DESIGN AND BEHAVIOR OF LARGE CONCRETE CANTILEVER OVERHANGS WITH COMBINATIONS OF PRESTRESSED AND NON-PRESTRESSED REINFORCEMENT

APPROVED BY
SUPERVISING COMMITTEE:

John E. Breen

Michael E. Kreger

DESIGN AND BEHAVIOR OF LARGE CONCRETE CANTILEVER OVERHANGS WITH COMBINATIONS OF PRESTRESSED AND NON-PRESTRESSED REINFORCEMENT

by

SCOTT DOUGLAS ARMSTRONG, B.S.

THESIS

Presented to the Faculty of the Graduate School of

The University of Texas at Austin

in Partial Fulfillment

of the Requirements

for the Degree of

MASTER OF SCIENCE IN ENGINEERING

THE UNIVERSITY OF TEXAS AT AUSTIN
August 1994

ABSTRACT

DESIGN AND BEHAVIOR OF LARGE CONCRETE CANTILEVER OVERHANGS WITH COMBINATIONS OF PRESTRESSED AND NON-PRESTRESSED REINFORCEMENT

by

Scott Douglas Armstrong, M.S.E.
The University of Texas at Austin, 1994
Supervising Professor: John E. Breen

The application of current guide specifications for the design of cantilever overhangs in concrete bridge piers can result in structures which are overdesigned, expensive, and difficult to construct. This is because the appropriate application of current design equations is often times ambiguous to the designer due to the wide variety of cantilever lengths and depths which are possible. The design is further complicated by the treatment of reinforced concrete and prestressed concrete in separate chapters and according to different strength and serviceability criteria in the current AASHTO Standard Specifications for Highway Bridges.

An alternative design approach is presented in this report. This proposed approach makes use of what is referred to as "structural concrete", which spans the full spectrum from reinforced to fully prestressed concrete, including combinations of prestressed and non-prestressed reinforcement. Also inherent in the "structural concrete" approach is the use of strut-and-tie modelling which offers a transparent design tool based on visualizing the flow of forces in the structure, and placing the reinforcement as needed to accommodate the force flow. This allows the designer to avoid the uncertainty often associated with application of design specification equations.

Four specimens, each with two overhangs, were constructed and tested. Six unique reinforcing patterns were represented among the eight overhangs. Two of the overhangs were designed according to the current AASHTO Specification. One was reinforced concrete while the other was fully prestressed concrete. The other overhangs were designed with varying combinations of prestressed and non-prestressed reinforcement. Each of the overhangs was evaluated on the basis of its service and ultimate load behavior, constructability, and reinforcement costs.

Based on the results of the research it was possible to recommend a design procedure consistent with the "structural concrete" approach considering both service limit state and ultimate limit state criteria. This approach has advantages over methods dictated by current design specifications by being more intuitive in its application and by leading to more easily constructed and potentially more economical overhangs.

ACKNOWLEDGEMENTS

The physical testing for this research was performed at the Ferguson Engineering Laboratory at the University of Texas at Austin. Completion of this work would not have been possible without the assistance of a great many people who are deserving of recognition.

I would first like to express sincere gratitude to my supervising professor, Dr. John E. Breen, for his guidance, suggestions, and encouragement throughout all phases of the research and for the many enlightening conversations which he freely shared. Thanks also to Dr. Michael E. Kreger for his many helpful suggestions throughout the project and for his review of this thesis. I truly considered it a privilege to work with both of you.

A special thanks is also extended to fellow graduate students Sarah Billington, Ruben Salas, and Brad Wood for all their help in planning and conducting the research and analyzing the results. Thanks also to undergraduate assistants Tim Abel, Pete Almarez, Jim Doran, Mohamed Najah, Steve Smith, David Vliet, and Todd Zatopek. You were a great group of people to share this experience with.

Thanks you also to David Hartmann and Mike Tanner of the Austin Bridge and Road Company for their generous assistance in providing cost estimates.

I would also like to express my appreciation to the staff of the Ferguson Engineering Laboratory including Pat Ball, Sharon Cunningham, Wayne Fontenot, Laurie Golding, Ryan Green, April Jenkins, Wayne Little, Ray Madonna, and Blake Stassney for your help in guiding me toward the most practical way of getting things done and for the countless hours that saved.

I am also very greatful to the Texas Department of Transportation for giving me this opportunity.

Most especially I thank my wife, Mary, who in her characteristic unselfish manner was willing to go the extra mile in the care of our children and home during the many required hours of my absence. Your love, support, and shared commitment to this endeavor have made it possible.

Scott Armstrong
August 1994
Austin, Texas

TABLE OF CONTENTS

LIST OF TABLES

LIST OF FIGURES

CHAPTER 1
INTRODUCTION

1.1 Background

1.1.1 Large Cantilever Bridge Piers used on San Antonio Downtown "Y" Project

The need for this research originated at the Texas Department of Transportation where large cantilever piers were designed as substructure elements for segmental box girder bridges in San Antonio Downtown "Y" projects. This project involved the construction of an elevated freeway over an existing section of at-grade freeway. Frontage roads paralleled the lower level mainlanes and access to and from the lower level freeway was provided by entrance and exit ramps. The large cantilever piers were required where entrance or exit ramps prevented positioning the bridge piers directly below the superstructure. Figure 1.1 illustrates the typical situation where the large cantilever piers were used.

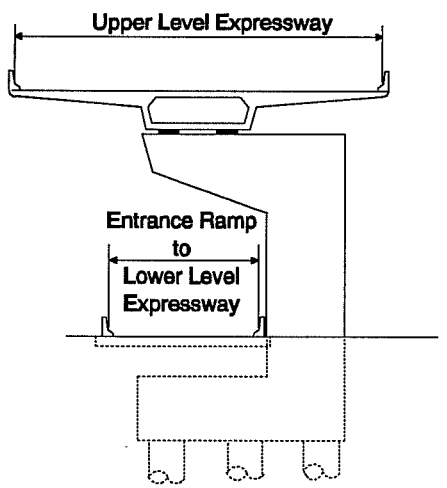

Figure 1.1 Typical Cantilever Bridge Pier

A large number of cantilever overhang lengths were required to accommodate the variety of relative positions of the superstructure, lower level mainlanes, frontage roads, and entrance and exit ramps. Loads were transferred from the superstructure through two transversely spaced bearings at the end of each span. Thus, each pier was loaded with two left bearings and two right bearings. For shorter overhangs, only the two left bearings loaded the overhang. These bearings were close to the column. For longer overhangs, both the left bearings and right bearings loaded the overhang, and these could be at a considerable distance from the column.

The current AASHTO Standard Specification for Highway Bridges (1) requires the use of corbel provisions when the shear span to depth ratio (a/d) is less than one. For shorter overhangs where all bearings were within this limit, it was appropriate to apply the AASHTO corbel provisions providing reinforcement to resist a shear-friction failure through the overhang at the face of the column. In the case of longer overhangs, where all bearings were outside this limit, AASHTO could reasonably be applied to the member by treating it as a beam, although very often they would be deep beams because of the low span to depth ratios.

However, because of the variety of pier sizes needed to accommodate the overall roadway geometrics, many overhangs had lengths for which the appropriate AASHTO design provisions were not obvious. Several overhangs had an a/d ratio for the inside bearing of less than one and an a/d ratio for the outside bearing of greater than one. In these instances, reinforcement was provided for both deep beam provisions as well as resistance to a shear-friction failure even though it may not have been necessary. Consequently, reinforcing cages were heavily congested and difficult to construct, and may have been significantly over-designed.

The design of the overhangs was further complicated by the use of both reinforced (ie. non-prestressed) concrete and post-tensioned concrete. The current AASHTO bridge design specification places different strength and serviceability requirements on each, treating them in separate chapters as essentially separate and unique materials.

For reinforced concrete, only mild reinforcement is used and the design is largely in accordance with an ultimate strength design philosophy. The serviceability provisions guard against fatigue failure of the reinforcement, excessive crack widths, and excessive deflections. Fatigue failure of the reinforcement is prevented by providing sufficient reinforcement to control the range of stress experienced by the steel as loads cycle on and off the member. Crack widths are controlled by providing the required area of steel, but also by using a large enough number of bars that the crack width formulae are indirectly satisfied. This leads to cracking patterns in

which the cracks are well distributed and in which crack widths are acceptably small. However, the required number of bars to satisfy the crack width provisions can become quite numerous, leading to highly congested reinforcing cages which are difficult to assemble and which create problems with the placement and consolidation of concrete. Furthermore, the cracking can significantly reduce the stiffness of the member and can lead to difficulties in obtaining acceptable service load deflections.

Post-tensioned concrete, on the other hand, is designed under the AASHTO criteria primarily in accordance with a service load, or working stress, design philosophy. Members are required to be "fully post-tensioned" which means that the tensile stresses in the concrete under service loads are limited to levels below which cracking would be expected to occur. This results in quantities of post-tensioning which are much greater than what would be required if an ultimate strength design approach governed. Excessive camber of a member can be a problem when the large amounts of post-tensioning required by service load stress criteria are used. The high camber occurs over time with creep and shrinkage of the concrete under the large post-tensioning force. In the event that a fully post-tensioned member does crack due to poor construction or an extreme overload, a sufficient number of reinforcing elements often may not be present to control the cracking. Additionally, fully-post tensioned concrete exhibits considerably less ductility than reinforced concrete. This results in less warning of distress and less general structural integrity when the structure is subjected to unanticipated accidental loads.

As previously mentioned, some of the piers in San Antonio were designed using AASHTO reinforced concrete provisions while others were designed using AASHTO fully post-tensioned concrete provisions. Because of the greatly different design approaches required by the AASHTO provisions, it was not uncommon for two adjacent overhangs, having only slightly different strength requirements, to be designed with significantly different strengths and service load behavior. This would occur when the first overhang was designed using reinforced concrete, but it would not be possible to provide enough mild reinforcement in the second overhang, without the cage becoming excessively congested. The second overhang would have to be redesigned as a fully post-tensioned member, basically governed by the service load design provisions of AASHTO.

1.1.2 Strut-and-Tie Modelling

The ambiguity associated with the design of the overhangs with intermediate a/d ratios (in which deep beam, corbel, and shear-friction provisions all were applied), and the highly congested reinforcing cages which resulted, could have been alleviated with the use of strut-and-tie modelling.

In strut-and-tie modelling (2), the designer is directed toward an approach which emphasizes tracing the flow of forces through a structure. The flow of forces, or load paths, are made up of zones of compressive and tensile stresses. The zones of compressive stresses are referred to as struts and the load carrying capacity of the struts is a function of the compressive strength of the concrete. The zones of tensile stresses are referred to as ties. The ties are made up of reinforcement which is provided in sufficient quantities to carry the tension forces.

The strut-and-tie modelling approach is in contrast to the section by section approach to design inherent in today's design codes. It is this section by section approach that caused the difficulty faced by the designers in determining whether overhangs with intermediate a/d ratios should be designed as corbels or as deep beams. Strut-and-tie modelling offers an approach which is transparent and allows the designer to visualize more clearly where reinforcement is needed, giving a more rational approach to the design of members for which application of more empirical code equations is not obvious.

It is commonly recognized that the traditional section by section analysis and design works satisfactorily, and may be the preferred method of design, in those regions of a structure where the Bernouli assumption that plane sections remain plane is valid. These regions are referred to as B-regions. The longer cantilever overhangs in San Antonio could reasonably be treated as having a large portion of B-region.

The strut and tie approach is preferred in those regions of a structure where the Bernouli assumption is not valid and the appropriate application of existing and generally highly empirical code equations is not clear to the designer. These regions are referred to as Discontinuity regions or D-regions. The overhangs of the large cantilever piers in San Antonio with bearings close to the column should be treated as D-regions.

1.1.3 "Structural Concrete"

The situation described in Section 1.1.1 where two adjacent overhangs would have significantly different strengths and service load performance is fundamentally irrational and is a

consequence of the AASHTO treatment of reinforced concrete in one chapter as if one material, while post-tensioned concrete is treated in a separate chapter as if a separate material. A more reasonable approach would involve the use of what many researchers traditionally referred to as partial prestressing, but which now is giving way to a more unified approach termed "structural concrete".

Partial prestressing was a term used for designs based on combinations of mild and pretensioned (or post-tensioned) reinforcement. An ultimate strength design approach is taken considering the contributions at ultimate of both non-prestressed and prestressed reinforcement so that the member strength is in proportion to the demand from factored loads. This design approach is closely patterned after the procedure for a member designed with only mild reinforcement.

Members designed with combinations of non-prestressed and prestressed reinforcement offer many advantages over either reinforced concrete or fully post-tensioned concrete for cases like the large cantilever overhangs used in San Antonio. The highly congested cages of the reinforced concrete members could be greatly reduced by substitution of post-tensioning for some of the mild reinforcement. This would lead to cages which would be much easier to assemble and to members for which good placement and consolidation of concrete would be easier to achieve. The overhangs might be expected to be cracked at loads below or slightly above service loads, but the mild reinforcement would be available to distribute the cracks and control the crack widths. The expected amount of cracking would be less than for the reinforced concrete overhangs, so greater member stiffness would be available to control service load deflections.

The reduction of post-tensioning offers advantages over fully post-tensioned members in that excessive cambering of the member could be avoided, ductility could be improved, cost savings are possible, and the presence of some mild reinforcement would help to control cracking in the event that a crack did occur.

The term partial prestressing is not advocated here because it has historically been the source of confusion among researchers and structural engineers. The confusion has centered around the manner in which the degree of partial prestressing would be defined. Several different definitions have been proposed through the years but no single definition has earned universal acceptance and usage.

The proposed term "structural concrete" would apply to the full spectrum from plain concrete, to mild, prestressed, or mixed reinforcement. With this term, the need for a single,

universally accepted, definition of the degree of prestressing is eliminated and the related confusion is avoided. Also embodied in the structural concrete approach is a unified design methodology which is applicable to all structural concrete, regardless of the type of reinforcement that is used. It is hoped that eventually this integrated approach will replace the current approach taken in AASHTO and other codes which treats reinforced and prestressed concrete in separate chapters and with different strength and serviceability criteria.

1.2 Objectives of Research

The primary objective of this research is to develop a design procedure for use on large cantilever bridge pier overhangs of intermediate length for which application of the current AASHTO provisions is ambiguous. The procedure should be rational, transparent, and easy to use. It should result in overhangs which have acceptable service load performance as well as ultimate strength, and which would be more easily constructed and economical than designs resulting from current AASHTO standards. It is envisioned that this procedure will incorporate combinations of mild reinforcement with prestressed reinforcement and use of strut-and-tie modelling in any D-regions.

Toward this end, an experimental program was conducted involving the construction and testing of multiple cantilever overhangs, some designed in accordance with current AASHTO standards, and others designed according to alternative procedures incorporating mixed non-prestressed and prestressed reinforcement. Where appropriate, strut-and-tie modelling was also used.

The test results should provide the basis for evaluating the strength, serviceability, and constructability inherent in current AASHTO designs and in suggested new designs. This experimental evidence will allow for a realistic comparison to be made between the contrasting approaches.

1.3 Organization of Thesis

This thesis is divided into seven chapters. The contents of Chapters 2 through 7 are briefly described here:

Chapter 2: Experimental Program -------- detailed description of specimen design, fabrication, and testing.

Chapter 3: Test Results ---------- presentation of data collected during the testing of each specimen.

Chapter 4: Analysis of Test Results ------ analysis and discussion of service load and ultimate load behavior of each specimen as well as comparison between specimens.

Chapter 5: Overhang Constructability ---- discussion of construction related topics and costs and Economics

Chapter 6: Design Recommendations ---- discussion of recommended design procedure.

Chapter 7: Summary and Conclusions --- summary of key elements of experimental program and significant findings from research.

CHAPTER 2
EXPERIMENTAL PROGRAM

2.1 Introduction

The experimental program involved the construction and testing of eight cantilever overhangs. All eight overhangs had the same external dimensions. Four specimens were constructed, each with two overhangs. Four different approaches were taken to design the primary moment reinforcement for each of the four specimens. The moment reinforcement on both overhangs of each specimen was the same. The shear reinforcement was the same on both overhangs of the first two specimens and different on each overhang of the third and fourth specimens. Thus, a total of six different reinforcement patterns and design schemes were represented in the eight overhangs.

The test specimens had similar geometries and loading to the intermediate length overhangs used on the San Antonio project. The reinforcement in the first two specimens was designed in accordance with the current AASHTO provisions for reinforced and fully post-tensioned concrete. The third specimen was post-tensioned concrete, but based on an ultimate strength design philosophy. The fourth specimen was of structural concrete with a mix of prestressed and non-prestressed main reinforcement based on an ultimate strength design philosophy.

Each specimen was loaded to failure with specific observation made of the service load behavior. Service loading of the test specimens simulated superstructure dead loads and traffic live loads.

2.2 Design and Loading of the Specimens

2.2.1 Specimen Dimensions

The dimensions of the specimen overhang was determined by examining typical cantilever piers utilized on the San Antonio Downtown "Y" project. Overhang lengths varied in these piers from less than 2 feet to approximately 25 feet. The maximum depths of the caps, at the column

face, varied from 8 feet to as much as 13 feet, and the widths of the piers averaged 8 to 10 feet. The average distance between the left and right bearings was approximately 12 feet.

Each of these dimensions was considered to arrive at a typical prototype overhang of intermediate length for which design of the reinforcement by the current AASHTO provisions would be ambiguous. The overall dimensions of this overhang are shown in Figure 2.1.

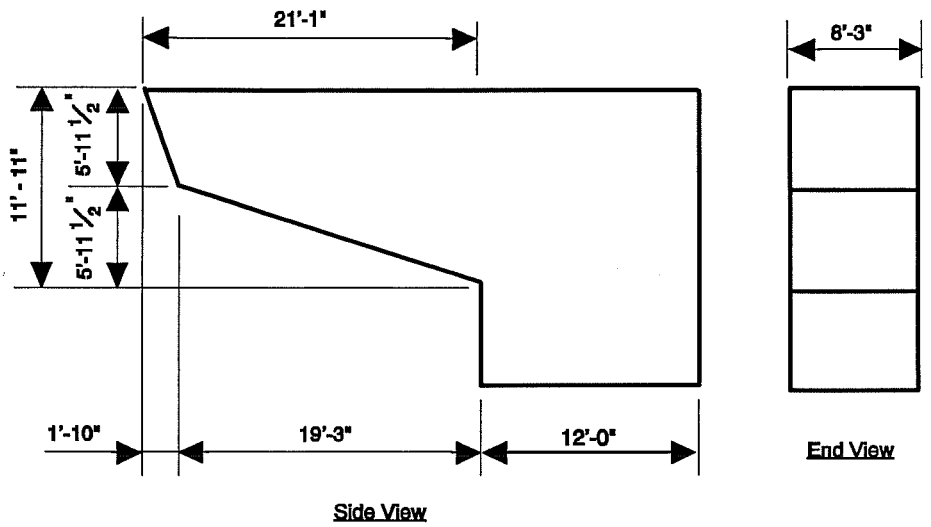

Figure 2.1 Prototype Dimensions

An attempt was made to keep the model dimensions as close as possible to the prototype, but, because of the practicality of handling and loading specimens of such enormous size, a scale factor of 5.5:1 was selected. Also, the decision was made to construct "T" shaped specimens with two cantilever overhangs rather than "L" shaped specimens with one overhang. This was to simplify the loading of the specimens. By loading "T" shaped specimens symmetrically on both sides, the complicated details of anchoring the column of an "L" shaped specimen to develop the column moment was eliminated. The resulting overall specimen dimensions are shown in Figure 2.2.

The position of the bearings relative to the column face are shown in Figure 2.3. The a/h ratios were 0.5 for the inside bearings and 1.5 for the outside bearings.

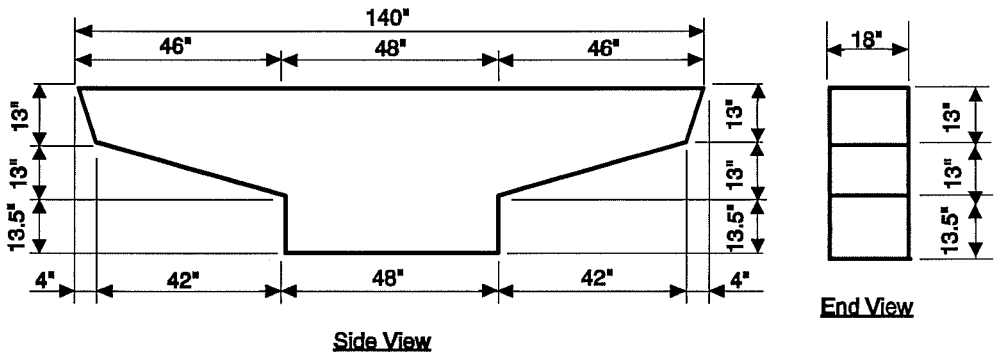

Figure 2.2 Overall Specimen Dimension

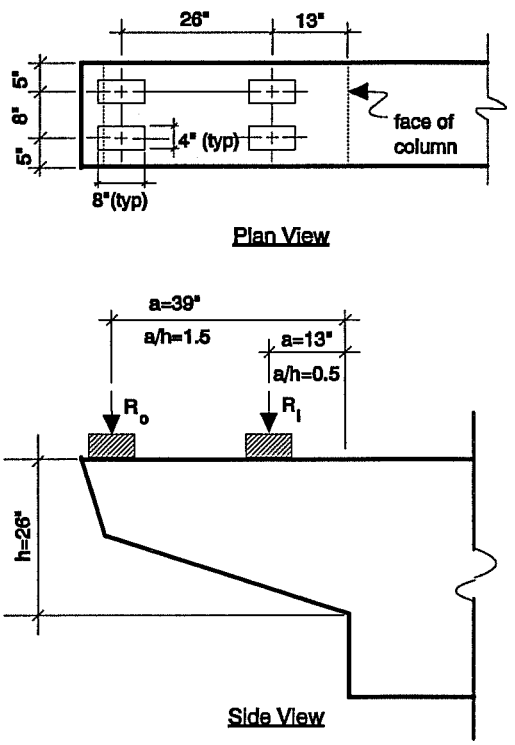

Figure 2.3 Location of Loads and Bearing Arrangement

2.2.2 Size and Arrangement of Bearings

The size and arrangement of bearings used was also derived from the typical full scale bridge. Bearing sizes varied in the full-scale piers depending on whether the bearing was fixed, sliding, or sliding at an expansion joint. The average dimensions and distances between these three bearing types was considered in the selection of bearing sizes and arrangements to be used on the model piers. The size of the bearings used in the tests was 4" x 8".

Since each pier supported a back span and a forward span, each cantilever overhang had four bearing locations, as shown in Figure 2.3.

2.2.3 Size and Grade of Reinforcement

It was desired that the same number and equivalent size of bars be used in the models that would have been used if full scale piers were being constructed. This was important because the distribution of the reinforcement was of primary concern for controlling crack widths.

An examination was made of the typical full scale piers to determine the bar sizes that were used for each of the different types of mild reinforcement. Each model overhang was designed initially with the prototype dimensions giving the required number and size of each bar. Reinforcing bars or wires were then selected for the models by scaling each bar by using the closest available bar or wire diameter resulting when the full scale diameter was divided by 5.5. A slight adjustment to the number of bars was permitted where the exact diameter was not available. Similarly, if the yield strength of the model reinforcement was significantly different than the assumed grade of the prototype reinforcement, 60 ksi, the number of bars or wires was again adjusted. This was the case for the No. 2 reinforcing bars and the 7 and 9 gauge wires. The No. 3 reinforcing bars and 10 gauge wire had measured yield strengths close to 60 ksi so no adjustment was made to the number of these on the basis of yield strength.

The adjustments ensured that the tensile yield provided by the reinforcement in the models was nearly equivalent to the tensile yield force in the prototype. Table 2.1 lists the size of reinforcement for the prototype design and the number of bars or wires used in the model specimens to substitute for each prototype bar.

The post tensioning in the models was similar to what would have been used in a full-scale design. It was observed that the most common size of tendon used in the San Antonio project was a 19-strand, 0.6" diameter tendon. The required number of these tendons, with the effective depth at the location typically observed in the San Antonio designs, was determined for

Type of Mild Reinforcement	Size of Prototype Reinforcement	Size of Model Reinforcement	Number of Model Bars or wires Used For Each Prototype Bar
Moment Bars Top Bars Bottom Bars	No. 11	No. 2	0.86
Side Face Bars Shear-Friction Bars Horizontal Shear Bars Top Bars Bottom Bars	No. 8	7 ga. wire	0.77
Double Shear Stirrups Anchorage Zone Stirrups	No. 6	10 ga. wire	1.08
Vertical Column Steel	No. 18	No. 3	1.20
Column Ties	No. 4	9 ga. wire	0.61

Table 2.1 Mild Reinforcement in Models

each overhang. The models were designed with approximately the same number of tendons at an equivalent effective depth by selecting appropriate combinations of 3/8", 1/2", and 0.6" diameter strands. In the models, each tendon was a single strand of one of these sizes. The result was that each single strand tendon in the model represented approximately one 19-strand tendon in the prototype.

Double vertical shear stirrups were used as web reinforcement, as this was observed to be typical in the full-scale piers.

2.2.4 Concrete Cover and Strength

The typical concrete cover used in the specimens was 0.41 inches. This is in direct scale with a cover of 2-1/4" which was typically used in the full scale piers. The concrete strength assumed in the design of the models was 5000 psi which is the same as that typically used in the full-scale piers.

2.2.5 Critical Load Cases

Load Group I from the AASHTO Bridge Design Specifications was assumed to be critical for the member so only dead load (D) and live load plus impact (L + I) were considered.

A superstructure was assumed with similar characteristics to that used in San Antonio. The bridge was wide enough for four lanes of traffic. It was arbitrarily decided that the pier would be an interior pier in a four span continuous unit with 110 ft spans.

The dead load of the superstructure was taken as the weight of 110 feet of the typical superstructure increased by a continuity factor of 1.143 since an interior pier was assumed. This load was assumed to be split evenly between all bearings.

The live loading was based on AASHTO lane loads increased by a continuity factor of 1.223 for the case of the first, third, and fourth spans of the unit loaded. This was further increased by a factor of 1.213 to account for impact loading.

Two different live load cases were determined to be critical for the design of the specimen. The case of the outside three lanes loaded was found to produce the maximum moment at the column face. The case of all four lanes loaded was critical for producing the maximum shear at the column face. These two cases are referred to as flexure loading and shear loading, respectively.

Factored loads were determined by application of AASHTO code Equation (3-10):

$$\gamma \left[\beta_D \cdot D + \beta_L (L + I) \right] \qquad [2\text{-}1]$$

For flexural and tension members and a Group I load combination, this equation reduces to the following:

$$1.3 \left[1.0D + 1.67(L + I) \right] = 1.3D + 2.17(L + I).$$

Table 2.2 summarizes critical loads for the specimen.

2.2.6 Load Similitude

Table 2.2 includes values for Simulated Dead Load Blocks. These loads are applied in addition to the superstructure and traffic loads to maintain equal bending and shearing stresses in the scale model as would occur in the prototype structure under equivalent loads.

	Inside Bearing (kips)	Outside Bearing (kips)	Inside Ram Load, Ri (kips)	Outside Ram Load, Ro (kips)	Moment at Column Face (kip-in)	Shear at Section a-a *** (kips)	Shear at Column Face (kips)
SERVICE LOADS							
Simulated Dead Load Blocks			4.47	1.47			
Superstructure Dead Load	39	39	43.47	40.47	M dead load = 2169*		
Flexure live loads plus impact	-4.9	16.5					
Shear live loads plus impact	6.5	6.5					
	Service Flexure Loads		38.57	56.97	M serv flex = 2749*		
	Service Shear Loads		49.97	46.97			
FACTORED LOADS							
Superstructure Dead Load	50.7	50.7					
Flexure live loads plus impact	-10.63	35.81					
Shear live loads plus impact	14.11	14.11					
	Factored Flexure Loads		44.54	87.98	Mu = 4036*	Vu = 88.6**	
	Factored Shear Loads		69.28	66.28			Vu = 136.9*

* includes self weight of overhang = 1.32 kips

** includes self weight of outside 27.17" of overhang = 0.64 kips

*** Section a-a shown on Figure 2.6

Table 2.2 Design and Test Loads

The laws of similitude give the relationship between prototype and model loads applied to the structure as:

$$\textit{Model Loads} = \textit{Prototype Loads} \;/\; (\textit{scale factor})^2 \qquad [2\text{-}2]$$

For loads applied to the structure, the relationship is maintained by simply dividing the prototype loads by the square of the scale factor.

However, since the self weight is related to the volume and mass density of the structure, the weight of a scale model is reduced from the prototype weight by the cube of the scale factor. Therefore, to maintain the relationship of Equation [2-2], the weight of the model must be increased by one times its scale factor. This is often accomplished through the use of supplementary dead load blocks which are suspended from the bottom of the specimen during testing. For the specimens on this project, it was possible to slightly increase the loads applied to the structure through the loading rams to simulate the placement of dead load blocks.

The required increase in loads, ΔR_i and ΔR_o, was determined by solving the following expressions to give the shear and moment at the face of the column equal to that which would result from the self weight of the overhang times the scale factor:

Shear at Column Face = $\Delta R_i + \Delta R_o + 1.32 = 5.5(1.32) = 7.26$, and

Moment at Column Face $= 13(\Delta R_i) + 39(\Delta R_o) + 19.44(1.32) = 19.44(7.26) = 141.13$

Solving these equations gives:

$$\Delta R_i = 4.47 \text{ kips, and}$$
$$\Delta R_o = 1.47 \text{ kips.}$$

2.3 Reinforcement Details and Design Procedures

2.3.1 Introduction

Design procedures used to determine the reinforcement pattern for each overhang, the column, and the anchorage zones are provided in this section. All designs were based on an assumed concrete compressive strength of 5000 psi. The actual yield strength was used to determine the required areas of steel for the No. 2 reinforcing bars and 7 and 9 gauge wires. A nominal yield strength of 60 ksi was assumed for the No. 3 reinforcing bars and 10 gauge wire,

and all strand was assumed to be Grade 270. All designs included the use of AASHTO strength reduction factors, Φ, of 0.9 for flexure and 0.85 for shear.

The following pnemonic labels were created for each overhang:

Specimen #	Overhang	Pnemonic Label
1	north and south	CO-RU
2	north and south	CO-PS-100S
3	north	CO-PU-100S-I
3	south	CO-PU-100S-V
4	north	CO-PU-74S-I
4	south	CO-PU-74S-V

The label provides information relevant to the reinforcement pattern and design philosophy utilized for each overhang, as explained in Figure 2.4.

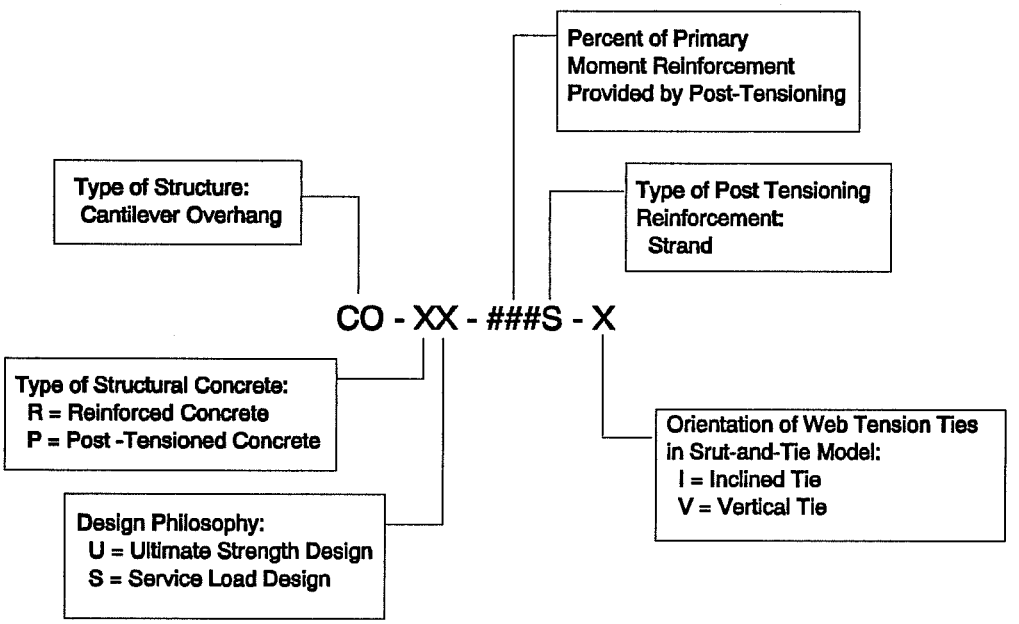

Figure 2.4 Overhang Labels

2.3.2 CO-RU (Specimen #1 - north and south overhangs)

This overhang was designed as reinforced concrete in accordance with the provisions of AASHTO. The reinforcing details are shown in Figure 2.5.

The primary moment reinforcement was determined from AASHTO Equation (8-15):

$$M_u \le \phi M_n = \phi \left[A_s f_y \, d \left(1 - 0.6 \frac{\rho f_y}{f_c'} \right) \right] \qquad [2\text{-}3]$$

where M_u was the moment at the face of the column from the factored flexure load case. The number of bars was slightly increased to satisfy AASHTO Equation (8-61):

$$f_s = \frac{z}{(d_c A)^{1/3}} \le 0.6 f_y \qquad [2\text{-}4]$$

The shear stirrup design was based on a 45° truss model implicit in AASHTO (see Figure 2.6). The quantity of vertical stirrups was determined from AASHTO Equations (8-46) and (8-47):

$$V_u \le \phi V_n = \phi (V_c + V_s), \qquad [2\text{-}5]$$

equation (8-49):

$$V_c = 2\sqrt{f_c'} \, b_w \, d \, , \qquad [2\text{-}6]$$

and equation (8-53):

$$V_s = \frac{A_v f_y \, d}{s} \, , \qquad [2\text{-}7]$$

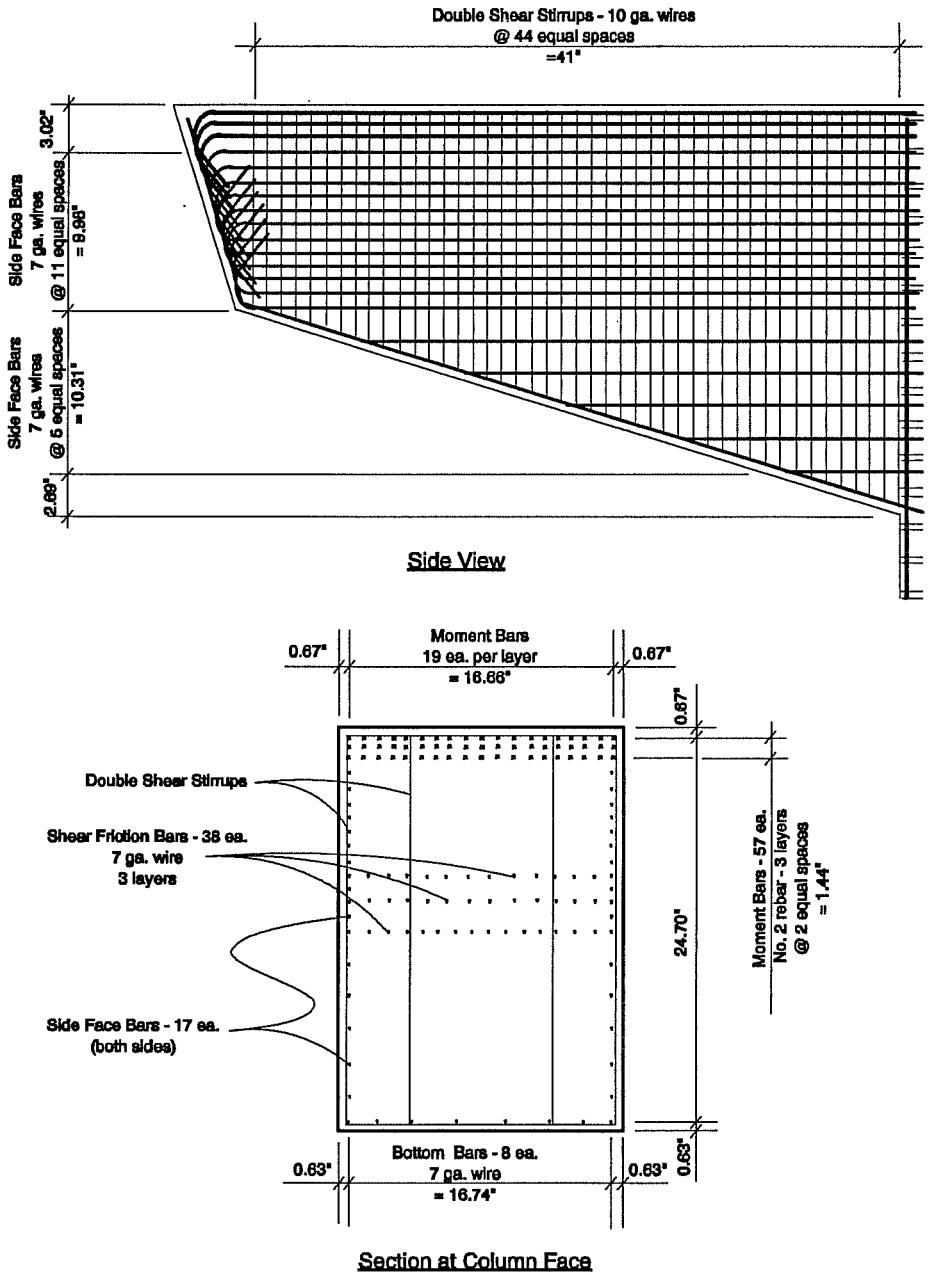

Figure 2.5 Reinforcing Details for the CO-RU Overhang

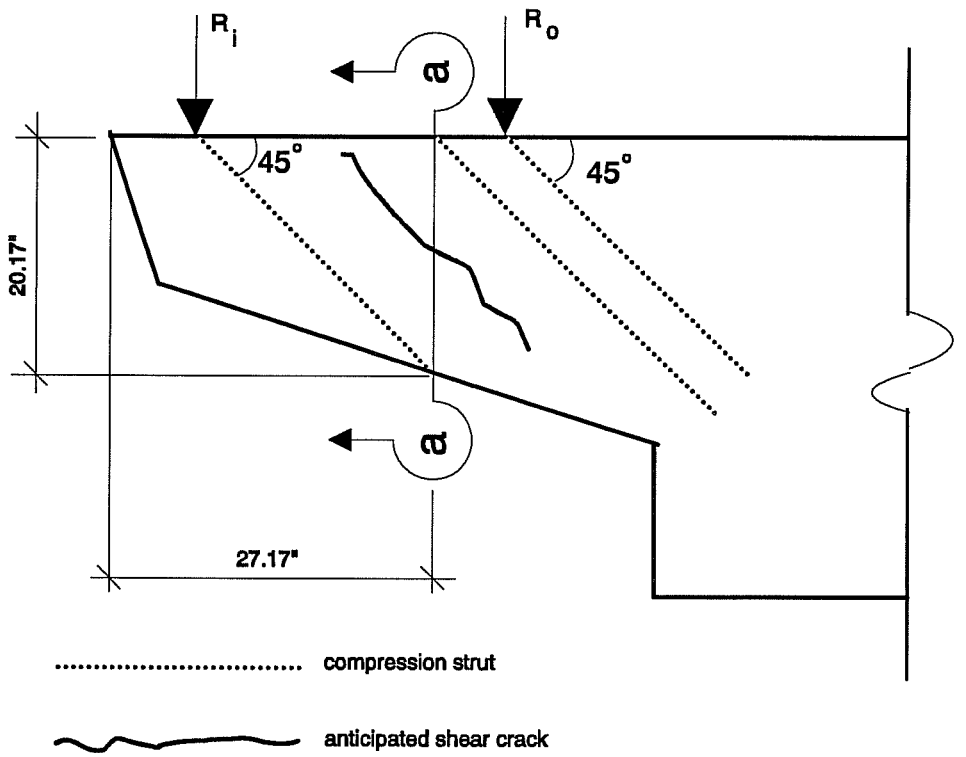

Figure 2.6 45° Compression Strut Implicit in AASHTO Shear Provisions

V_u was taken as the sum of the outside reaction from the factored flexure load case and the factored weight of the outside 27.17" of the overhang. The effective depth of the overhang at Section a-a in Figure 2.6 was used to determine V_c and V_s.

The side face bars were designed according to the recommendations of Frantz and Breen (3) for deep flexural members:

For d > 100" (prototype dimension),

$$\rho_{sk} \geq 0.011 + 0.000058d \qquad [2\text{-}8]$$

and

$$\rho_{sk} = \frac{A_{sk}}{2\ [d/2 \cdot 2d_c]} \qquad [2\text{-}9]$$

The corbel provisions of AASHTO were used to determine the shear-friction steel requirement. V_u was taken from the factored shear loading case for the maximum shear at the face of column. The corbel provisions require the primary moment reinforcement, A_f, be made greater than the larger of A_s, as determined above by Equation [2-3], and

$$\frac{2A_{vf}}{3} \qquad [2\text{-}10]$$

where A_{vf} is determined from AASHTO Equation (8-56):

$$\phi V_n = A_{vf} f_y \mu \qquad [2\text{-}11]$$

A_s from Equation [2-3] was found to control.

The corbel provisions further require that longitudinal steel with an area equal to 1/2 A_f be distributed within 2/3 of the depth of the section adjacent to A_s. The side face bars within this region were counted toward partially fulfilling this requirement.

2.3.3 CO-PS-100S (Specimen #2 - north and south overhangs)

This overhang was designed as fully post-tensioned concrete in accordance with the current AASHTO provisions. The reinforcing details are shown in Figure 2.7.

The quantity of primary moment reinforcement was determined by solving Equation [2-12], which limits the tensile stresses in the extreme fiber of an uncracked section to $3\sqrt{f_c'}$, with service flexure loads applied.

$$\textit{Extreme Fiber Tensile Stress} = 3\sqrt{f_c'} = -\frac{P}{A} + \frac{Pey}{I} + \frac{M_{serv}\textit{flex}\ y}{I}$$

where P = the effective prestressing force = $A_{ps} \cdot f_{se}$,

A = the cross-sectional area at the face of column,

e = the post tensioning eccentricity,

y = the distance from the centroid of the section to the extreme fiber,

I = the moment of inertia at the section, and

$M_{serv\ flex}$ = the moment due to unfactored self weight and service flexure live loading.

The effective prestress level, f_{se} , was assumed to be equal to 160 ksi.

The shear stirrup design was identical to that of Specimen #1, as this was the typical manner for determining the vertical stirrup requirement in the fully post tensioned piers in San Antonio.

The side face reinforcement consisted of 7 Gauge wires at a spacing of 2.07" along both faces of the cap. This spacing corresponded to No. 8 bars at 12" in the typical full-scale post-tensioned design.

The corbel provisions of AASHTO were used to determine the shear-friction requirement, but a slightly different procedure was followed than for Specimen #1. It was recognized that the post-tensioning provided was governed by service load stress requirements and was substantially more than was required for factored flexural strength. This was used to advantage in determining the quantity of shear-friction steel. The ultimate post-tensioning force was converted to an equivalent area of 82.2 ksi steel (82.2 ksi is the yield strength of the 7 Gauge wire which was used for the shear-friction steel). Then the area of 82.2 ksi steel required for flexural strength was determined and subtracted from the equivalent area provided by the post tensioning. The remaining area was considered to be available to partially fulfill the shear-friction steel requirement in the upper 1/3 of the beam. The remainder was provided by two No. 2 bars and three 7 Gauge wires used for the top layer of steel in the overhang. Eight side face bars were counted towards partially fulfilling the requirement for the middle 1/3.

Ten No. 2 bars were provided along the bottom of the cap which is equivalent to the typical amount of steel used in the full-scale post-tensioned pier caps.

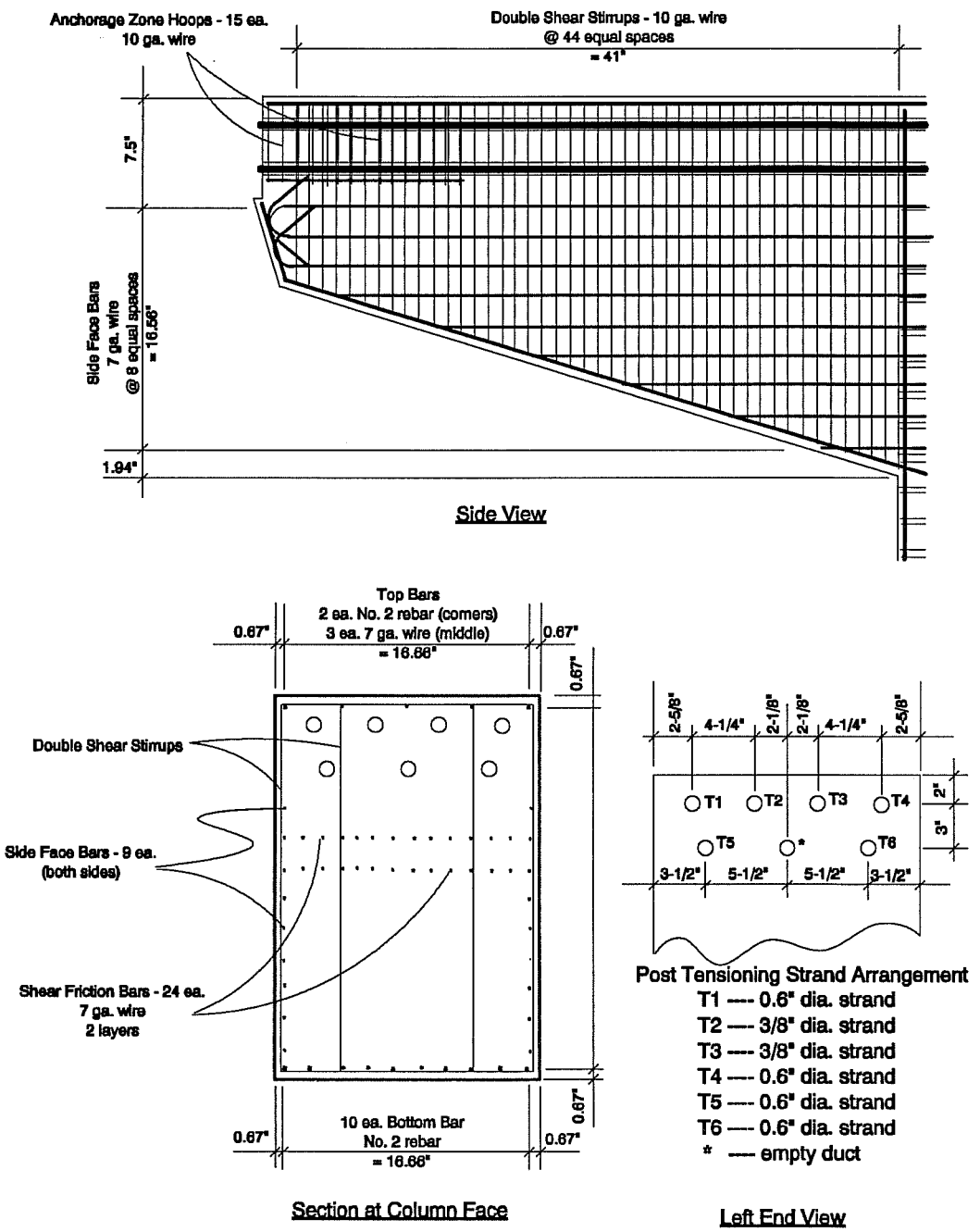

Figure 2.7 Reinforcing Details for the CO-PS-100S Overhang

2.3.4 CO-PU-100S-V (Specimen #3 - south overhang)

This overhang was designed with 100% of the primary moment reinforcement consisting of post-tensioning strand, but it was determined ignoring AASHTO service load concrete stress limits and was totally based on an ultimate strength design philosophy. Strut-and-tie modelling was used in the shear design. The reinforcing details for this overhang are shown in Figure 2.8.

The primary moment reinforcement was determined from AASHTO Equations (9-13):

$$M_u \leq \phi M_n = \phi\left[A_s^* f_{su}^* d\left(1 - 0.6\frac{\rho^* f_{su}^*}{f_c'}\right)\right], \qquad [2\text{-}13]$$

and (9-17):

$$f_{su}^* = f_s'\left(1 - 0.5\frac{\rho^* f_s'}{f_c'}\right), \qquad [2\text{-}14]$$

where f^*_{su} = the average stress in prestressing steel at ultimate load,

ρ^* = the ratio of prestressing, and

f'_s = the ultimate strength of the prestressing steel.

The shear reinforcement consisted of vertical stirrups only and was designed using a strut-and-tie model incorporating the horizontal compressive stress block from Equation [2-13]. This strut-and-tie model is shown in Figure 2.9. This model is one representation of the flow of forces in the overhang.

Development of the model began with a finite element analysis of the overhang under the effect of factored flexure loads and the effective post-tensioning force. The finite element analysis program used was ANSYS. The effective post tensioning force was based on an assumed stress in the strand of 160 ksi.

Plots of the principal compressive and tensile stress vectors, shown in Figures 2.10 and 2.11, were generated to obtain a visual image of the elastic stress distribution under factored loads. The orientation of struts and ties for the model were chosen to resemble the orientation of the stress vectors. However, struts C2, C_{sw}, C5, and C6 were forced to converge at the center of the horizontal compressive stress block, and the inclined tensile stresses in the middle of the web were approximated with a vertical tie T4.

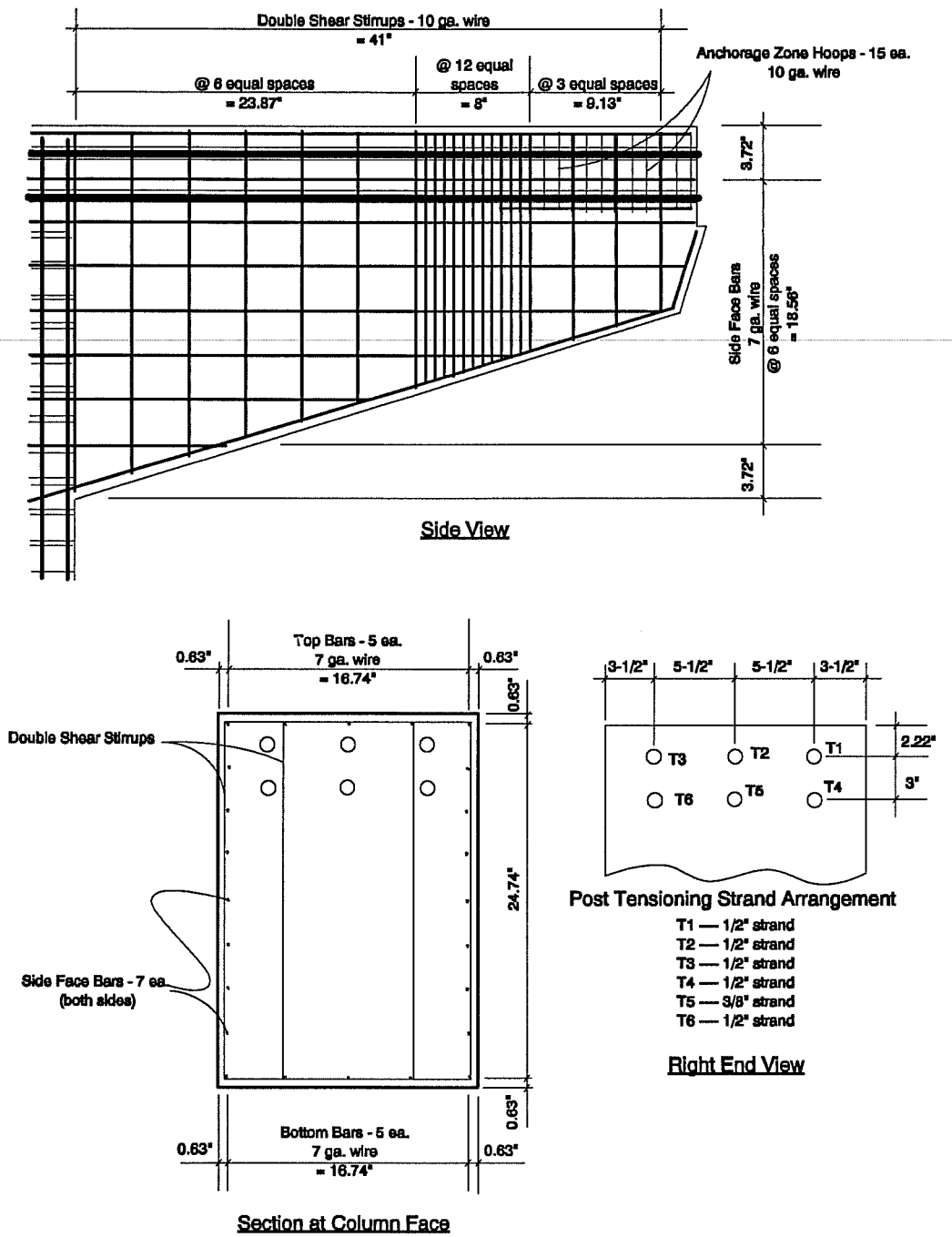

Figure 2.8 Reinforcing Details for the CO-PU-100S-V Overhang

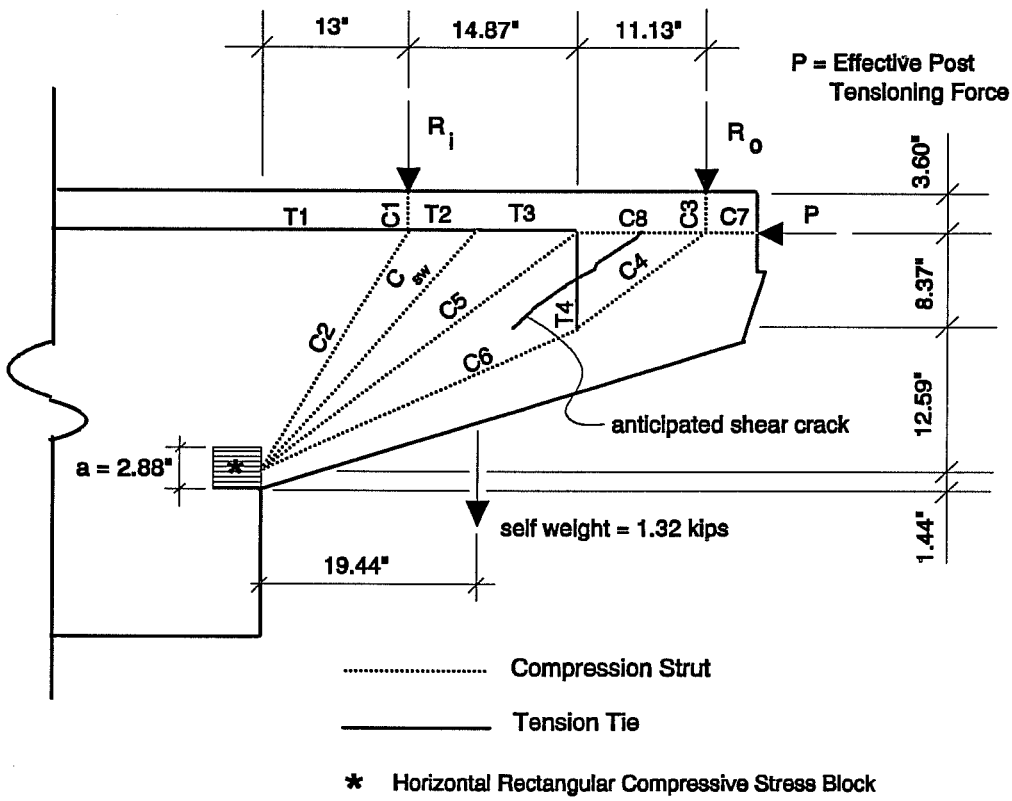

Figure 2.9 Strut-and-Tie Model for the CO-PU-100S-V Overhang

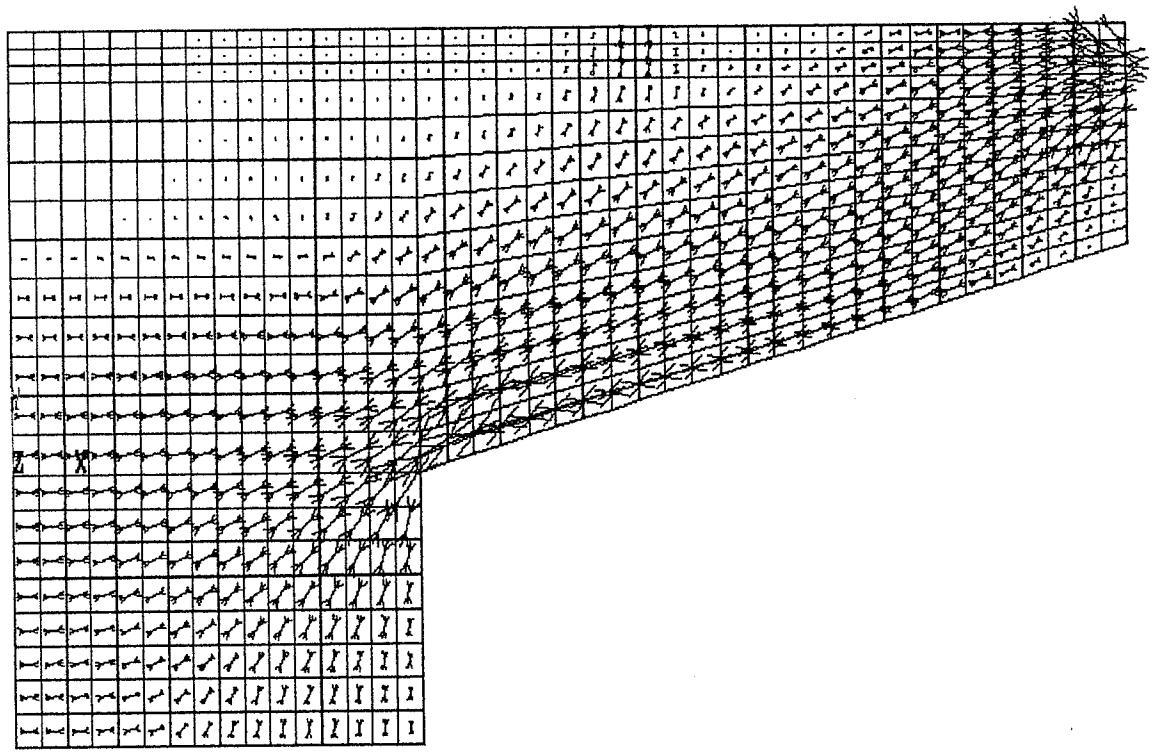

Figure 2.10 Principal Compressive Stress Vectors for the CO-PU-100S Overhangs with Factored Flexure Loads Applied

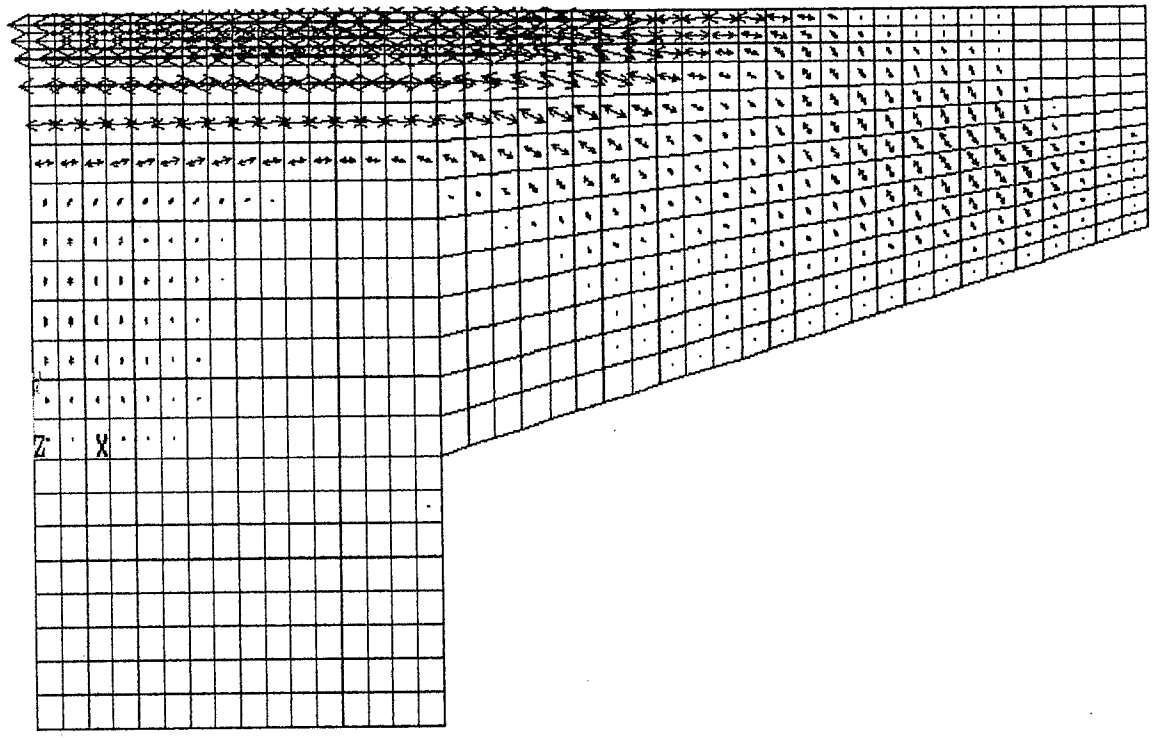

Figure 2.11 Principal Tensile Stress Vectors for the CO-PU-100S Overhangs with Factored Flexure Loads Applied

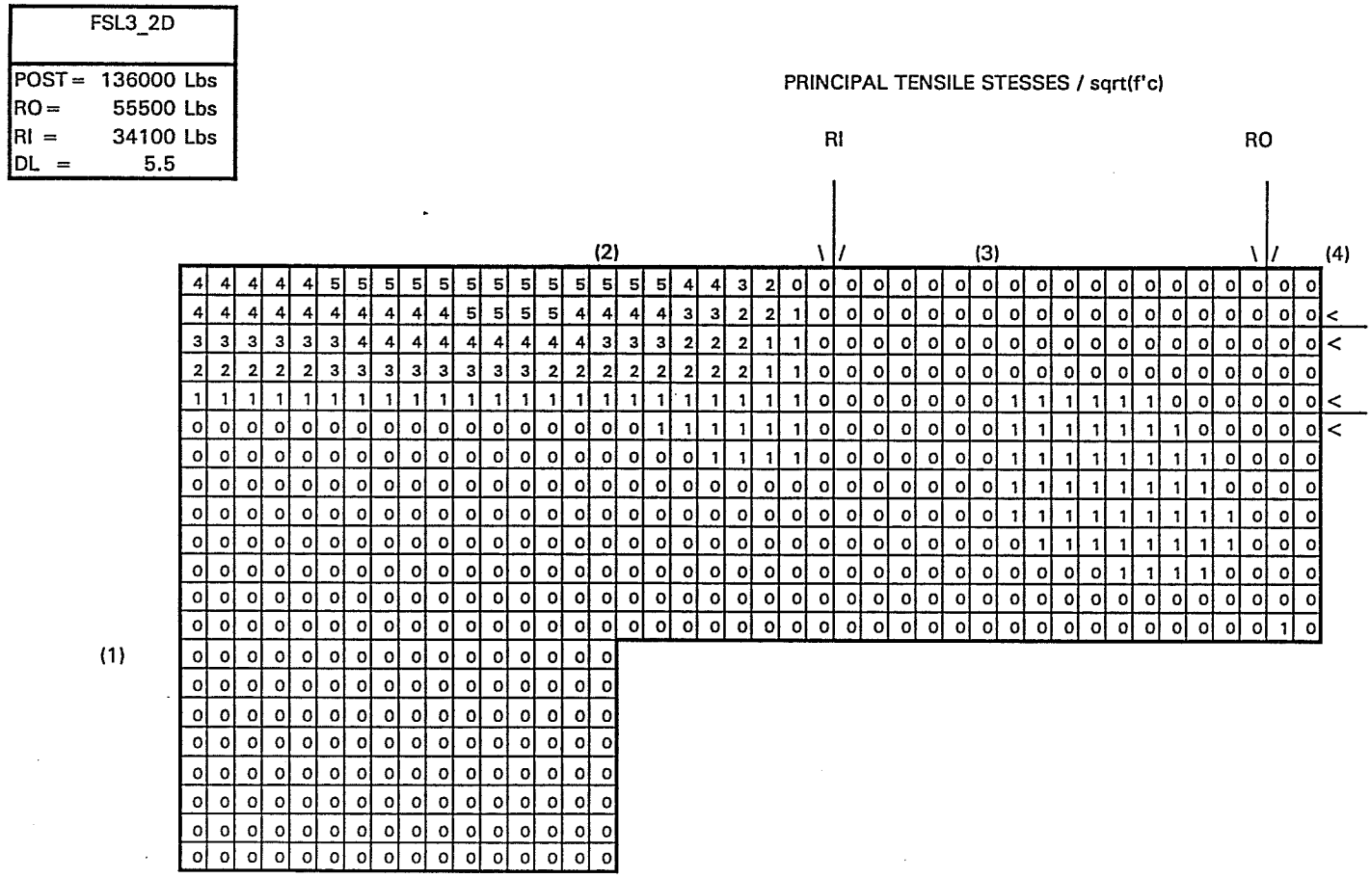

Figure 2.12 Magnitude of Principal Tensile Stresses for the CO-PU-100S Overhangs with Service Flexure Loads Applied

The force in tie T4 was determined from nodal equilibrium with factored flexure loads applied to the model. The number of stirrups used for tie T4 was determined from this force divided by a Φ-factor of 0.85. The width over which to distribute the vertical stirrups of tie T4 was determined from another finite element analysis with service flexure loads and the effective post-tensioning force applied to the overhang. Figure 2.12 shows the results of this analysis where each number represents the magnitude of the principal tensile stress in terms of multiples of $\sqrt{f_c'}$. The steel for tie T4 was distributed over the region within the middle of the web with principal tensile vectors greater than or equal to $1\sqrt{f_c'}$. The stirrups were placed at a minimum spacing of 1/2". This was determined from 1.5 times the maximum coarse aggregate size. This resulted in an 8" tie width between centers of the outside bars. Stirrups were placed at a maximum spacing of 4.36" throughout all other regions along the overhang. This spacing corresponds with 24" in the full scale.

Minimum skin steel was used on the sides, top, and bottom faces of the cap. The maximum spacing of this steel was 3.27", which corresponds to 18" in the full scale.

2.3.5 CO-PU-100S-I (Specimen #3 - north overhang)

The primary moment, side face, top, and bottom reinforcement were the same as in CO-PU-100S-V. The shear reinforcement was determined from strut-and-tie modelling, but it consisted of both vertical and horizontal steel. The reinforcing details are shown in Figure 2.13.

The shear reinforcement was designed using the strut-and-tie model shown in Figure 2.14. This strut-and-tie model is similar to the one used for the CO-PU-100S-V overhang in that it incorporates the compressive stress block from the flexural design. However, this model uses inclined ties in the web. The inclined ties more closely match the orientation of principal tensile stress vectors shown in Figure 2.11.

Vertical stirrups were provided for the vertical component of each tie. The stirrups for tie T5 were spaced evenly over the horizontal length of the tie. The stirrups for tie T6 were placed at the minimum spacing of 1/2" and centered on the horizontal center of the tie. This led to a band of stirrups that was 6.7" between the centers of the outside bars.

The horizontal steel was distributed over three levels at the same height as the side face bars. Tie T6 required more horizontal steel than tie T5. As a matter of good detailing, the steel required for T6 was extended through the cap to provide an equal area of steel for T5. This steel

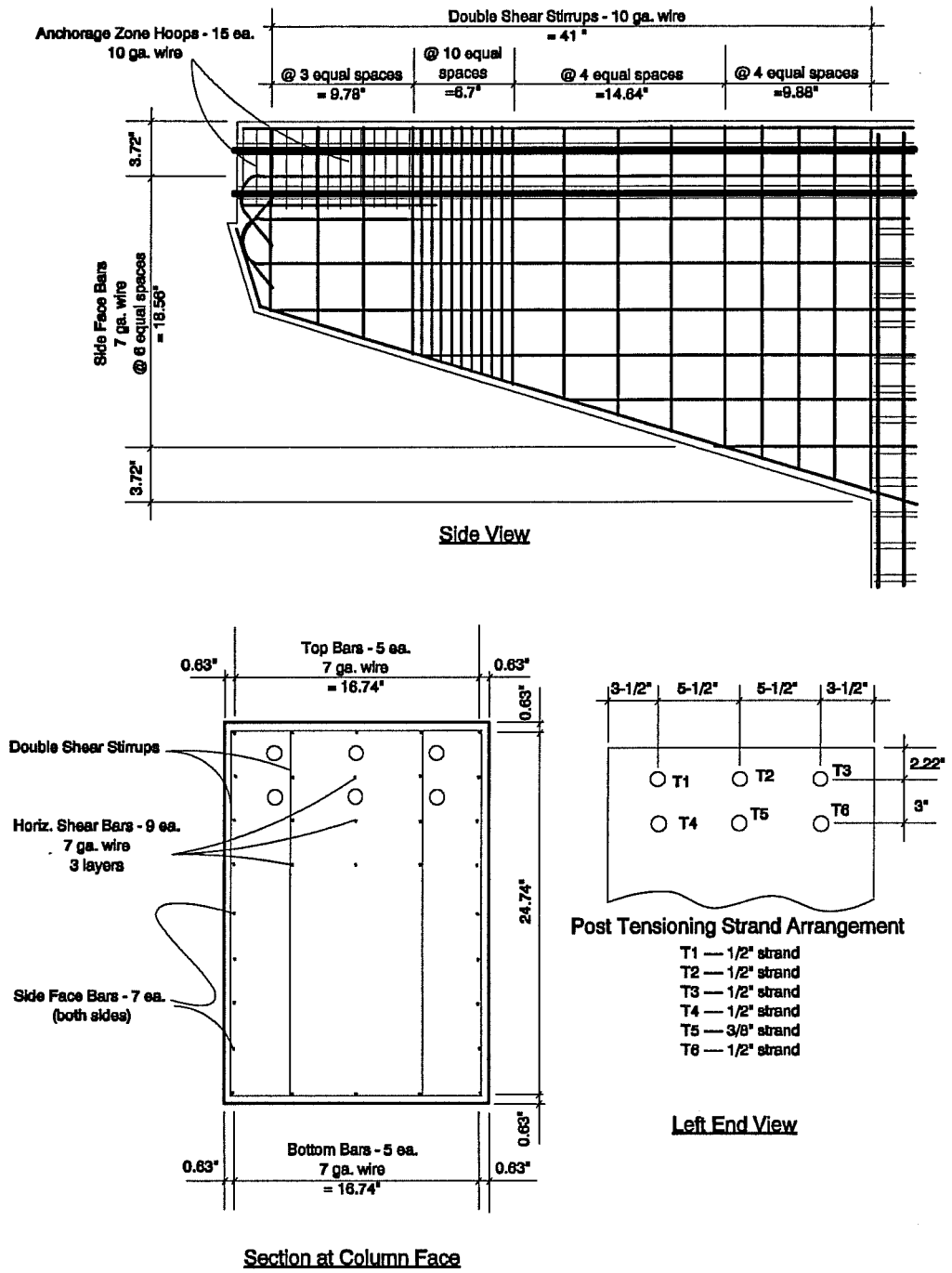

Figure 2.13 Reinforcing Details for the CO-PU-100S-I Overhang

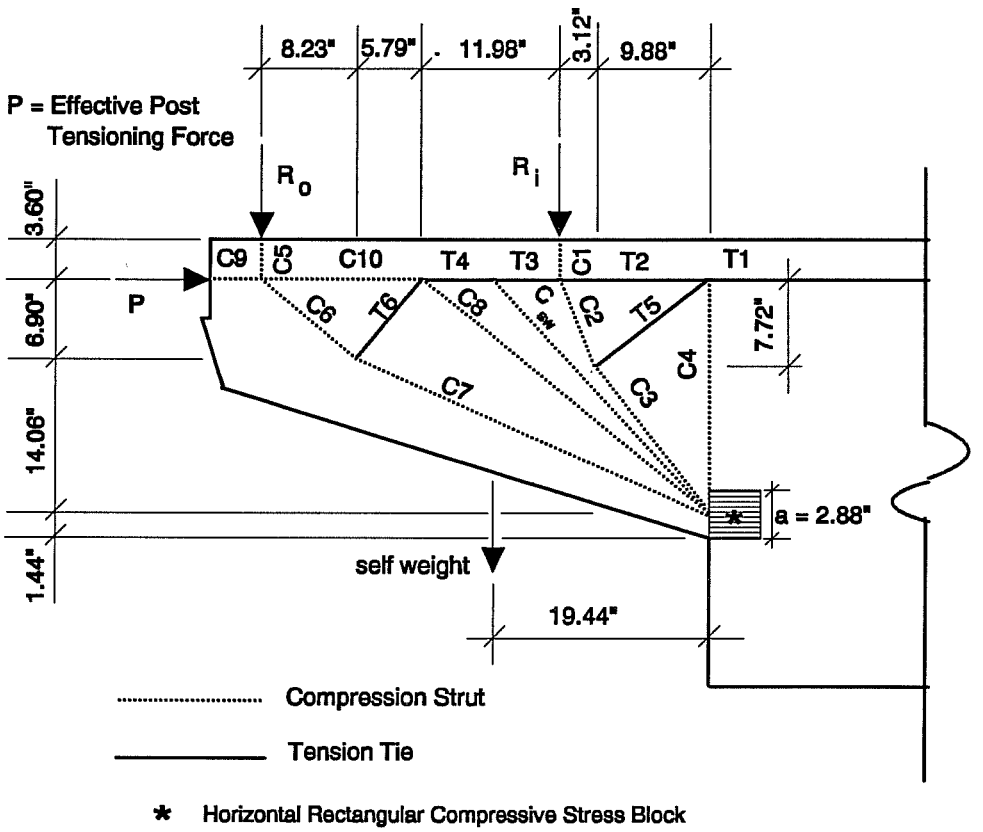

Figure 2.14 Strut-and-Tie Model for the CO-PU-100S-I Overhang

was further extended into the column. Six of the side face bars were used to partially fulfil the horizontal shear steel requirement.

2.3.6 CO-PU-74S-V (Specimen #4 - south overhang)

This overhang was designed as a structural concrete member using a combination of non-prestressed and prestressed reinforcement based on an ultimate strength design approach. Seventy-four percent of the primary moment reinforcement was provided by post tensioning strand and the remaining twenty-six percent was provided by mild reinforcement. The shear

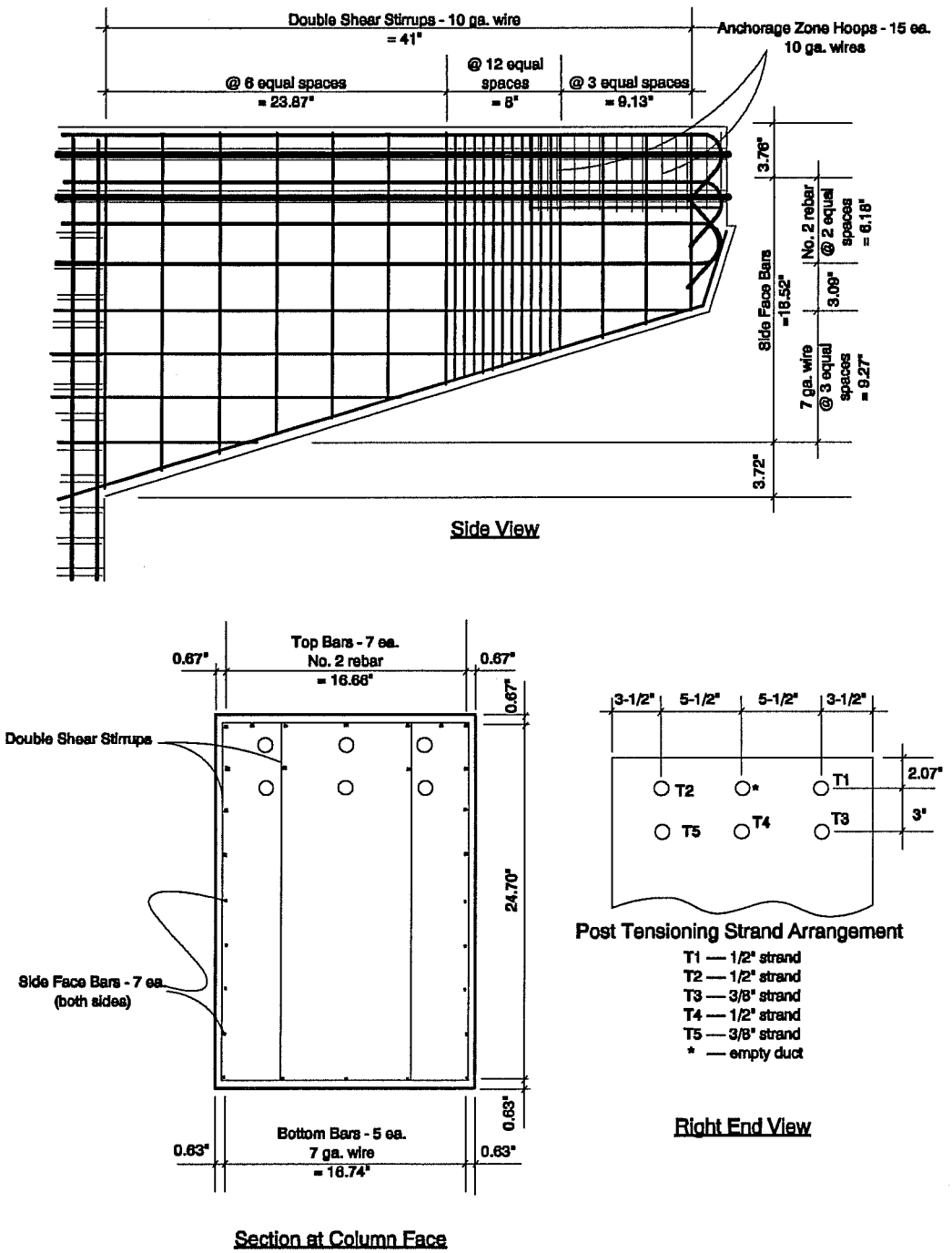

Figure 2.15 Reinforcing Details for the CO-PU-74S-V Overhang

reinforcement was identical to that used in CO-PU-100S-V. The reinforcing details for this overhang are shown in Figure 2.15.

Finite element analyses of the overhang under factored and service loads with the reduced effective post-tensioning force were performed. The magnitude and orientation of the principal stresses did not change appreciably from what was determined for Specimen # 3 with the higher post tensioning force, so the shear reinforcement was not changed.

The side face, top, and bottom bars were also similar to CO-PU-100S-V. The differences were that the top bars and the upper four side face bars were replaced with No. 2 bars of the primary moment reinforcement.

2.3.7 CO-PU-74S-I (Specimen #4 - north overhang)

The primary moment, side face, top, and bottom bars were identical to that used for CO-PU-74S-V. The shear reinforcement was the same as for CO-PU-100S-I, except that the horizontal shear steel requirement was not partially fulfilled by the side face bars. The reinforcing details for this overhang are shown in Figure 2.16.

2.3.8 Columns

The column portion of all specimens was identical. Vertical reinforcement and ties were placed in amounts that were direct scaled models of details typically observed in the full-scale piers constructed in San Antonio. Reinforcing details for the column are shown in Figure 2.17.

2.3.9 Anchorage Zone Stirrups

The anchorage zone hoops were designed according to the provisions of NCHRP Report No. 356 (4). The required number of hoops were determined for the post-tensioning force of Specimen #2 and the same number of hoops was used for all other models.

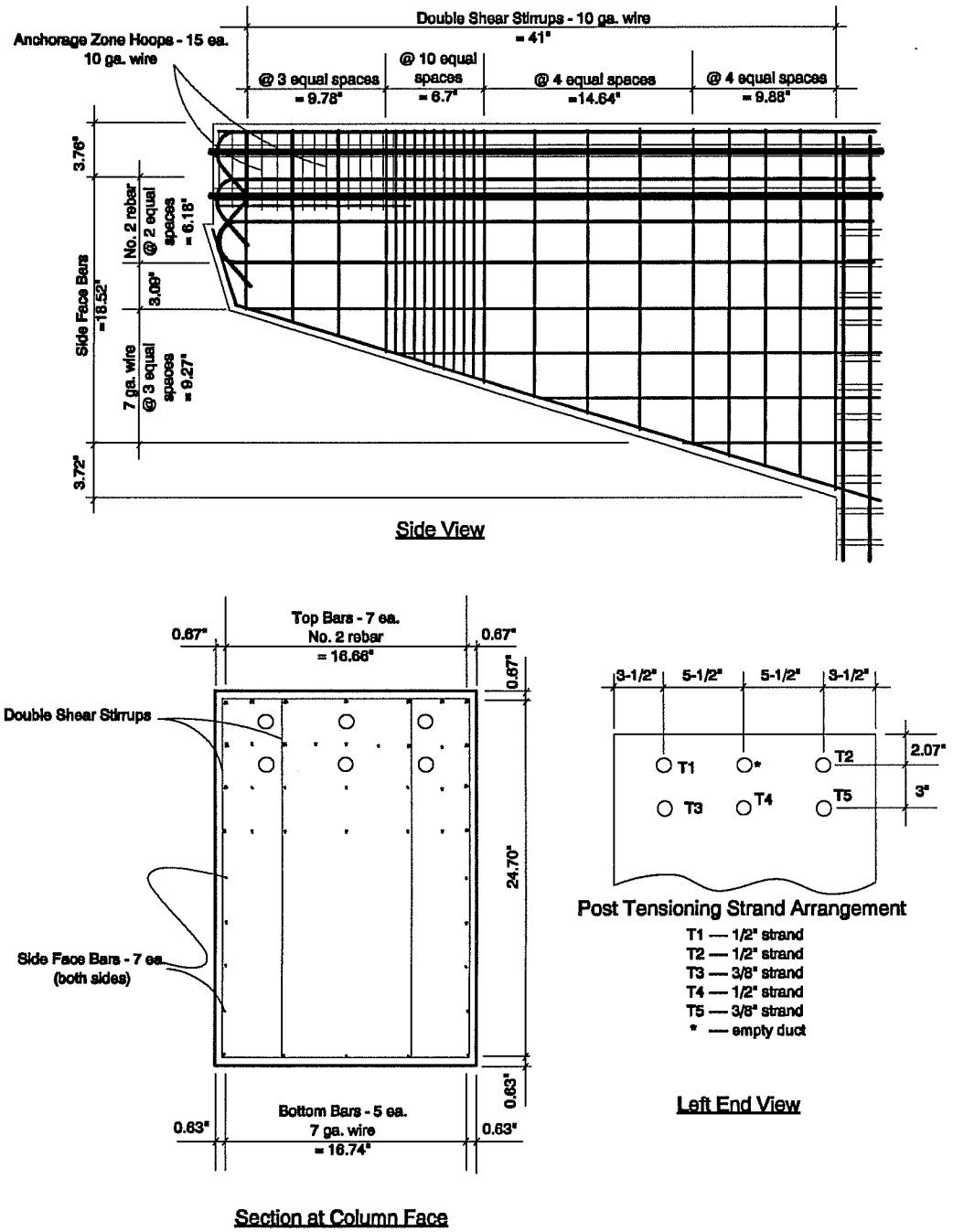

Figure 2.16 Reinforcing Details for the CO-PU-74S-I Overhang

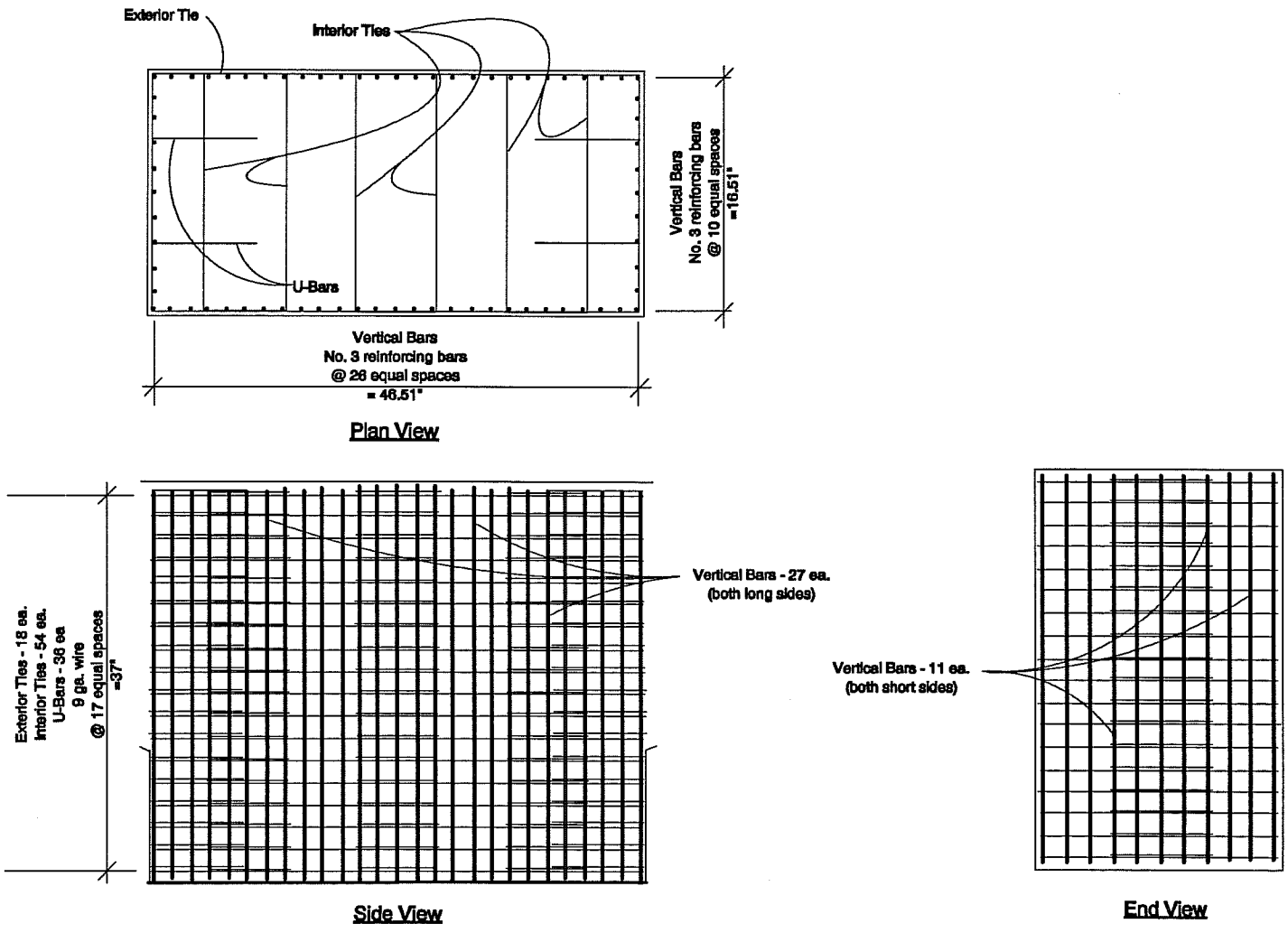

Figure 2.17 Reinforcing Details for Columns

2.4 Materials

2.4.1 Concrete

The mix design used for all four specimens is shown in Table 2.3. The proportions were selected to produce a mix that would reach a maximum strength of 5000 psi in 7 days. A set retarder was added to the concrete at the batch plant because the casts were made in the hot summer months and the travel time from the batch plant was approximately 45 minutes. A superplasticizer was added to the concrete both at the batch plant and at the laboratory after delivery. The first dose was used to improve the early strength gain of the concrete. The concrete slump was measured upon arrival at the laboratory and the second dose of superplasticizer was used to adjust the slump to the desired level of 9-10 inches. The high slump was required because of the highly congested reinforcing cages of the scale models.

Mix Constituent	Quantity
Cement	564 #
3/8" Aggregate	1463 #
Sand	1631 #
Water	200 #
Retarder	25 oz
Superplasticizer	45 oz

Table 2.3 Concrete Mix Proportions

Concrete compressive strengths from standard 6" x 12" cylinders broken at the time of testing are shown for each specimen in Table 2.4.

2.4.2 Mild Reinforcement

Tensile tests were conducted in the laboratory to determine the yield strengths of all mild reinforcement as shown in Table 2.5. A 60 kip load controlled test machine and Satec Systems Model T-6M Extensometer were used to load the steel specimens and monitor the strains. The

Specimen #	Overhang	Concrete Strength, f ' c	Age at Testing
1	CO-RU	5620 psi	23 days
2	CO-PS-100S	6270 psi	49 days
3	CO-PU-100S-I	7350 psi	40 days
	CO-PU-100S-V	"	"
4	CO-PU-74S-I	5440 psi	29 days
	CO-PU-74S-V	"	"

Table 2.4 Concrete Compressive Strengths

Mild Reinforcement	Diameter (inches)	Area (sq. in.)	yield strength, (ksi)	yield strain, (in/in)
No. 2 reinf. bar	0.247	0.048	75.1	0.00259
No. 3 reinf. bar	0.375	0.11	62.6	0.00216
10 ga. wire	0.131	0.0135	68.7	0.00237
9 ga. wire	0.1505	0.0178	36.5	0.00126
7 ga. wire	0.177	0.0246	82.2	0.00283

Table 2.5 Mild Reinforcement Properties

No. 2 bars and 7 gauge wires were tested to failure and stress-strain curves for these materials are shown in Figures 2.18 and 2.19. The 9 and 10 gauge wire were only tested to yielding.

The 7 and 10 gauge wires, and the No. 2 reinforcing bars were annealed through a process of heat treating to restore their ductility and reduce their yield strengths to values acceptable for use in place of grade 60 reinforcement. The 9 gauge wire was purchased as "soft

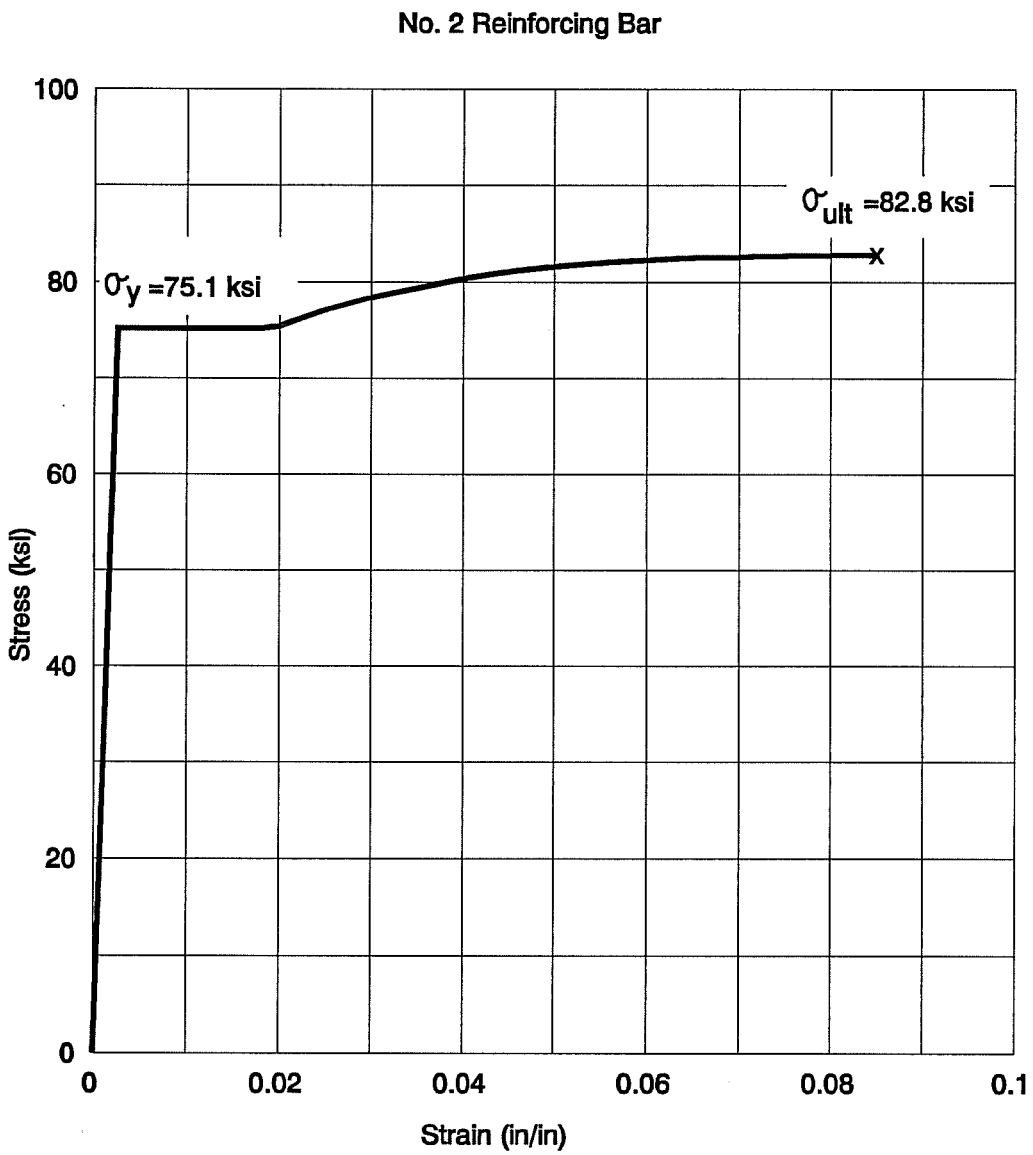

Figure 2.18 Stress-Strain Curve for No. 2 Reinforcing Bars

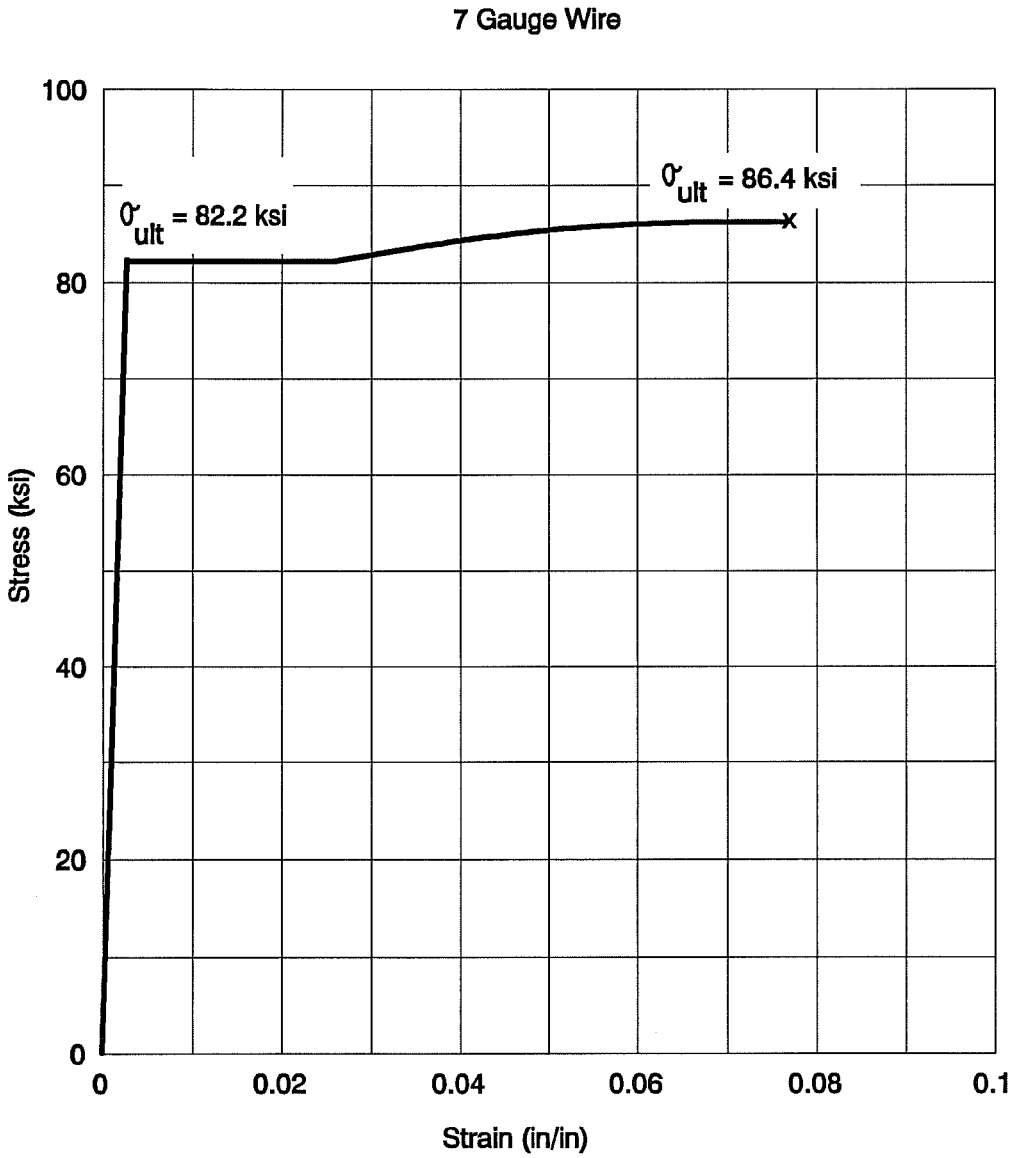

Figure 2.19 Stress-Strain Curve for 7 Gauge Wire

Black Annealed" which has very ductile properties so it did not have to receive any additional heat treatment.

2.4.3 Post-Tensioning Strand, Ducts, and Anchorage Hardware

Grade 270 Lo-Lax 7-wire strand was used for all tendons. Three-quarter inch diameter flexible steel electrical conduit was used as duct material for the tendons.

Anchorage plates were fabricated from 7/8 steel plate. Stressing wedges were anchored on the dead end with open chucks and on the stressing end with threaded chucks, which were fitted with nuts which were tightened after stressing to eliminate seating losses.

Stress-strain curves were developed for the strand using the same equipment described for the mild reinforcement tests. Aluminum collars with brass set screws were fabricated and placed on the strands at the points where the extensometer gripped the strand. The curves are shown in Figures 2.20 through 2.22. Strands were secured within the test machine using chucks and wedges. The strands consistently failed at the wedges so it is expected that the ultimate strength of the strands might be slightly higher than was achieved in the tests.

2.4.4 Post-Tensioning Grout

The mix design for the grout used on all tendons is shown in Table 2.6. The w/c ratio for the grout was 0.487. This ratio was taken from the Standard Specifications of the Texas Department of Transportation (5). Interplast N was used as an expansive admixture to help accomplish complete filling of the ducts. The Interplast N was added at a rate of 1% of the weight of the cement, as recommended by the manufacturer.

Compressive strength from standard 2" x 2" grout cubes broken at the time of testing is shown for each tendon in Table 2.7.

2.5 Fabrication

The scale factor of 5.5 required that strict tolerances be maintained in the fabrication of the specimens. Minor variations in the steel cages or forms could have resulted in a significant variation in the cover or changes in the structural performance.

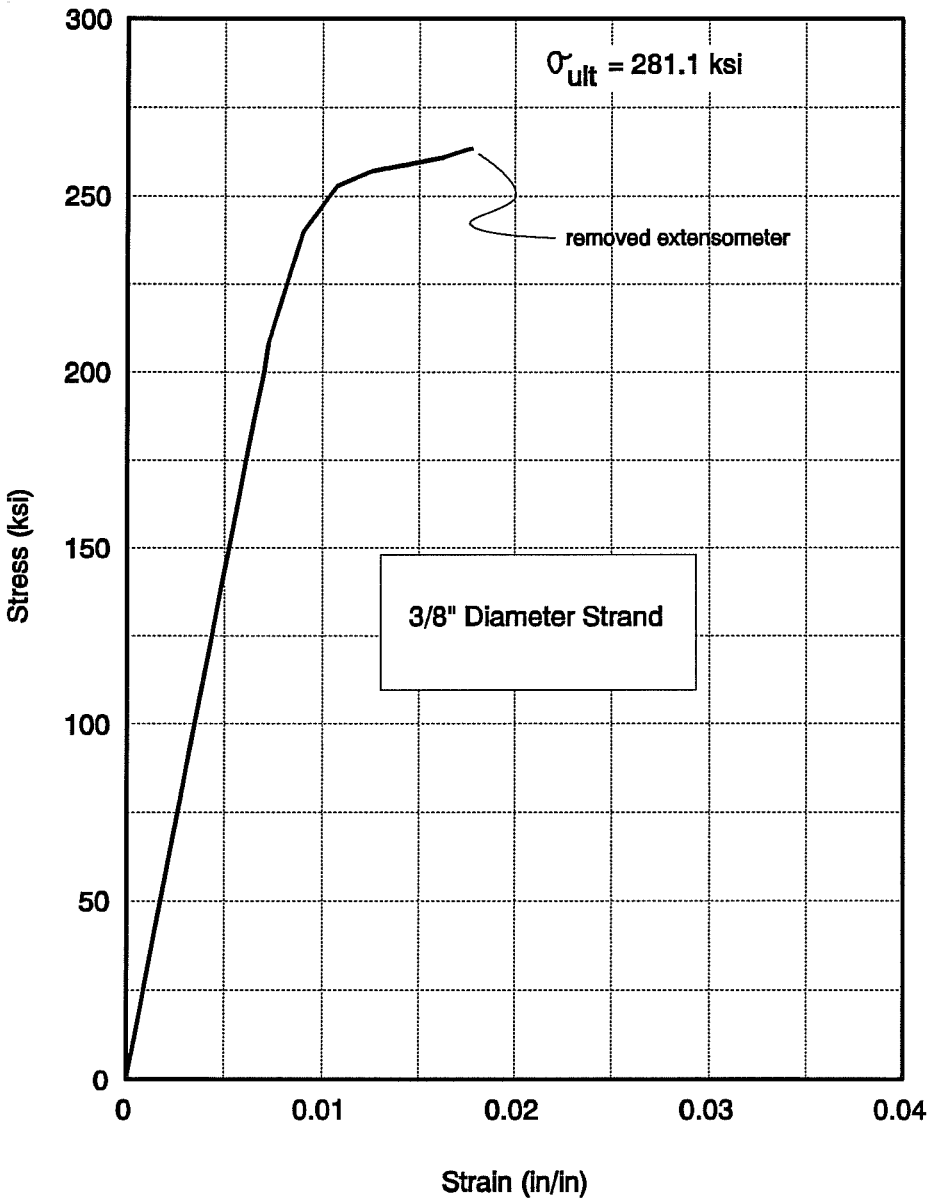

Figure 2.20 Stress-Strain Curve for 3/8" Diameter Strand

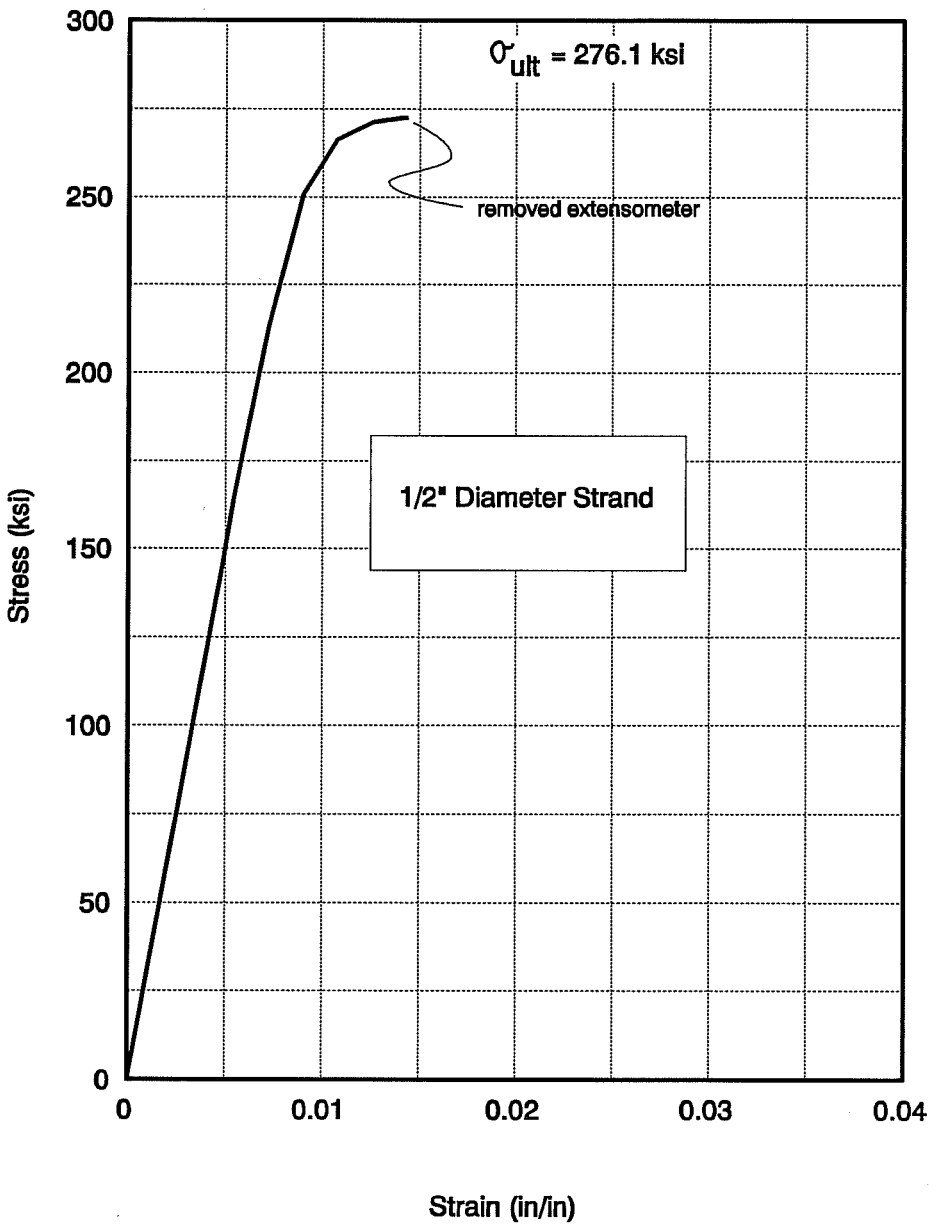

Figure 2.21 Stress-Strain Curve for 1/2" Diameter Strand

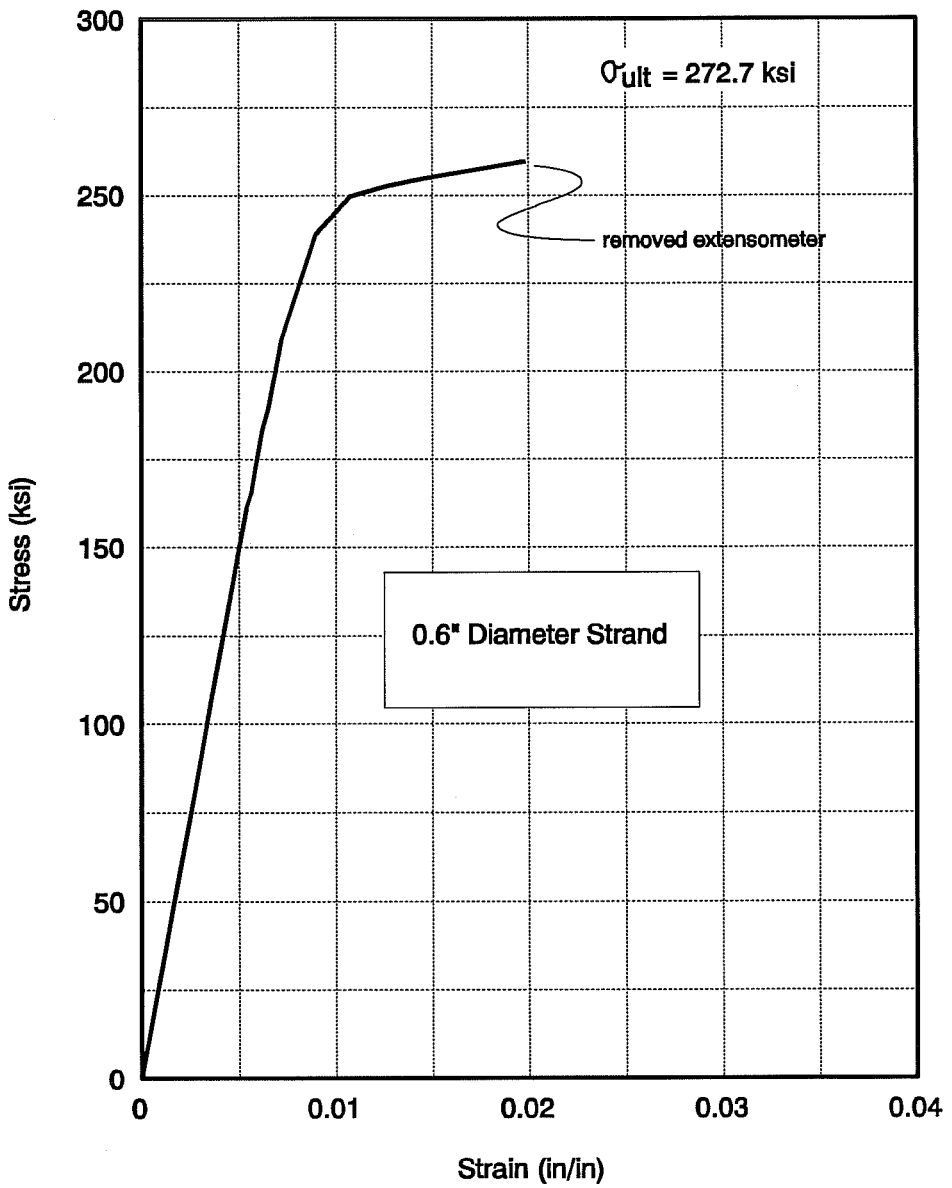

Figure 2.22 Stress-Strain Curve for 0.6" Diameter Strand

Ty 1 Cement	Water	Interplast N
30#	14.6#	0.3#

Table 2.6 Grout Mix Proportions

Specimen #	Overhang	Tendon Number	Grout Strength, f ' cu	Age at Testing
2	CO-PS-100S	1,2,3,4,5	1647	2 days
3	CO-PU-100S-I and V	1,4,5	2326	4 days
"	"	2,3,6	1669	3 days
4	CO-PU-74S-I and V	1,2,3,4,5	1913	3 days

Table 2.7 Grout Compressive Strengths

2.5.1 Formwork

All specimens were cast in the same set of timber forms. The forms were constructed in five separate sections and fastened together with bolts. This facilitated stripping the forms after the concrete had hardened. Foam rubber weather stripping was used at the contact joint between sections of the forms to prevent leaking during casting. The forms were arranged for casting the specimens in a horizontal position as shown in Figure 2.23.

Figure 2.23 Formwork

2.5.2 Reinforcing Cages

Each bar was individually bent in the laboratory to the required shape. The 10 gauge wire was received in coil form and had to be straightened by pulling the wire through a series of brass pulleys. Shear and anchorage zone stirrups were bent to shape by hand on a jig that was prepared using wood boards and nails placed at the required spacing. Reinforcing used for moment, shear-friction, and horizontal shear was hooked on the ends using a reinforcing steel bender.

Strain gages were placed on the reinforcement. Each gage was connected to the steel on a small smoothed area on the surface of the bar, then coated with waterproofing compounds.

Reinforcement cages were assembled in an upright position (see Figure 2.24) and laid on their side inside the formwork. The cages were tied together using steel and plastic ties. Circular

Figure 2.24 Assembly of Reinforcing Cage

sections of 1-1/2" pvc pipe were used as chairs which were attached to the cage before placing it in the forms.

Wooden insert forms were attached to the steel cages on both ends of the post tensioned specimens to create a vertical face to post tension against (see Figure 2.25). The forms also served the purpose of holding the post tensioning ducts in place during casting.

Holes were drilled into each post tensioning duct at both ends and 1/2" polyethylene tubing was attached at each hole to serve as grouting conduits.

2.5.3 Placement and Consolidation of Concrete

The concrete was delivered to the lab in ready-mix trucks and the slump was measured upon arrival. A superplasticizer was added to increase the slump to 9-10 inches. Concrete was

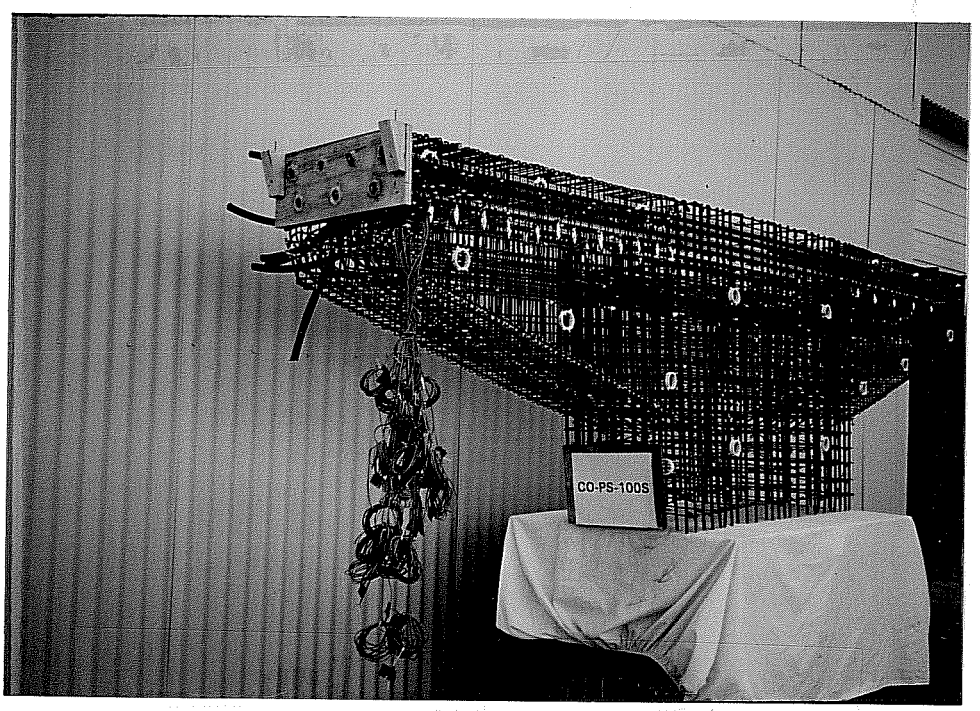

Figure 2.25 Wooden Insert Forms

placed in the forms with a crane operated hopper (see Figure 2.26). Internal vibrators and form vibrators were used to consolidate the concrete (see Figure 2.26). The concrete surface was finished with hand trowels.

2.5.4 Curing and Form Removal

Each specimen was cured in the forms with burlap and polyethylene sheeting covering the open face for four days. After four days, the forms were removed and the specimens were cured for an additional three days with the burlap and polyethylene.

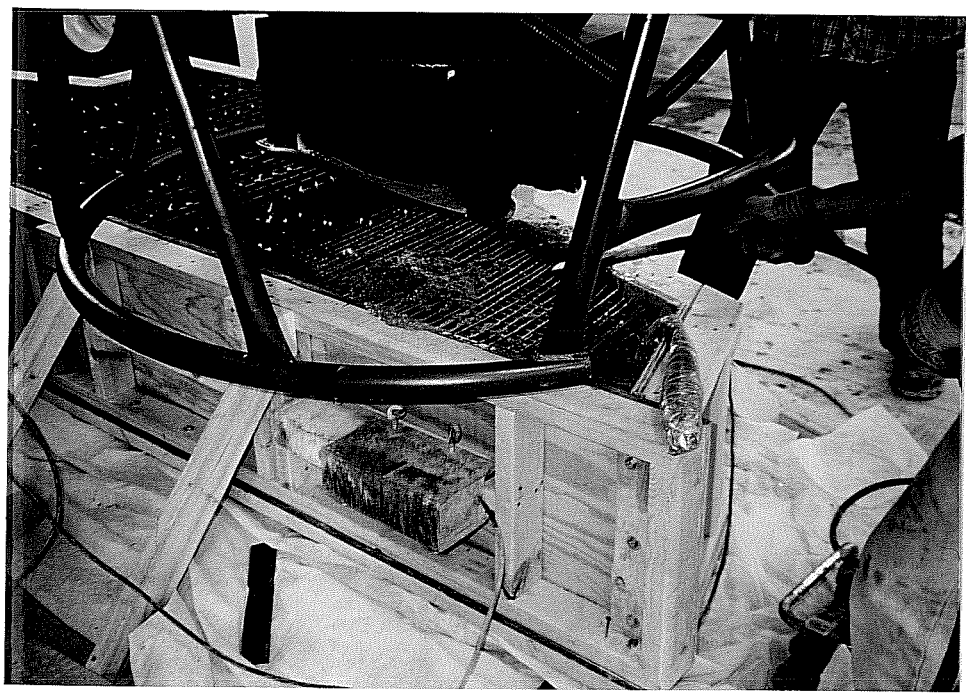

Figure 2.26 Placement and Consolidation of Concrete

2.5.5 Post-Tensioning Operation

All post-tensioning of specimens was done after the specimens were in place within the test setup. Strands were placed in the ducts and the anchorage hardware was secured. Each tendon was stressed to 160 ksi with a 60 kip hydraulic ram with pressure supplied by a hand pump. Figure 2.27 shows the setup of the stressing equipment. All tendons were grouted with a hand operated grout pump.

A stress level of 160 ksi was chosen to correspond with the stress level that would be expected in the strand after all long term losses. This stress is equal to 59% of F_{pu} for grade 270 strand. The specimens were tested from 2 to 4 days after the post-tensioning operation.

A diligent attempt was made to control the post-tensioning force and eliminate seating losses. This was accomplished by stressing all the tendons on each specimen to their final load

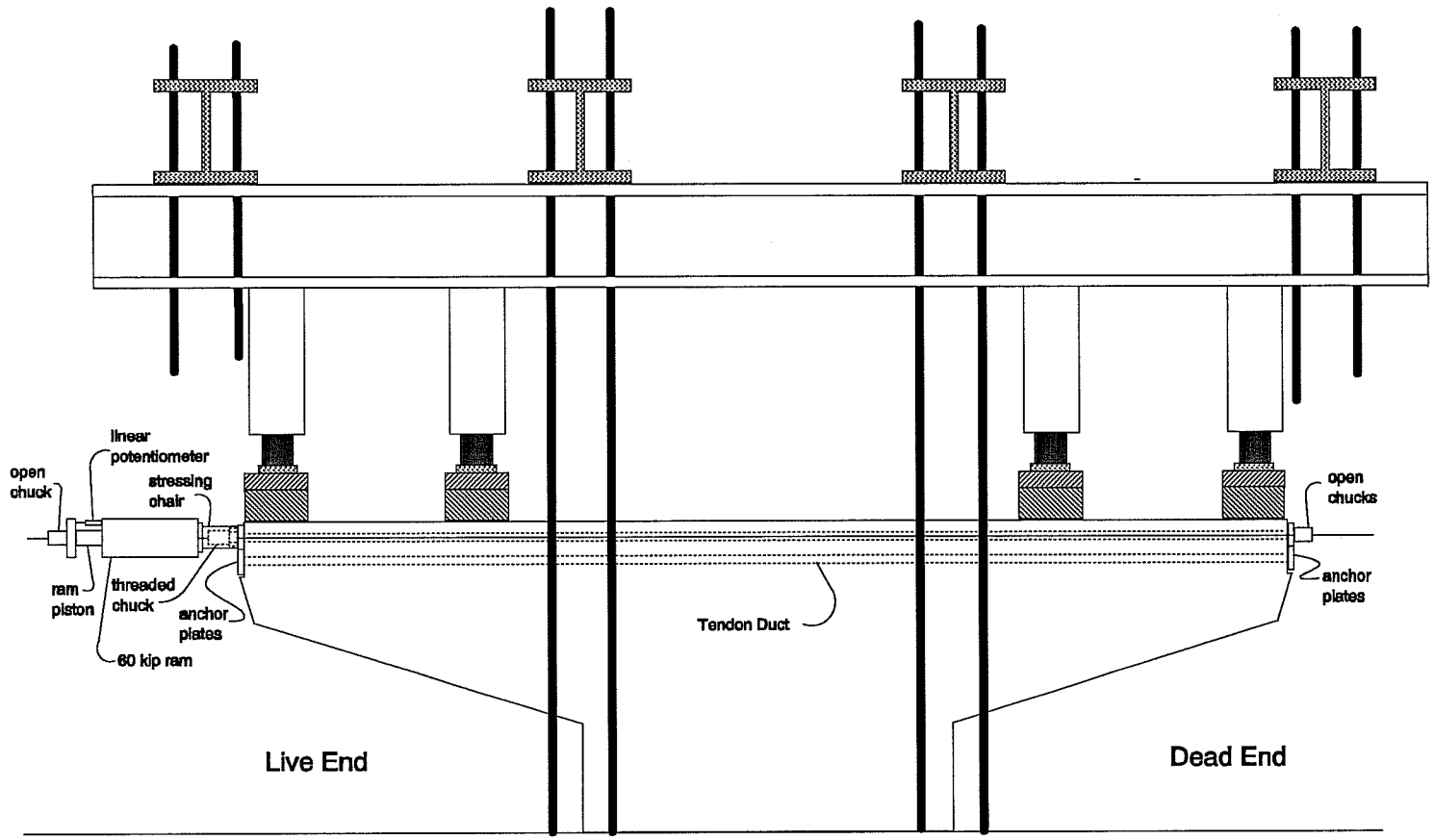

Figure 2.27 Post-Tensioning Equipment

in one pass and then making a second pass through each tendon to "bump-up" the load back to the required force. After the second pass through the tendons, a lift-off procedure was performed on each tendon. Threaded chucks with a nut secured onto them were extended after each stressing operation to eliminate the live end seating losses.

The lift-off procedure utilized a linear potentiometer to measure piston displacement, a pressure transducer to measure the load from the stressing ram, and a chart recorder. A plot was generated on the chart recorder, as shown in Figure 2.28, with the output from the pressure transducer on the vertical axis and the output from the linear potentiometer on the horizontal axis. The initial steep slope resulted from the elongation of only that portion of the tendon from the wedges at the outside of the ram piston to the wedges at the face of the specimen. When the stress in this portion of the tendon reached the stress in the tendon inside the specimen, the wedges at the specimen face "lifted-off" and any increase in load from the ram was applied to the entire strand length. Consequently, the axial stiffness of the strand was reduced and a much flatter slope resulted. The load at which the break in slope occurred was the load on the tendon inside the specimen. The lift-off procedure was repeated with adjustments to the nut on the threaded chuck until the required force was attained.

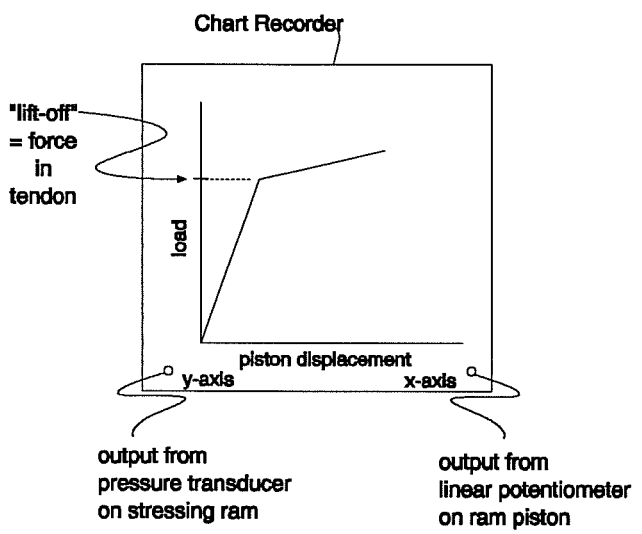

Figure 2.28 Lift-Off Plot

The stressing sequence was slightly different for each specimen as shown in Tables 2.8 through 2.10. A stressing sequence was determined for each specimen that would avoid stresses greater than $3\sqrt{f_c'}$ in the bottom fiber of the overhang. For Specimen #2 and #3 this required stressing a limited number of tendons, then applying loads through the loading rams that simulated the placement of the back span of the superstructure before stressing the remaining tendons. An attempt was also made in the selection of the sequence to avoid excessive bending of the specimen in the horizontal plane. For Specimen #2, this required stressing Tendon #5 to less than its final load initially until after Tendon #6 was stressed.

Step #	Operation
1	Apply Simulated Dead Load Blocks
2	Stress Tendon # 5 to 15 kips
3	Stress Tendon # 6 to 34.4 kips
4	Stress Tendon # 5 to 34.4 kips
5	Apply Simulated Back Span Dead Load
6	Stress Tendon # 2 to 13 kips
7	Stress Tendon # 3 to 13.6 kips
8	Stress Tendon # 1 to 34.4 kips

Table 2.8 Stressing Sequence for the CO-PS-100S Overhang

Step #	Operation
1	Apply Simulated Dead Load Blocks
2	Stress Tendon # 5 to 13.6 kips
3	Stress Tendon # 4 to 24.5 kips
4	Stress Tendon # 6 to 24.5 kips
5	Apply Simulated Back Span Dead Load
6	Stress Tendon # 2 to 24.5 kips
7	Stress Tendon # 1 to 24.5 kips
8	Stress Tendon # 3 to 24.5 kips

Table 2.9 Stressing Sequence for the CO-PU-100S-I and V Overhangs

Step #	Operation
1	Apply Simulated Dead Load Blocks
2	Stress Tendon # 4 to 24.5 kips
3	Stress Tendon # 3 to 13.6 kips
4	Stress Tendon # 5 to 13.6 kips
5	Stress Tendon # 1 to 24.5 kips
6	Stress Tendon # 2 to 24.5 kips

Table 2.10 Stressing Sequence for the CO-PU-74S-I and V Overhangs

The grout initially used on Tendons #2, #3, and #6 of Specimen #3 contained excessively high amounts of Interplast N and it was not clear that the grout would gain sufficient strength quickly enough to bond the tendons before testing. The decision was made to replace the grout in these tendons with new grout. The strands were de-tensioned and the old grout was flushed out with water. The strands were then re-stressed and new grout was placed in the ducts. This procedure was performed one tendon at a time.

2.6 Specimen Instrumentation and Data Measurement

2.6.1 Loading Rams

Ram loads were controlled by measuring the pressure on the calibrated hydraulic system. The load was considered to be equal to the product of the ram piston area and the hydraulic pressure.

The pressure on each set of loading rams was measured using hydraulic pressure transducers. Each pressure transducer had a 10,000 psi capacity and 10 mv/v output. The output voltage from the transducer was displayed on a voltmeter located next to each pump which allowed the pump operator to control the amount of pressure applied to the system. Each pump was additionally fitted with a hydraulic dial gage which was used to verify the pressure given by the transducers.

2.6.2 Post-Tensioning Ram

Hydraulic pressure supplied to the post-tensioning ram was measured by a pressure transducer with a 10,000 psi capacity and 3mv/v output. The output from the pressure transducer was also displayed on a voltmeter located next to the pump during the post tensioning operation.

2.6.3 Strains

Steel strains were measured with electronic resistance strain gages. Strain gages were placed on the primary moment, vertical shear stirrup, side face, shear-friction, and horizontal shear reinforcement. Strain gages on the No. 2 bars and 7 gauge wires were 5 mm wide and strain gages on the post tensioning strand and 10 gauge wire were 2 mm wide.
The locations of most of the strain gages are shown in Chapter 3, Section 3.3, on sketches accompanying the strain gage results.

2.6.4 Deflections

Deflections were measured using linear displacement potentiometers and mechanical dial gages. The range of the potentiometers was 2.0 inches with an accuracy of ± 0.001 inches. The range of the mechanical gages was 1 inch with an accuracy of ± 0.001 inches.
Potentiometers and mechanical dial gauges were located as shown in Figure 2.29.

2.6.5 Crack Widths

Crack widths were measured using an optical crack comparator. The accuracy of the crack comparator was ± 0.0005 inches.

2.7 Test Setup

Two different test setups were utilized in the course of the project.
Specimen #1 was tested in the setup shown in Figure 2.30. The frame consisted of structural steel elements bolted together. The frame was bolted to the floor of the testing laboratory. This setup required the use of a 2 foot high concrete pedestal to bring the specimen up to the level of the loading rams.

Specimens #2, #3, and #4 were all tested in the second setup. This setup, shown in Figure 2.31, used vertical tension rods connected to the laboratory floor and structural steel elements.

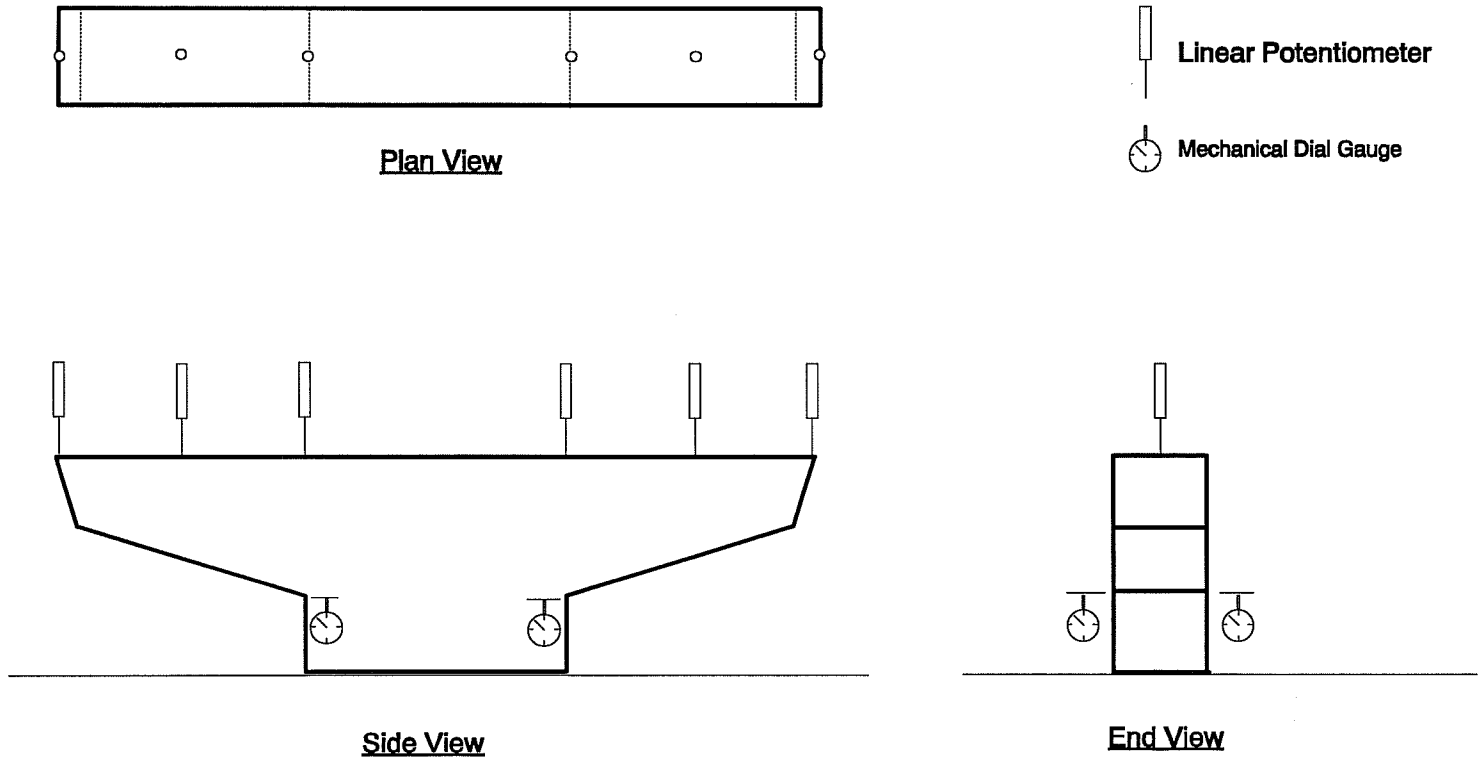

Figure 2.29 Deflection Gages

Both test set-ups utilized a longitudinal steel beam parallel to and centered on the long axis of the specimen onto which four 200 kip hydraulic loading rams were fastened. The two inside rams were connected in parallel to one pressure source and the two outside rams were connected in parallel to a separate pressure source. Thus, loads from the two inside rams were equal, loads from the two outside rams were equal, and the two pairs of rams could be operated independently. This resulted in symmetrical loads being applied to each overhang and it gave the ability to simulate different live load conditions. Hydraulic pressure was supplied to the rams by the use of hand pumps.

Loads were transferred from each ram to the specimen through the loading assembly shown in Figure 2.32. Fabric bearings were used between the 5"x7"x1" plate and the 8"x12"x2" plate for the testing of Specimen #1. These bearings were not used in the loading assemblies for Specimens #2, #3, and #4. However, after testing was completed it was determined that the bearings should have been used on all specimens to minimize lateral restraint.

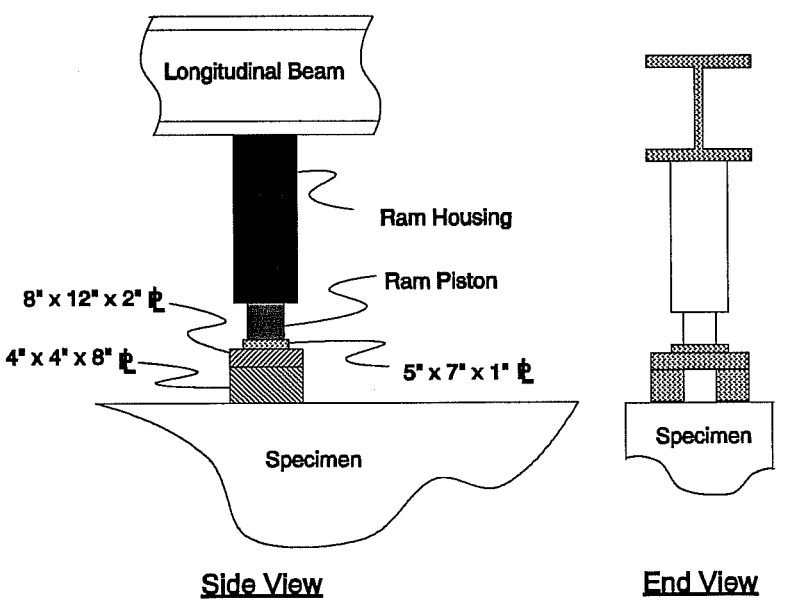

Figure 2.32 Loading Assembly

2.8 Testing Procedure

2.8.1 Preparation for Testing

Specimens were maneuvered into position in the test frame and seated in a 1/4" layer of quick setting grout (see Figure 2.33). Assembly of the test frame was completed. Instrumentation was set in place and connected to the data acquisition system.

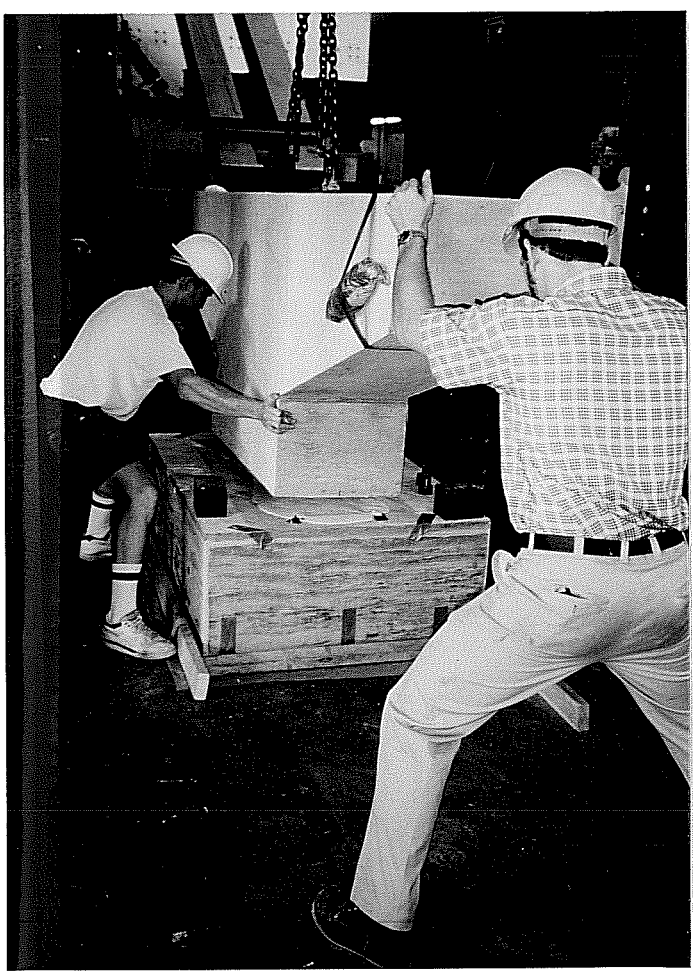

Figure 2.33 Positioning Specimen in Test Setup

Each specimen was marked with the 4" x 4" grid shown in Figure 2.34. The grid served as a reference for numbering and recording the location of each crack for which width measurements were taken. Line A was at the top of the specimen. An additional line A' was added to each specimen at the centroid of the primary moment reinforcement.

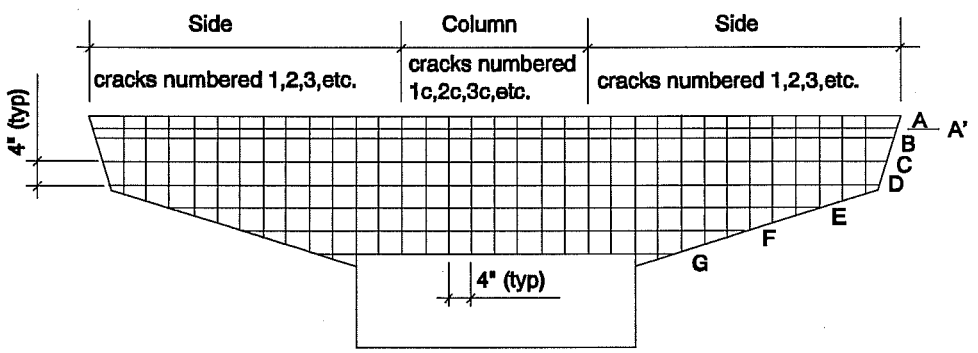

Figure 2.34 Crack Reference Grid

2.8.2 Loading of Specimens

The same loading sequence was applied to each specimen in the following stages:

Load Stage #	Description of Loading
1.	Simulated Dead Load Blocks
1a.	Post Tensioning of specimen (if applicable)
2.	Superstructure Dead Load
3.	Service Flexure Loads (3 outside lanes loaded)
4.	Superstructure Dead Load
5.	Service Shear Loads (4 lanes loaded)
6.	Superstructure Dead Load
7.	Service Flexure Loads
8.	Factored Flexure Loads
9.	Superstructure Dead Load
10.	Service Shear Loads
11.	Factored Shear Loads

12. Superstructure Dead Loads
13. Service Flexure Loads
14. Factored Flexure Loads
15. Ultimate Flexure Loads

Loads were increased between load stages by a number of smaller steps. The number of steps between load stages was determined by increasing the outside reaction in 4 kip increments. The inside reaction was increased or decreased linearly between corresponding stages by the same number of load steps.

When increasing from service flexure to factored flexure loads, the outside reaction increased 30.01 kips (from 56.97 kips to 87.98 kips). The number of 4 kip increments corresponding to this increase is 7.75. The inside reaction increased 5.97 kips (from 38.57 kips to 44.54 kips). Thus, the inside reaction increased 0.77 kips per step.

For loads approaching ultimate, the outside reaction was increased by 4 kips per step and the inside reaction was increased by 0.77 kips per step.

2.8.3 Data Collection

All electronic instrumentation was read at each load step. Data from pressure transducers, strain gages, and linear potentiometers was collected and stored using a data acquisition system. The system consisted of a Hewlett Packard 3497A scanner driven by an in-house computer program (HPDAS2) operating on an IBM XT personal computer.

Mechanical gages were read at each load stage.

Crack widths were measured at initiation and at every following load stage up to and including Load Stage #11. The cracks were numbered sequentially in the order of appearance within each of the six regions shown on Figure 2.34.

CHAPTER 3
TEST RESULTS

3.1 Introduction

The results of the testing of each overhang are presented in this chapter. Data was collected for the overhangs which provides the basis for evaluating both the service load and ultimate load behavior. In the testing of each overhang, deflections, loads, and steel strains were recorded at each load step from beginning of loading, through service loads, and beyond to ultimate loads.

Significant differences were observed in both the service load performance and ultimate capacity of each overhang. The service load performance of each overhang will be evaluated on the basis of cracking loads, crack patterns and widths, deflections, and reinforcement fatigue considerations. The ultimate behavior of each overhang was evaluated on the basis of the overhang capacity and ductility at maximum test loads and the modes of failure. Only one overhang on each specimen was loaded to failure since the manner in which hydraulic pressure was supplied to the loading rams prevented the application of higher loads once one of the adjacent overhangs failed.

In general, this chapter contains the basic test results for each overhang and a more detailed analysis of the results is given in Chapter 4.

3.2 Cracking Loads

The cracking loads for each overhang are summarized in Table 3.1. The loads given are for the inside and outside reactions that were applied when cracking of the overhang was first detected. The cracking moment includes the self weight of the overhangs.

The moment at the face of the column corresponding to superstructure plus overhang dead load is 2169 k-in. The moment corresponding to service flexure live loads plus impact is 580 k-in. The combination of these is the service flexure moment (DL + LL + I) which is 2749 k-in.

Specimen #	Overhang	Observed Cracking Loads		
		Inside Reaction, Ri (kips)	Outside Reaction, Ro (kips)	Moment, Mcr Test (kip-in)
1	CO-RU (north and south)	28.47	25.59	1394
2	CO-PS-100S (north)	41.11	69.53	3272
3	CO-PU-100S -I	40.02	65.15	3087
	CO-PU-100S-V	39.29	61.20	2923
4	CO-PU-74S--I	41.29	49.66	2499
	CO-PU-74S-V	41.29	49.66	2222

Table 3.1 Cracking Loads

The CO-RU overhangs cracked at the lowest loads, which were below the full superstructure dead load. The CO-PS-100S overhangs cracked at the highest loads, which were above the service flexure loads. This was expected because of the service load design approach taken. The CO-PU-100S-I and CO-PU-100S-V overhangs cracked at lower loads than the CO-PS-100S overhang, however, the loads were still above the service flexure moment. The CO-PU-74S-I and CO-PU-74S-V overhangs cracked at lower loads than the CO-PU-100S overhangs but at higher loads than the CO-RU overhang. These overhangs cracked at loads above the full superstructure dead load but below the service flexure moment. As expected, the cracking loads for each overhang increased with increasing levels of post-tensioning.

The presence of cracking at service loads was shown to have a significant influence on the service load deflections (see Section 3.6). Cracking under service loads also has a significant effect on the fatigue life of the reinforcement. This is discussed in greater detail in Section 4.3.

3.3 Crack Patterns

The crack pattern for each overhang was indicative of typical flexural behavior. Cracks initiated perpendicular to the top fiber near the region of maximum moment at the face of the column. The first cracks propagated nearly vertically toward the compression zone at the juncture

of the bottom of the overhang and the column. Subsequent cracks occurring outside the maximum moment region initiated perpendicular to the top fiber, but developed inclination toward the compression zone as they propagated, in the fashion of typical inclined-shear cracks.

As previously mentioned, only the CO-RU, CO-PU-74S-I, and CO-PU-74S-V overhangs were cracked at service loads. The crack patterns of the CO-PU-74S-I and CO-PU-74S-V overhangs were essentially the same. Typical crack patterns for the CO-RU and CO-PU-74S-V overhangs at service flexure loads are shown in Figures 3.1 and 3.2. A much larger number of cracks were present on the CO-RU overhang than on the CO-PU-74S overhangs. The cracks on the CO-RU specimen also extended much further out along the overhang.

Service shear loads were applied to each overhang after unloading to dead load. The cracking pattern did not change significantly from the pattern at service flexure loads, except that on the CO-RU and CO-PU-74S-I overhangs, one new flexural crack appeared. In each case, the new crack was located between the bearing for the inside reaction and the face of the column.

As loading progressed beyond service loads to maximum test loads, the crack patterns on each overhang remained indicative of typical flexural behavior. See Figures 3.3 through 3.6 which show each overhang after the maximum test loads had been applied. While the number of cracks on all overhangs increased, the number on the CO-RU overhang was far greater than on any of the prestressed overhangs. At high loads approaching ultimate, significant inclined cracking occurred on the CO-RU overhang parallel to the compression strut from the outside reaction. The location of these cracks coincided with the location of the anticipated shear crack shown in Figure 2.6. The CO-PU-74S overhangs had the next highest number of cracks which is not surprising because this overhang had the lowest amount of prestressing of all the prestressed overhangs. Some inclined cracking was observed but not to the same extent as observed on the CO-RU overhang. The CO-PS-100S and CO-PU-100S overhangs had the smallest number of cracks, with each of these overhangs having essentially the same number of cracks. Even at ultimate loads, no inclined cracks in the vicinity of the compression strut from the outside reaction were observed on either of these overhangs.

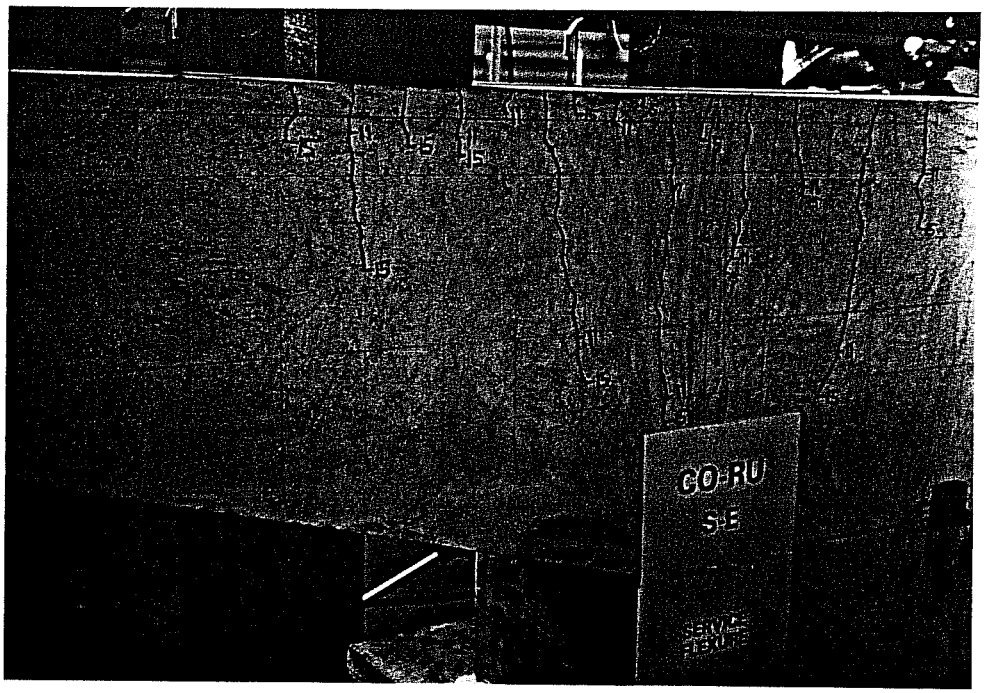

Figure 3.1 Cracks on Typical CO-RU Overhang at Service Flexure Loads

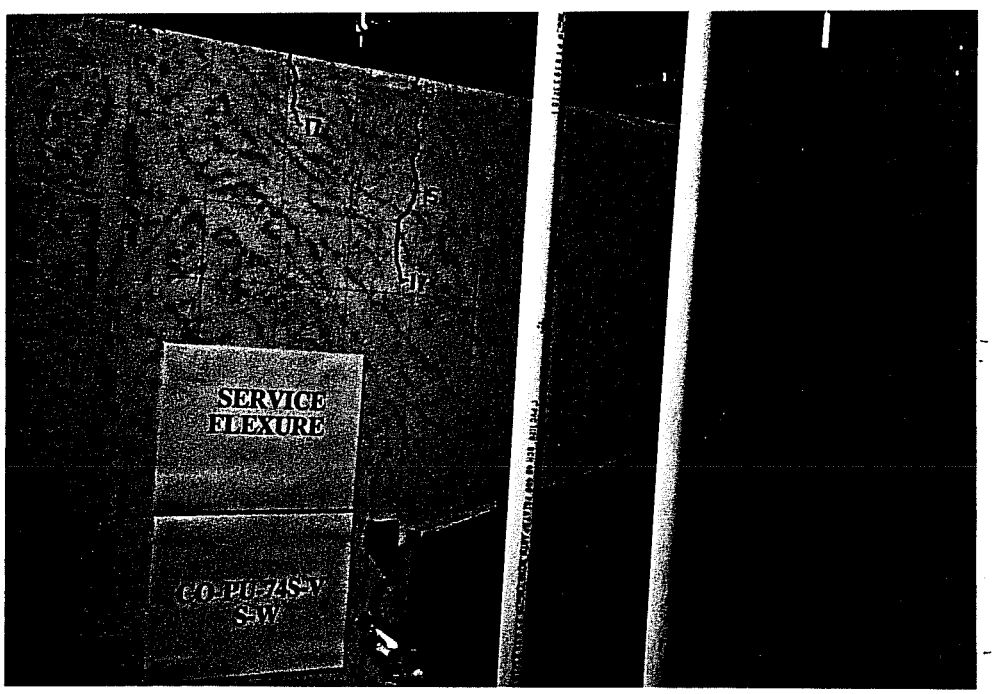

Figure 3.2 Cracks on Typical CO-PU-74S Overhang at Service Flexure Loads

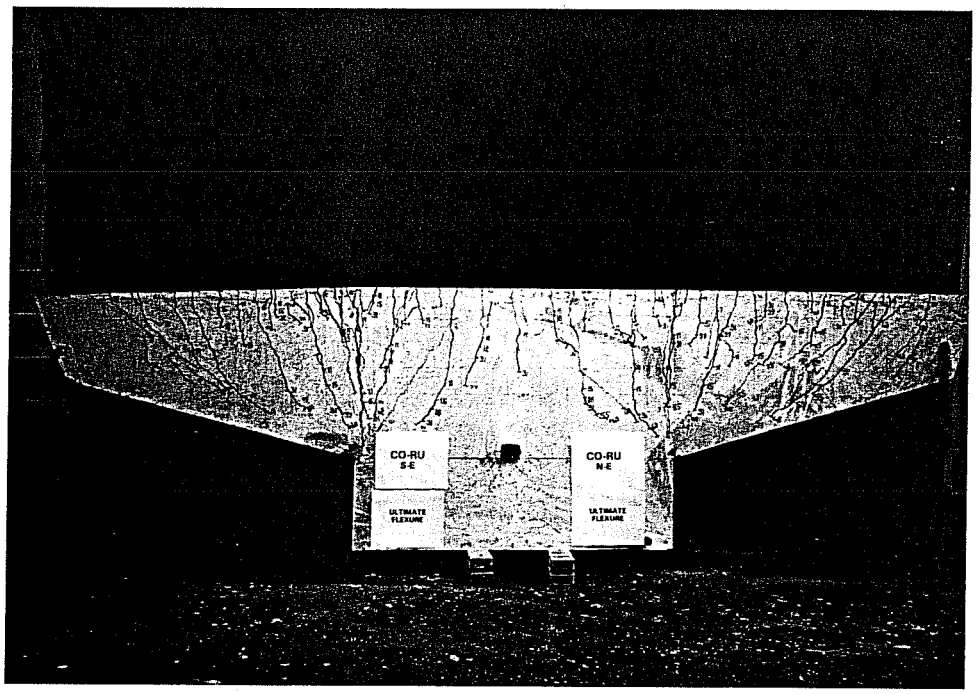

Figure 3.3 CO-RU Overhangs After Testing

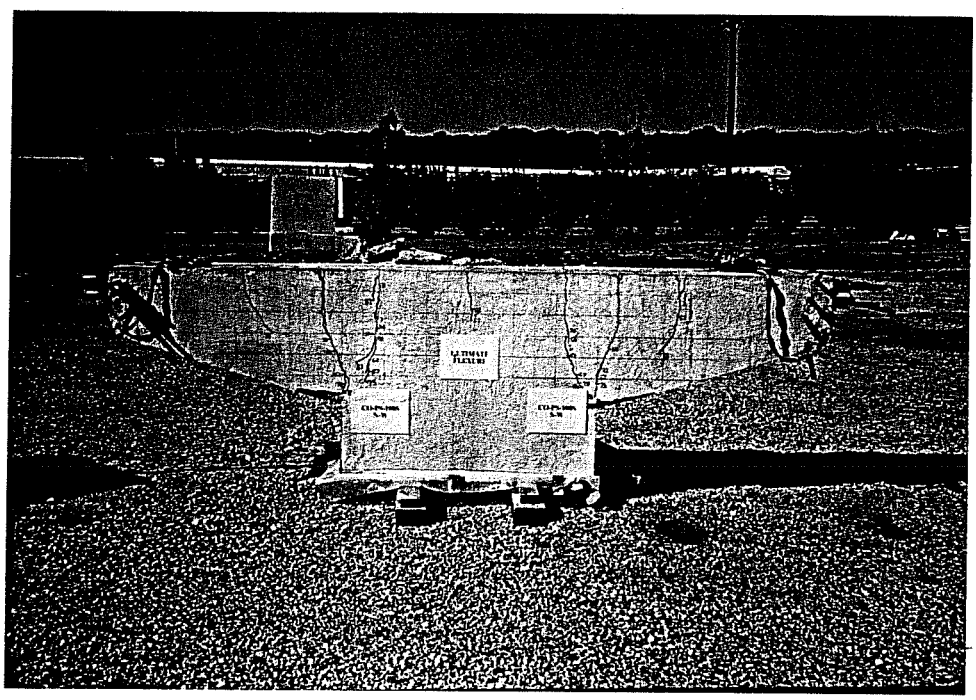

Figure 3.4 CO-PS-100S Overhangs After Testing

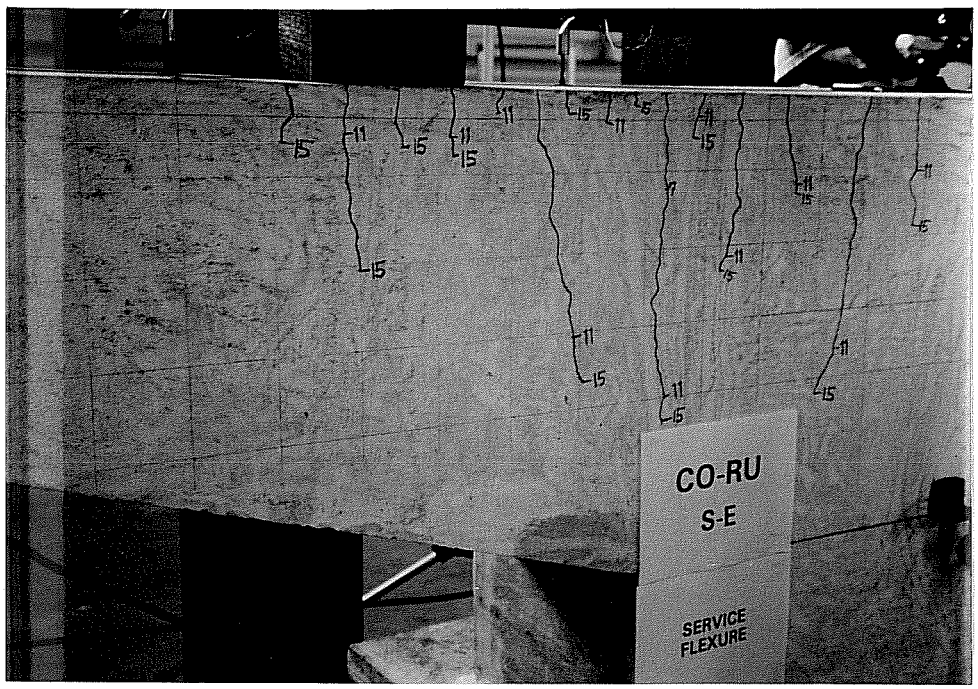

Figure 3.1 Cracks on Typical CO-RU Overhang at Service Flexure Loads

Figure 3.2 Cracks on Typical CO-PU-74S Overhang at Service Flexure Loads

Figure 3.3 CO-RU Overhangs After Testing

Figure 3.4 CO-PS-100S Overhangs After Testing

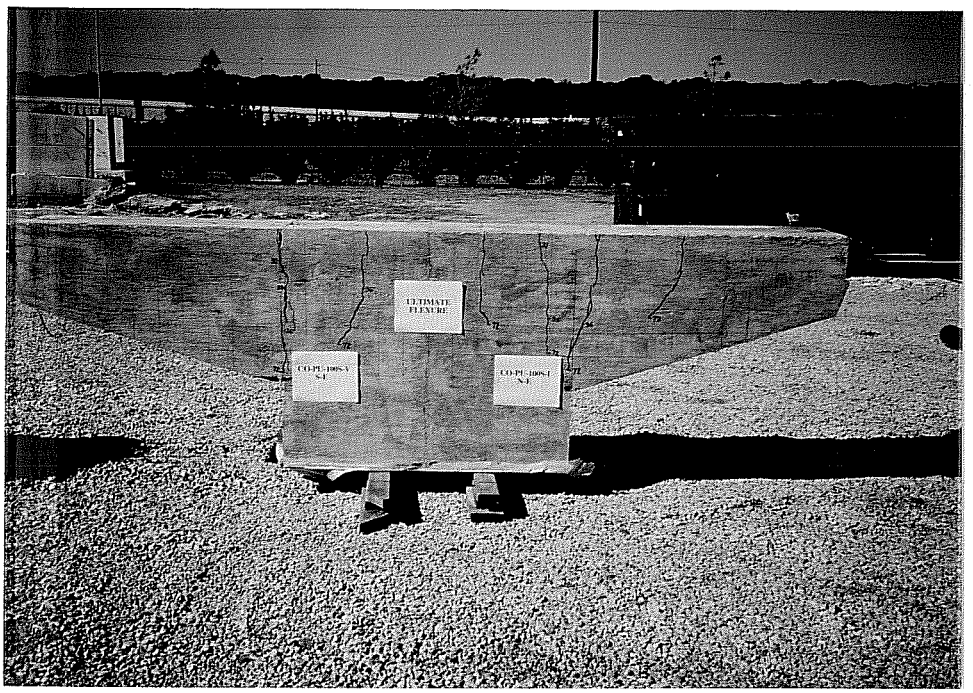

Figure 3.5 CO-PU-100S-I and CO-PU-100S-V Overhangs After Testing

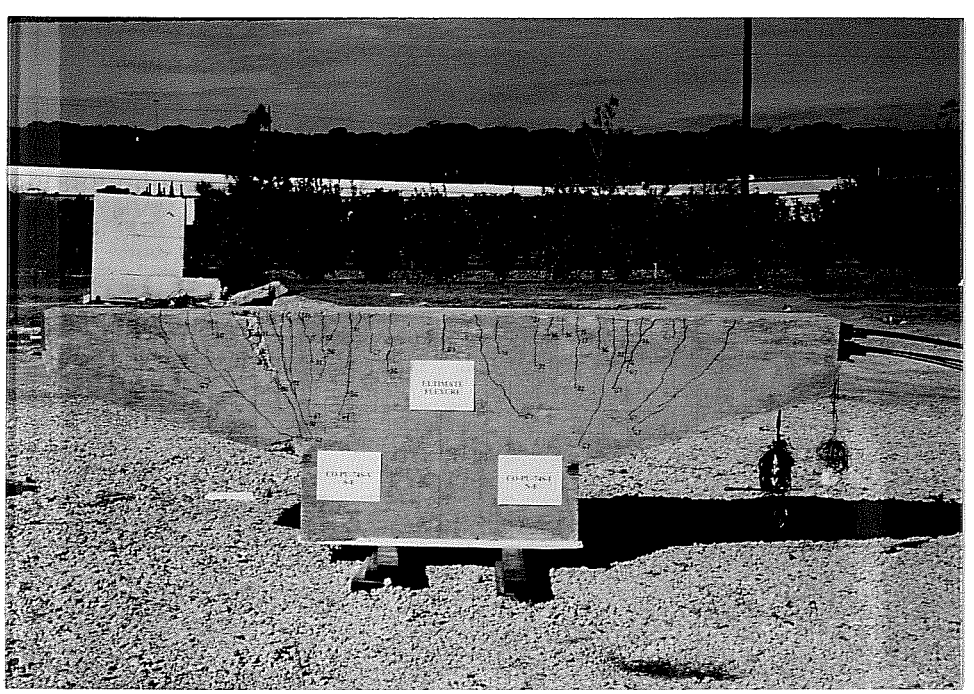

Figure 3.6 CO-PU-74S-I and CO-PU-74S-V Overhangs After Testing

3.4 Crack Width Measurements

This section summarizes the crack locations and numbers, and the crack width readings taken for each overhang. A detailed analysis of the data and a presentation of the relative crack width performance of each overhang is presented in Section 4.3.

Tables 3.2 through 3.9 list all of the cracks for which readings were taken on each of the 16 overhang faces. Accompanying each table is a drawing (Figures 3.7 through 3.14) showing the location and number of each crack. The data for each overhang face includes cracks on the side of the overhang plus half of the side of the column adjacent to the overhang.

Crack widths were measured at every level, A through G, and at least at every load stage up to and including Load Stage # 11 (Factored Shear Loads). The crack width data was reduced so that the tables include only the maximum widths that occurred on each crack, at each load stage. The maximum width occurred most often at the top of the overhang , level A. If the maximum width was measured at a level other than the top of the overhang, the level at which it occurred is indicated with a capitol letter following the width.

The crack width data was further reduced to determine the "major" cracks on each overhang. A crack was considered a "major" crack if its maximum width was greater than the maximum width of all other cracks on the overhang at the same load stage. The "major" cracks are indicated by the shaded columns in Tables 3.2 through 3.9.

Note that Table 3.2 indicates a maximum crack width of 0.004" at service shear loads (Load Stage # 4) for crack number 5 on the north west side of the CO-RU overhang. The widths of all other cracks were found to increase with increasing moment, when later load stages were considered, and yet at service flexure loads (Load Stage # 6), the width of this crack was measured to be 0.003". This width is more consistent with the maximum width of other "major" cracks on the overhang at the same load stage. Because of this, it is believed that the 0.004" reading was erroneous. Therefore, it was judged that this reading should be omitted from any further consideration.

CO - RU	North East Side			Maximum Crack Width (inches)												
Load Stage	Ri (kips)	Ro (kips)	Moment at Face of Column (kip-inches)	Crack Number 1	2	3	4	5	6	7	8	9	10	4c	5c	6c
cracking loads	28.47	25.59	1394	0.0005	0.0005	0.0005										
(1) Dead Load	43.47	40.47	2169	0.001 A'	0.001	0.0005	0.001	0.0005	0.0005	0.0005	0.0005	0.0005		0.001	0.001	
Dead Load plus	41.15	48.46	2451	0.0025 C	0.002		0.002									
(2) Service Flexure	38.57	56.97	2749	0.0025 B	0.0025	0.002	0.0025	0.002	0.002	0.003	0.0005	0.0015	0.002 A'	0.003 C	0.002	0.001 A'
(4) Service Shear	49.97	46.97	2507	0.002 C	0.003 B	0.0015 B	0.0015 B	0.001	0.0015	0.002 B	0.0005	0.001	0.001 A'	0.002 C	0.002	0.001 A'
(5) Dead Load *	43.47	40.47	2169	0.0005	0.002		0.002			0.0005				0.001	0.001	
(6) Service Flexure *	38.57	56.97	2749	0.001	0.002		0.0025			0.003				0.002	0.002	
Service Flexure plus *	41.51	72.95	3410	0.003	0.0035		0.004		0.002	0.004				0.004	0.0035	
(7) Factored Flexure	46.18	88.52	4078	0.004 B	0.006 B		0.005		0.004	0.006 B				0.0035	0.003	
(8) Dead Load *	43.47	40.47	2169	0.002	0.0025		0.003		0.0015	0.0025				0.003	0.001	
(9) Service Shear *	49.97	46.97	2507	0.002	0.003		0.004		0.003	0.003				0.002	0.0025	0.004
Service Shear plus *	58.00	55.13	2930	0.003	0.003		0.004		0.004	0.003				0.003	0.003	0.004
(10) Factored Shear	70.92	66.82	3554	0.006 B	0.0045 B		0.0045 B		0.0045	0.0055 B				0.003	0.004	0.005

CO - RU	North West Side			Maximum Crack Width (inches)												
Load Stage	Ri (kips)	Ro (kips)	Moment at Face of Column (kip-inches)	Crack Number 1	2	3	4	5	6	7	8	9	10	1c	2c	5c
cracking loads	28.47	25.59	1394													
(1) Dead Load	43.47	40.47	2169	0.002	0.002	0.002	0.0005	0.002	0.0005					0.005	0.0005	
Dead Load plus	41.15	48.46	2451	0.003		0.002		0.003								
(2) Service Flexure	38.57	56.97	2749	0.003	0.001	0.003	0.001	0.003	0.001	0.001	0.002	0.001		0.001	0.001	0.0005
(4) Service Shear	49.97	46.97	2507	0.003	0.002	0.002	0.0015	0.004 **	0.0015	0.0015	0.002 A'	0.001	0.0015	0.0005	0.001	0.0005
(5) Dead Load *	43.47	40.47	2169	0.003		0.002		0.003								
(6) Service Flexure *	38.57	56.97	2749	0.003		0.002		0.003								
Service Flexure plus *	41.51	72.95	3410	0.004		0.003		0.004						0.0015	0.002	
(7) Factored Flexure	46.18	88.52	4078	0.005		0.005		0.005						0.002	0.0025	
(8) Dead Load *	43.47	40.47	2169	0.004		0.002		0.003						0.001	0.001	
(9) Service Shear *	49.97	46.97	2507	0.0035		0.002		0.0045						0.001	0.0015	
Service Shear plus *	58.00	55.13	2930	0.003		0.0025		0.0045						0.001	0.003	
(10) Factored Shear	70.92	66.82	3554	0.0045		0.003		0.005						0.003	0.002	

* Crack Widths measured only at level A.

** omitted

Table 3.2 Maximum Crack Width Readings on the north CO-RU Overhang

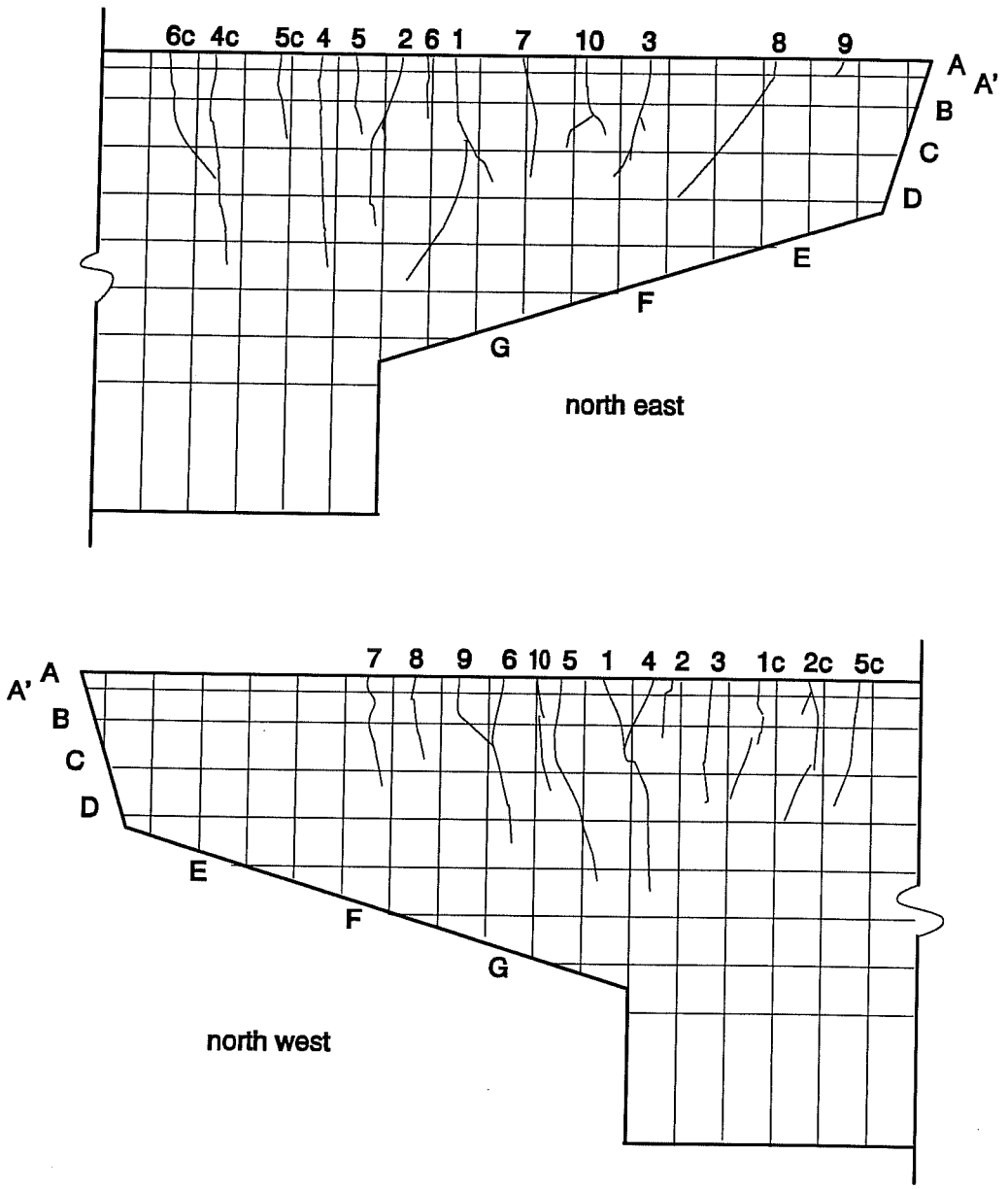

Figure 3.7 Crack Numbers and Locations on the north CO-RU Overhang

CO - RU	South East Side			Maximum Crack Width (inches)																
Load Stage	Ri (kips)	Ro (kips)	Moment at Face of Column (kip-inches)	Crack Number 1	2	3	4	5	6	7	8	9	10	11	12	13	1o	2o	3o	7o
cracking loads	28.47	25.59	1394	0.001																
(1) Dead Load	43.47	40.47	2169	0.002 C	0.0005	0.0005	5E-04	0.0005	0.001	0.0005	0.002						0.002	0.001	0.002	
Dead Load plus	41.15	48.46	2451	0.002 C				0.001			0.0015									
(2) Service Flexure	38.57	56.97	2749	0.002 C	0.001	0.002	5E-04	0.002 B	0.001	0.001	0.002	0.001	0.001	0.001	0.0005		0.002	0.003 C	0.002	0.002
(4) Service Shear	49.97	46.97	2507	0.0025 C	0.001	0.002	5E-04	0.002 B	0.001	0.001	0.0015	0.001	0.001	0.0005	0.0005	0.001 A'	0.002	0.003	0.001	0.0015
(5) Dead Load *	43.47	40.47	2169	0.001				0.0005			0.001						0.002	0.002		
(6) Service Flexure *	38.57	56.97	2749	0.002				0.0015			0.002						0.0025	0.003		
Service Flexure plus *	41.51	72.95	3410	0.003				0.002			0.004						0.0045	0.0036		
(7) Factored Flexure	46.18	88.52	4078	0.005 C				0.005 C			0.004						0.006	0.006		
(8) Dead Load *	43.47	40.47	2169	0.002				0.001			0.002						0.004	0.0045		
(9) Service Shear *	49.97	46.97	2507	0.0015				0.001			0.0025						0.005	0.004		
Service Shear plus *	58.00	55.13	2930	0.002	0.002	0.002		0.002			0.003						0.005	0.005		
(10) Factored Shear	70.92	66.82	3554	0.0055 C	0.0035	0.003		0.005 C			0.0055 C						0.006	0.006		

CO - RU	South West Side			Maximum Crack Width (inches)										
Load Stage	Ri (kips)	Ro (kips)	Moment at Face of Column (kip-inches)	Crack Number 1	2	3	4	5	6	7	3o	4o	6o	7o
cracking loads	28.47	25.59	1394											
(1) Dead Load	43.47	40.47	2169	0.0015 A	0.0005	0.0015 C	5E-04	0.0005	5E-04		0.0005	0.0005		
Dead Load plus	41.15	48.46	2451	0.001		0.0015 C		0.001 B						
(2) Service Flexure	38.57	56.97	2749	0.002	0.001	0.002 B	0.001	0.001 A'	0.002	0.001	0.001	0.0005	5E-04	0.0005
(4) Service Shear	49.97	46.97	2507	0.002	0.001 A'	0.0015 C	0.001	0.001	0.001	0.001 B	0.0005	0.0005	5E-04	0.0005
(5) Dead Load *	43.47	40.47	2169	0.002		0.001		0.0005						
(6) Service Flexure *	38.57	56.97	2749	0.002		0.0015		0.001						
Service Flexure plus *	41.51	72.95	3410	0.001		0.003		0.004			0.0015			0.003
(7) Factored Flexure	46.18	88.52	4078	0.004 A'		0.004 B		0.004 B			0.003			0.003
(8) Dead Load *	43.47	40.47	2169	0.001		0.001		0.0005			0.001			0.0015
(9) Service Shear *	49.97	46.97	2507	0.002		0.0015		0.001			0.001			0.002
Service Shear plus *	58.00	55.13	2930	0.003		0.002		0.001	0.003		0.001			0.002
(10) Factored Shear	70.92	66.82	3554	0.0045 A'		0.0045 C		0.0045 C	0.003		0.0025			0.003

* Crack Widths measured only at level A.

Table 3.3 Maximum Crack Width Readings on the south CO-RU Overhang

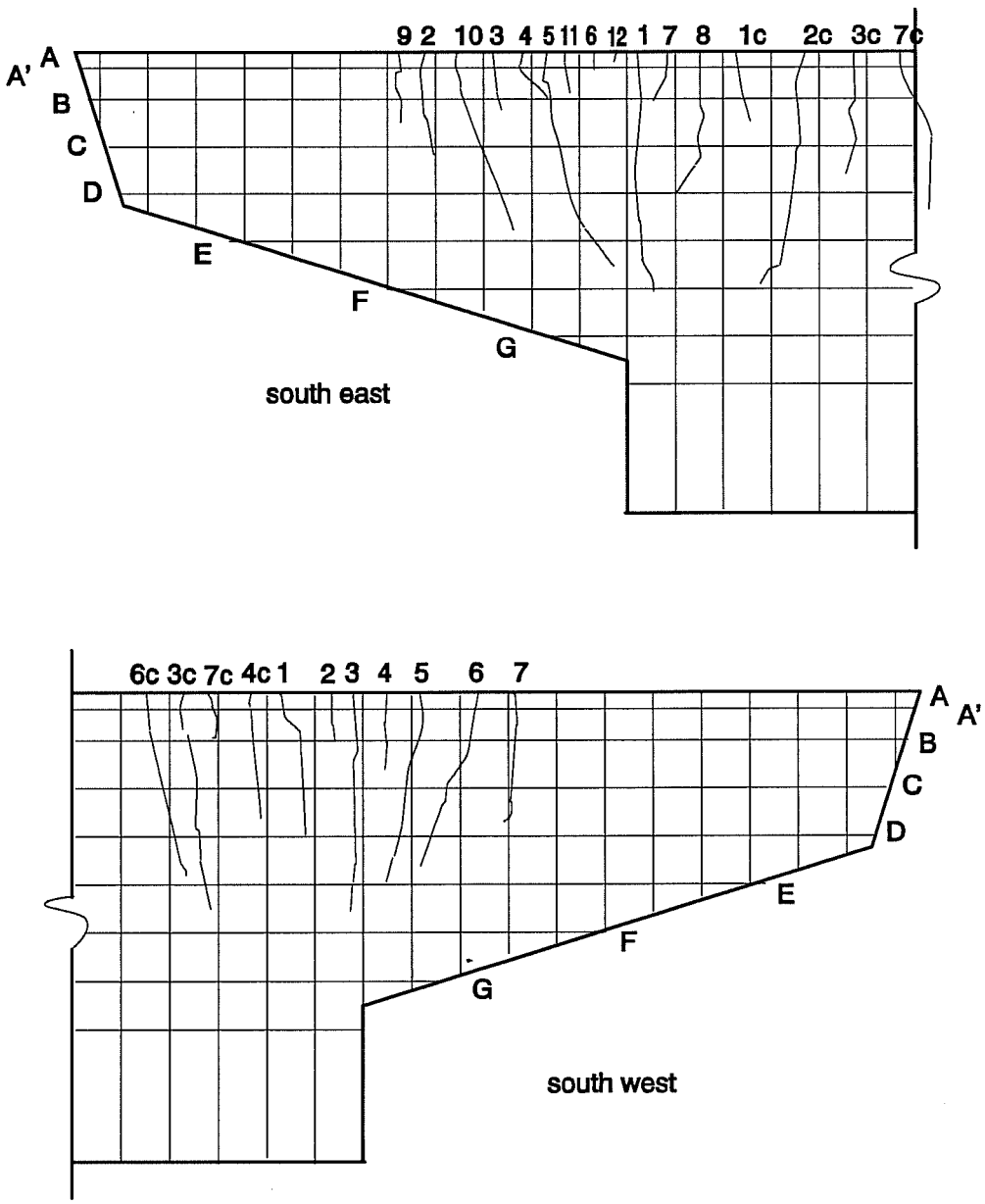

Figure 3.8 Crack Numbers and Locations on the south CO-RU Overhang

CO-PS-100S North East Side				Maximum Crack Width (inches)			
Load Stage	Ri (kips)	Ro (kips)	Moment at Face of Column (kip-inches)	Crack Number 1	2	3	1c
(7) Factored Flexure	46.18	88.52	4078	0.0045			
(8) Dead Load	43.47	40.47	2169	0.001			
(9) Service Shear	49.97	46.97	2507	0.001			
(10) Factored Shear	70.92	66.82	3554	0.004			
(11) Dead Load	43.47	40.47	2169	0.001			
(12) Service Flexure	38.57	56.97	2749	0.0015			
(13) Factored Flexure	46.18	88.52	4078	0.005			
Factored Flexure plus	51.12	121.25	5419	0.01	0.012		0.003
Factored Flexure plus	61.16	172.90	7564	0.04	0.06 A'	0.007	0.009

CO-PS-100S North West side				Maximum Crack Width (inches)			
Load Stage	Ri (kips)	Ro (kips)	Moment at Face of Column (kip-inches)	Crack Number 1	2	3	1c
cracking loads	41.11	69.53	3272	0.0015			
(7) Factored Flexure	46.18	88.52	4078	0.005 A'			
(8) Dead Load	43.47	40.47	2169	0.002			
(9) Service Shear	49.97	46.97	2507	0.002			
(10) Factored Shear	70.92	66.82	3554	0.0055			
(11) Dead Load	43.47	40.47	2169	0.002			
(12) Service Flexure	38.57	56.97	2749	0.003			
(13) Factored Flexure	46.18	88.52	4078	0.006			
Factored Flexure plus	51.12	121.25	5419	0.012	0.011		0.005
Factored Flexure plus	61.16	172.90	7564	0.05	0.06 A'	0.01	0.007

Table 3.4 Maximum Crack Width Readings on the north CO-PS-100S Overhang

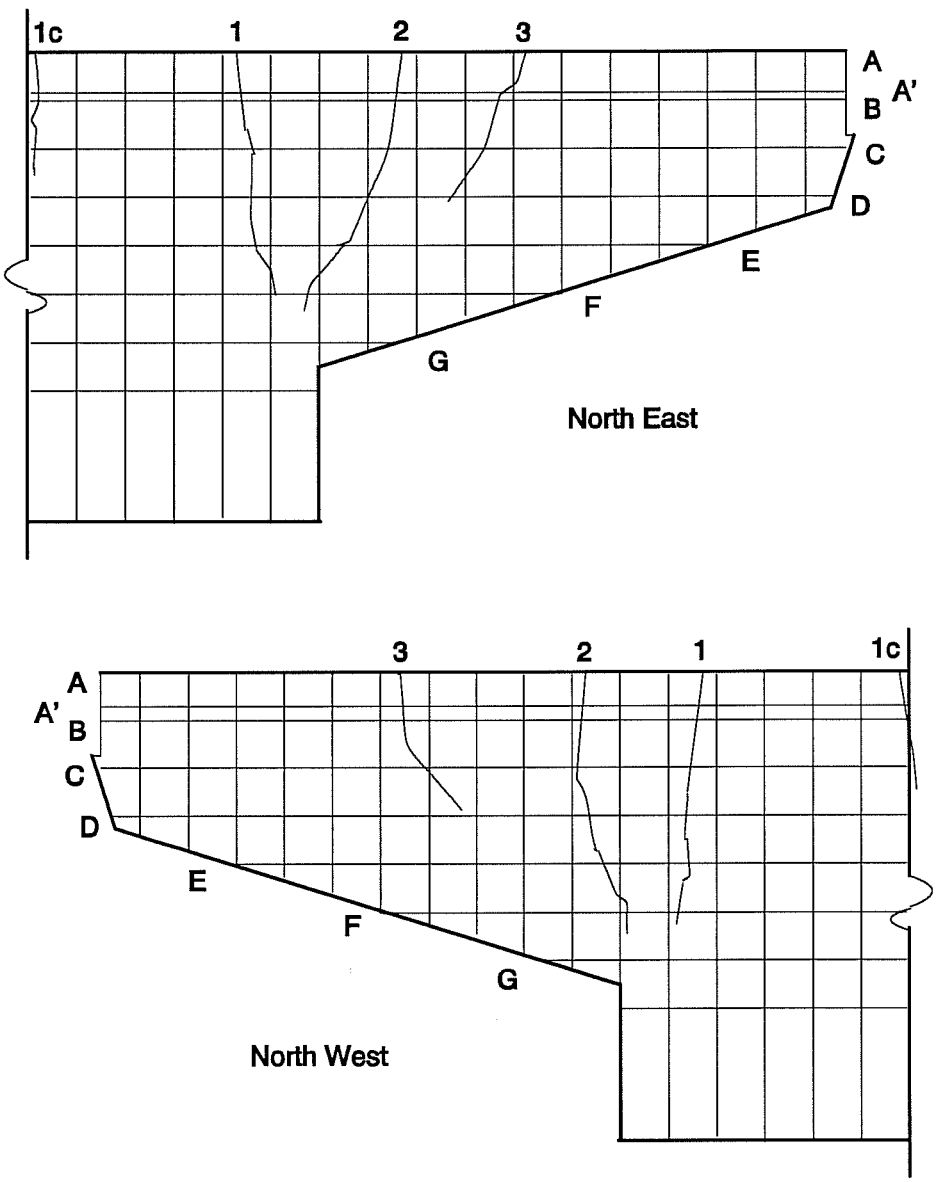

Figure 3.9 Crack Numbers and Locations on the north CO-PS-100S Overhang

CO-PS-100S South East side				Maximum Crack Width (inches)		
Load Stage	Ri (kips)	Ro (kips)	Moment at Face of Column (kip-inches)	Crack Number 1	2	3
(7) Factored Flexure	46.18	88.52	4078	0.004		
(8) Dead Load	43.47	40.47	2169	0.001		
(9) Service Shear	49.97	46.97	2507	0.001		
(10) Factored Shear	70.92	66.82	3554	0.003		
(11) Dead Load	43.47	40.47	2169	0.001		
(12) Service Flexure	38.57	56.97	2749	0.001		
(13) Factored Flexure	46.18	88.52	4078	0.005 B		
Factored Flexure plus	51.12	121.25	5419	0.008	0.016	
Factored Flexure plus	61.16	172.90	7564	0.04	0.05	0.01

CO-PS-100S South West side				Maximum Crack Width (inches)		
Load Stage	Ri (kips)	Ro (kips)	Moment at Face of Column (kip-inches)	Crack Number 1	2	3
(7) Factored Flexure	46.18	88.52	4078	0.005		
(8) Dead Load	43.47	40.47	2169	0.002		
(9) Service Shear	49.97	46.97	2507	0.002		
(10) Factored Shear	70.92	66.82	3554	0.0045		
(11) Dead Load	43.47	40.47	2169	0.002		
(12) Service Flexure	38.57	56.97	2749	0.0025		
(13) Factored Flexure	46.18	88.52	4078	0.007		
Factored Flexure plus	51.12	121.25	5419	0.014	0.014	
Factored Flexure plus	61.16	172.90	7564	0.04	0.06	0.009 B

Table 3.5 Maximum Crack Width Readings on the south CO-PS-100S Overhang

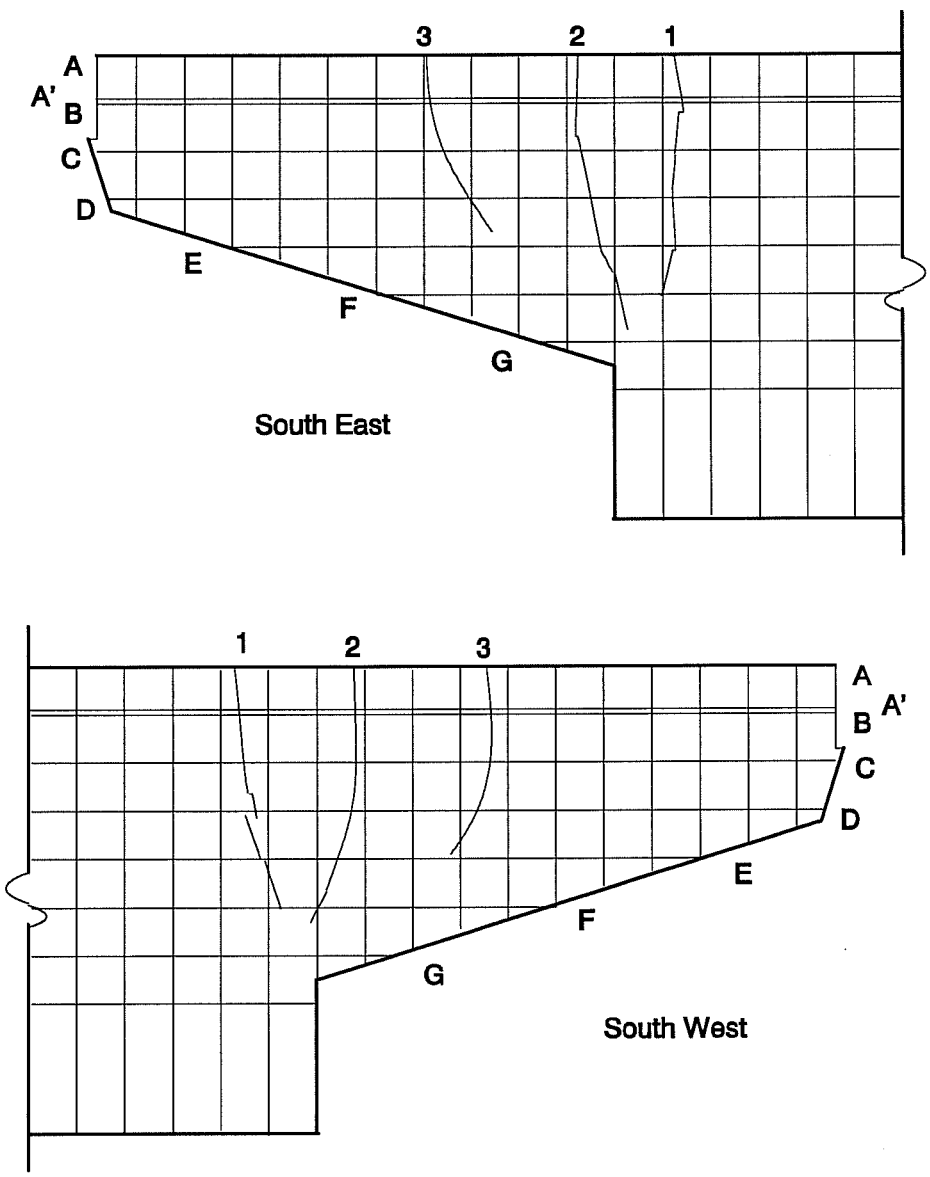

Figure 3.10 Crack Numbers and Locations on the south CO-PS-100S Overhang

CO-PU-100S-I North East side				Maximum Crack Width (inches)	
Load Stage	Ri (kips)	Ro (kips)	Moment at Face of Column (kip-inches)	Crack Number 1	2
cracking loads	41.48	73.27	3422	0.0015	
(7) Factored Flexure	46.18	88.52	4078	0.005	0.006 A'
(8) Dead Load	43.47	40.47	2169	0.002	0.001
(9) Service Shear	49.97	46.97	2507	0.002	0.003 A'
(10) Factored Shear	70.92	66.82	3554	0.003	0.004 A'
(11) Dead Load	43.47	40.47	2169	0.0015	0.002 A'
(12) Service Flexure	38.57	56.97	2749	0.002	0.003 A'
(13) Factored Flexure	46.18	88.52	4078	0.0055	0.007
Factored Flexure plus	51.12	120.88	5405	0.018	0.025

CO-PU-100S-I North West side				Maximum Crack Width (inches)			
Load Stage	Ri (kips)	Ro (kips)	Moment at Face of Column (kip-inches)	Crack Number 1	2	3	4
cracking loads	40.02	65.15	3087	0.002			
cracking NE	41.48	73.27	3422	0.005			
(7) Factored Flexure	46.18	88.52	4078	0.01	0.003	0.003	
(8) Dead Load	43.47	40.47	2169	0.004	0.001	0.001	
(9) Service Shear	49.97	46.97	2507	0.005	0.001	0.002 A'	
(10) Factored Shear	70.92	66.82	3554	0.0065	0.001	0.003	
(11) Dead Load	43.47	40.47	2169	0.004	0.0005	0.001	
(12) Service Flexure	38.57	56.97	2749	0.004	0.001	0.0015	
(13) Factored Flexure	46.18	88.52	4078	0.009	0.003	0.005	
Factored Flexure plus	51.12	120.88	5405		0.002	0.021	0.018

Table 3.6 Maximum Crack Width Readings on the CO-PU-100S-I Overhang

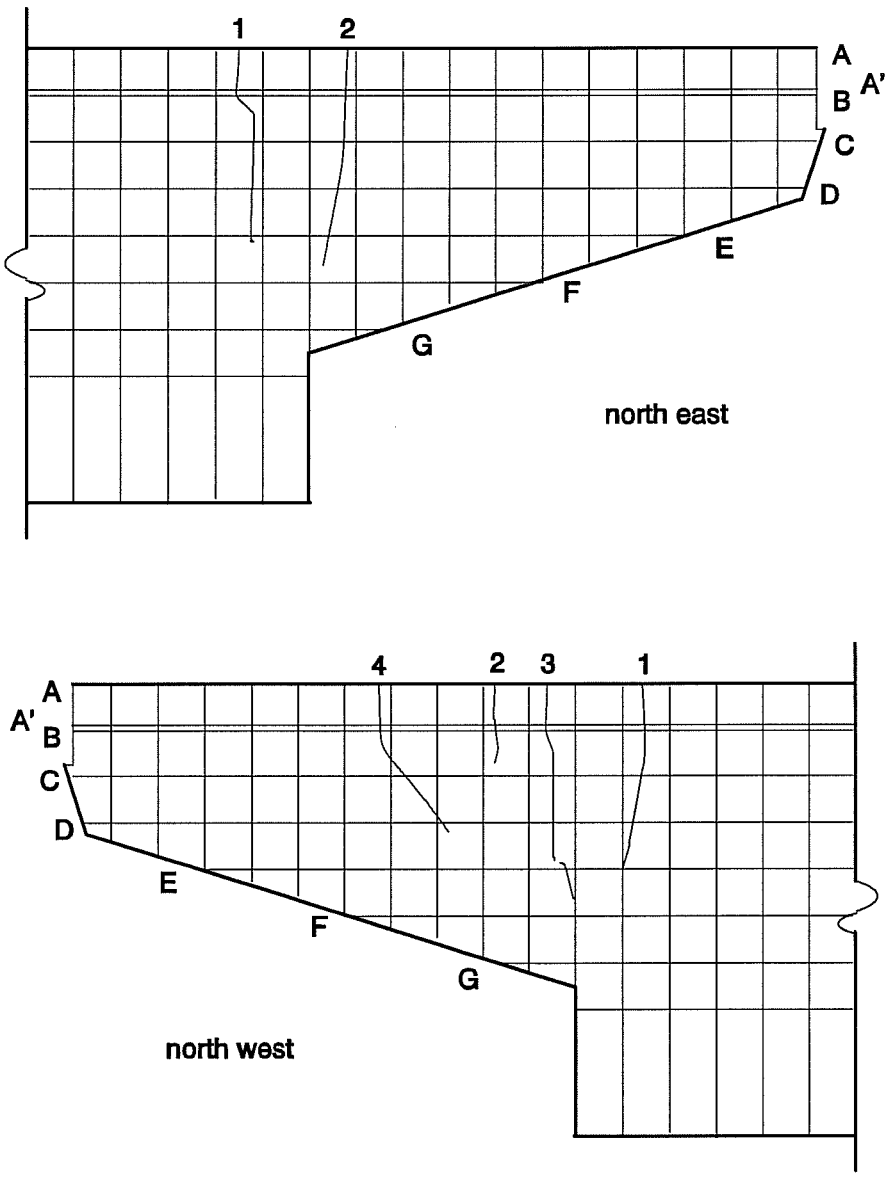

Figure 3.11 Crack Numbers and Locations on the CO-PU-100S-I Overhang

CO-PU-100S-V South East side				Maximum Crack Width (inches)	
Load Stage	Ri (kips)	Ro (kips)	Moment at Face of Column (kip-inches)	Crack Number 1	1c
cracking loads	40.02	65.15	3087	0.002	
cracking NE	41.48	73.27	3422	0.006	
(7) Factored Flexure	46.18	88.52	4078	0.015	0.004
(8) Dead Load	43.47	40.47	2169	0.006	0.002
(9) Service Shear	49.97	46.97	2507	0.007	0.002
(10) Factored Shear	70.92	66.82	3554	0.013	0.0035
(11) Dead Load	43.47	40.47	2169	0.005	0.001
(12) Service Flexure	38.57	56.97	2749	0.007	0.002
(13) Factored Flexure	46.18	88.52	4078	0.017	0.004
Factored Flexure plus	51.12	120.88	5405	0.074	0.016

CO-PU-100S-V South West side				Maximum Crack Width (inches)				
Load Stage	Ri (kips)	Ro (kips)	Moment at Face of Column (kip-inches)	Crack Number 1	2	3	4	1c
cracking loads	39.29	61.20	2923	0.002	0.001			
cracking SE,NW	40.02	65.15	3087	0.0025	0.001			
cracking NE	41.48	73.27	3422	0.003	0.001	0.003		
(7) Factored Flexure	46.18	88.52	4078	0.003	0.001	0.014	0.003	0.005
(8) Dead Load	43.47	40.47	2169	0.0015	0.001	0.005	0.001	0.002
(9) Service Shear	49.97	46.97	2507	0.002	0.001	0.007	0.001	0.002
(10) Factored Shear	70.92	66.82	3554	0.002	0.001	0.011	0.0015	0.004
(11) Dead Load	43.47	40.47	2169	0.002	0.001	0.007	0.001	0.001
(12) Service Flexure	38.57	56.97	2749	0.002	0.001	0.007	0.001	0.002
(13) Factored Flexure	46.18	88.52	4078	0.003	0.001	0.017	0.002	0.005
Factored Flexure plus	51.12	120.88	5405	0.003	0.001	0.077	0.001	0.02

Table 3.7 Maximum Crack Width Readings on the CO-PU-100S-V Overhang

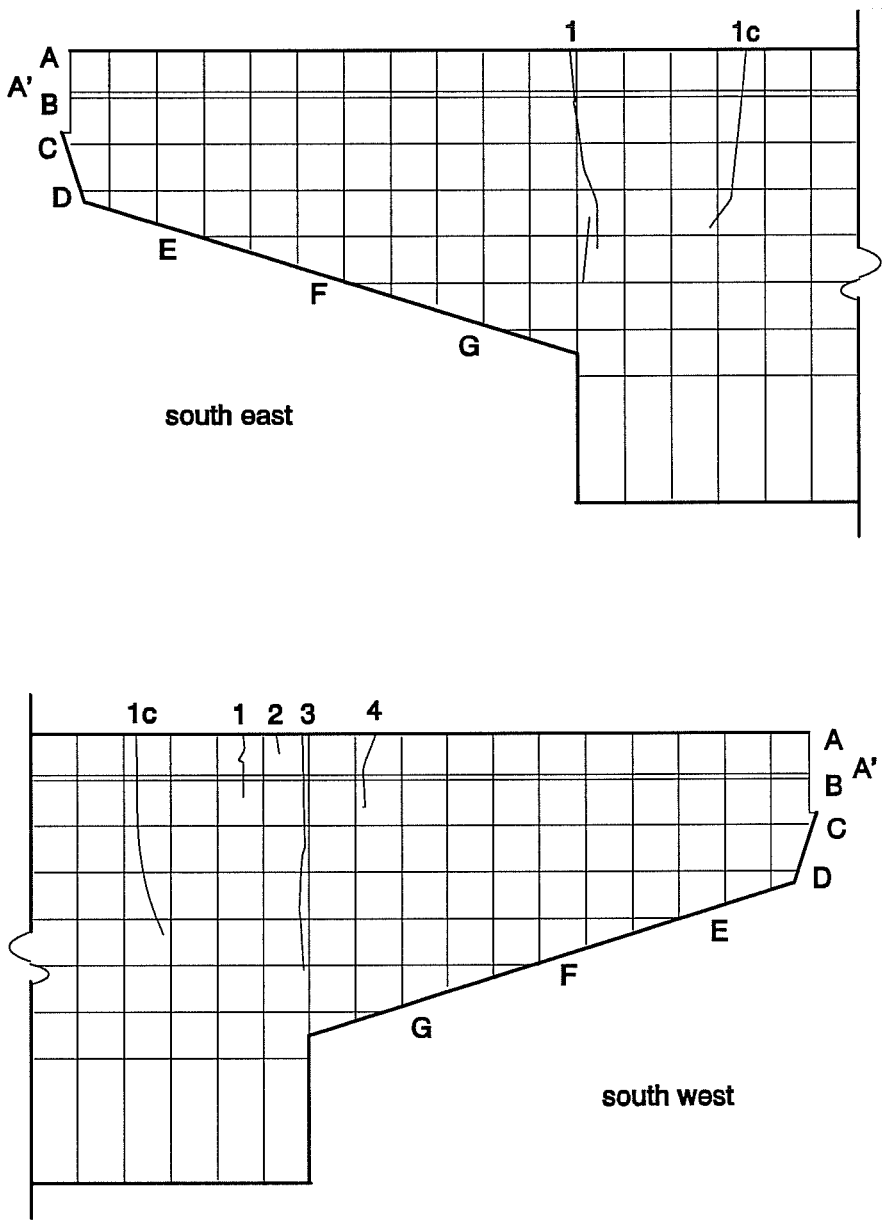

Figure 3.12 Crack Numbers and Locations on the CO-PU-100S-V Overhang

CO-PU-74S-I	North East side			Maximum Crack Width (inches)								
Load Stage	Ri (kips)	Ro (kips)	Moment at Face of Column (kip-inches)	Crack Number 1	2	3	4	5	6	7	8	1c
cracking loads	41.29	49.66	2499	0.0015								
(2) Service Flexure	38.57	56.97	2749	0.0025								
(3) Dead Load	43.47	40.47	2169	0.002								
(4) Service Shear	49.97	46.97	2507	0.002								
(5) Dead Load	43.47	40.47	2169	0.002								
(6) Service Flexure	38.57	56.97	2749	0.003	0.0005							
Service Flexure plus	41.91	73.94	3454	0.005	0.003	0.002						
(7) Factored Flexure	46.18	88.52	4078	0.005	0.004	0.0025	0.003	0.002	0.004	0.003	0.003	0.003 A'
(8) Dead Load	43.47	40.47	2169	0.003	0.002	0.0005	0.0005	0.0005	0.002	0.001	0.0005	0.002 A'
(9) Service Shear	49.97	46.97	2507	0.003	0.002	0.0005	0.001	0.0005	0.002	0.001	0.0005	0.002 A'
(10) Factored Shear	70.92	66.82	3554	0.003	0.003	0.002	0.003	0.001	0.003	0.002	0.002	0.003 A'
(12) Service Flexure	38.57	56.97	2749	0.002	0.002	0.001	0.0015	0.0005	0.002	0.001	0.0015	0.002
(13) Factored Flexure	46.18	88.52	4078	0.005	0.004	0.003	0.003	0.002	0.004	0.003	0.003	0.004 A'

CO-PU-74S-I	North West side			Maximum Crack Width (inches)							
Load Stage	Ri (kips)	Ro (kips)	Moment at Face of Column (kip-inches)	Crack Number 1	2	3	4	5	6	1c	2c
cracking loads	41.29	49.66	2499	0.0005							
(2) Service Flexure	38.57	56.97	2749	0.0025							
(3) Dead Load	43.47	40.47	2169	0.002							
(4) Service Shear	49.97	46.97	2507	0.002	0.0015						
(5) Dead Load	43.47	40.47	2169	0.002	0.0015						
(6) Service Flexure	38.57	56.97	2749	0.003	0.002	0.0005					
Service Flexure plus	41.91	73.94	3454	0.004	0.004 A'	0.007	0.0005				
(7) Factored Flexure	46.18	88.52	4078	0.007 A'	0.004	0.01	0.005	0.004	0.002	0.01	0.002
(8) Dead Load	43.47	40.47	2169	0.0005	0.003 A'	0.006	0.0015	0.001	0.0005	0.003	0.0005
(9) Service Shear	49.97	46.97	2507	0.004 A'	0.003 A'	0.007	0.003	0.002	0.0005	0.003	0.0005
(10) Factored Shear	70.92	66.82	3554	0.005 A'	0.005 A'	0.007	0.004	0.004	0.0015	0.004	0.001
(12) Service Flexure	38.57	56.97	2749	0.004 A'	0.004 A'	0.007	0.003	0.002	0.001	0.0035	0.001
(13) Factored Flexure	46.18	88.52	4078	0.005 A'	0.005 A'	0.009	0.007	0.004	0.003	0.005	0.002

Table 3.8 Maximum Crack Width Readings on the CO-PU-74S-I Overhang

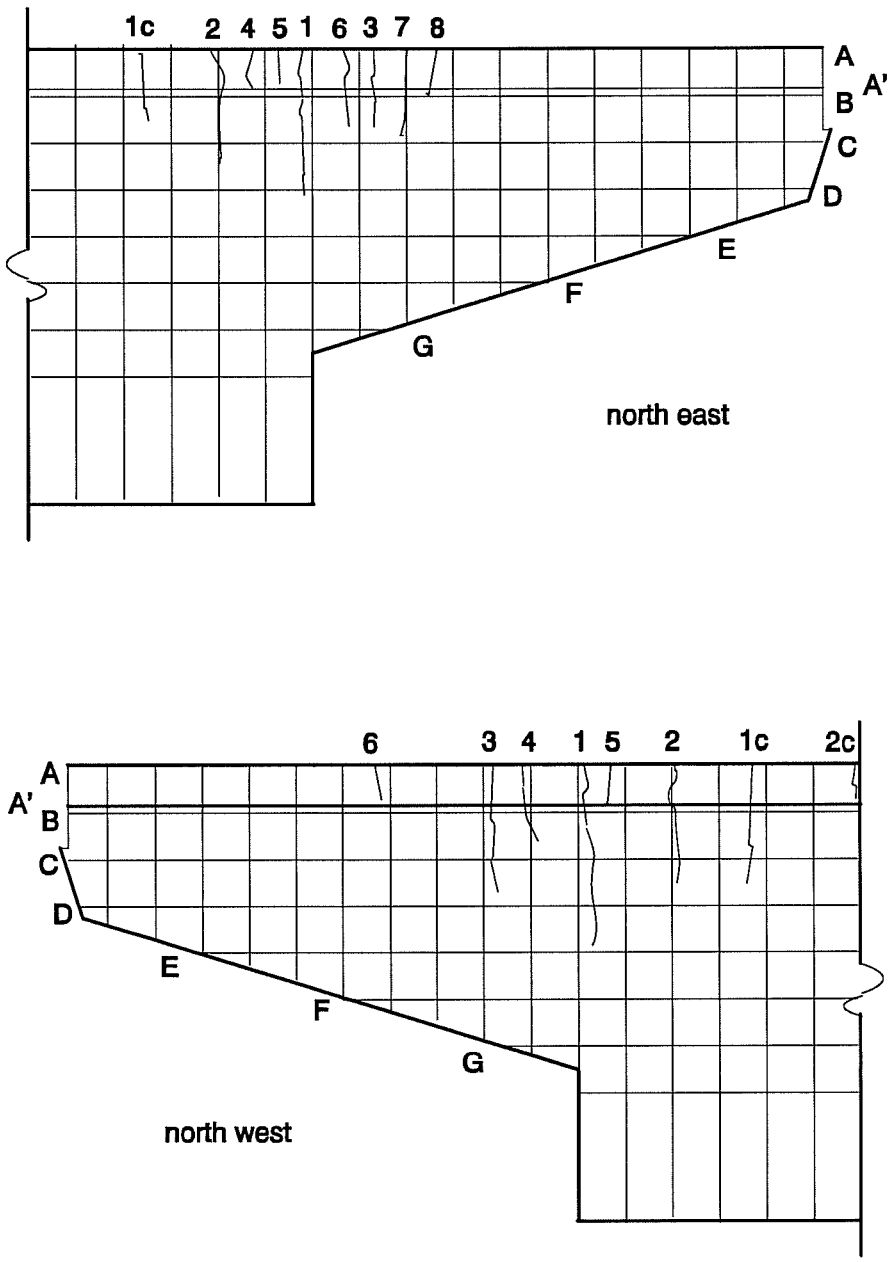

Figure 3.13 Crack Numbers and Locations on the CO-PU-74S-I Overhang

CO-PU-74S-V	South East side			Maximum Crack Width (inches)								
Load Stage	Ri (kips)	Ro (kips)	Moment at Face of Column (kip-inches)	Crack Number 1	2	3	4	5	6	7	2c	3c
cracking loads	41.29	49.66	2499	0.001								
(2) Service Flexure	38.57	56.97	2749	0.0028								
(3) Dead Load	43.47	40.47	2169	0.0022								
(4) Service Shear	49.97	46.97	2507	0.0025								
(5) Dead Load	43.47	40.47	2169	0.0022								
Service Flexure plus	41.91	73.94	3454	0.004	0.002	0.004	0.007	0.003				
(7) Factored Flexure	46.18	88.52	4078	0.005	0.005	0.005	0.006	0.005	0.005	0.003	0.004	0.001
(8) Dead Load	43.47	40.47	2169	0.0035	0.001	0.002	0.004	0.0035	0.002	0.0005	0.002	0.0005
(9) Service Shear	49.97	46.97	2507	0.002	0.001	0.002	0.004	0.003	0.002	0.0005	0.003	0.0005
(10) Factored Shear	70.92	66.82	3554	0.003	0.0025	0.003	0.006	0.005	0.003	0.0015	0.0035	0.001
(11) Service Flexure	38.57	56.97	2749	0.003	0.003	0.003	0.004	0.003	0.003	0.001	0.003	0.0005
(12) Factored Flexure	46.18	88.52	4078	0.006	0.005	0.005	0.0065	0.006	0.0045	0.003	0.004	0.002

CO-PU-74S-V	South West side			Maximum Crack Width (inches)						
Load Stage	Ri (kips)	Ro (kips)	Moment at Face of Column (kip-inches)	Crack Number 1	2	3	4	5	6	3c
cracking loads	43.36	41.86	2222	0.0005						
cracking NW	41.29	49.66	2499	0.002						
(2) Service Flexure	38.57	56.97	2749	0.003	0.0012					
(3) Dead Load	43.47	40.47	2169	0.0025	0.001					
(4) Service Shear	49.97	46.97	2507	0.003	0.001					
(5) Dead Load	43.47	40.47	2169	0.003	0.001					
(6) Service Flexure	38.57	56.97	2749	0.003	0.002					
Service Flexure plus	41.91	73.94	3454	0.0055	0.007	0.005	0.0025			
(7) Factored Flexure	46.18	88.52	4078	0.009	0.009	0.008	0.008	0.005	0.006	0.007
(8) Dead Load	43.47	40.47	2169	0.004	0.004	0.004	0.003	0.004	0.002	0.004
(9) Service Shear	49.97	46.97	2507	0.004	0.006	0.005	0.003	0.003	0.002	0.005
(10) Factored Shear	70.92	66.82	3554	0.0065	0.008	0.007	0.006	0.003	0.0035	0.007
(12) Service Flexure	38.57	56.97	2749	0.005	0.006	0.005	0.006	0.003	0.002	0.005
(13) Factored Flexure	46.18	88.52	4078	0.009	0.011	0.007	0.008	0.006	0.006	0.007

Table 3.9 Maximum Crack Width Readings on the CO-PU-74S-V Overhang

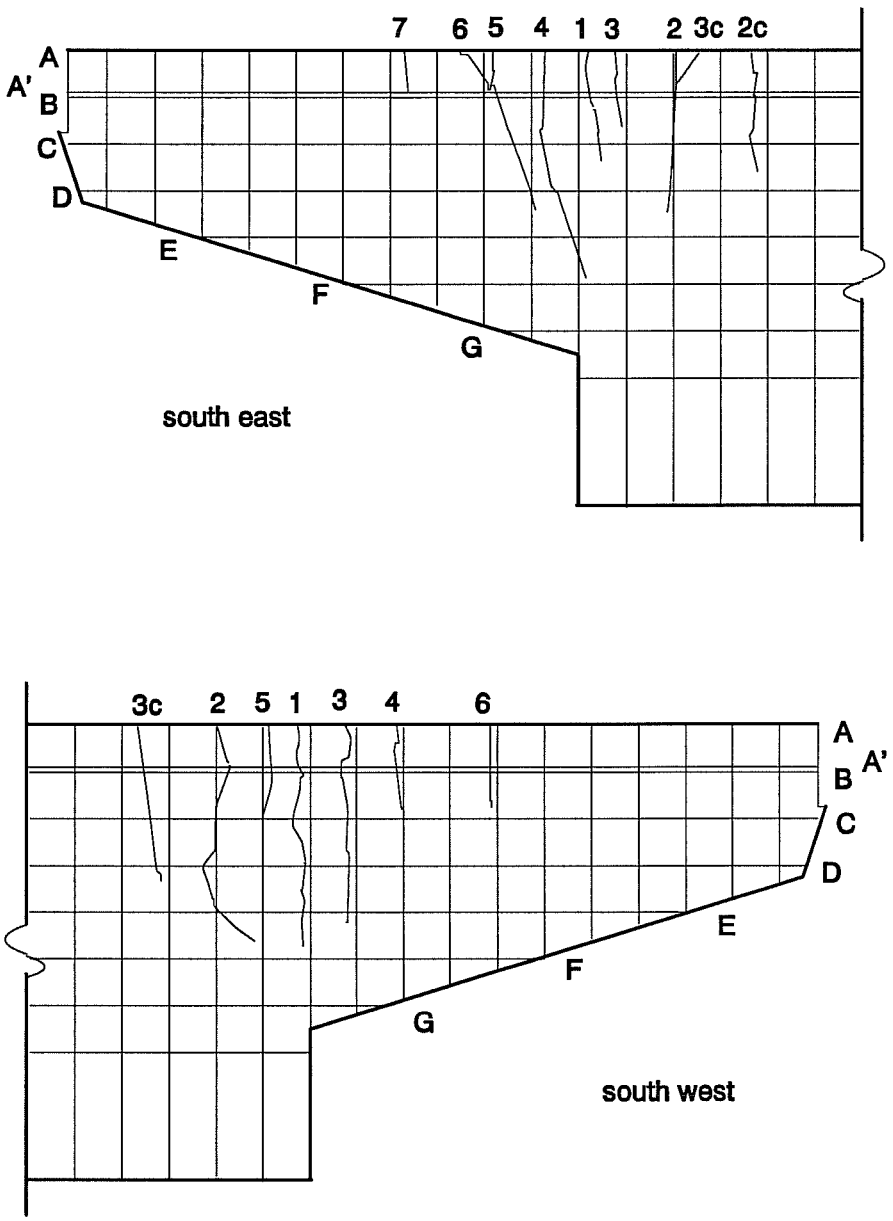

Figure 3.14 Crack Numbers and Locations on the CO-PU-74S-V Overhang

3.5 Moment-Deflection Curves

The recorded loads and tip deflections were used to generate moment-deflection curves for each of the eight overhangs. These curves are shown in Figures 3.15 through 3.18. The moment at the face of the column from applied loads plus self weight of the overhang is plotted on the vertical axis against the deflection at the tip of the overhang on the horizontal axis (downward deflection is positive). Because of scaling of the loads, it was possible in the tests to determine moment corresponding to superstructure dead load and service loads, and the corresponding deflections.

Each plot indicates the cracking loads, maximum test loads, dead load deflection, and service load deflection. Dead load and service load deflections are the maximum values measured for these loads respectively before factored loads were applied to the overhang. Larger deflections were measured at dead and service load levels when these load levels were reapplied after factored flexure loads had been applied. However, because of the wide cracking at factored load levels, the reloadings following factored loads are not considered to be representative of the service load performance.

The moment-deflection curves for each overhang follow basically the same slope (same stiffness) up to the load level at which cracking occurred. The CO-RU overhang cracked at the lowest loads and its moment-deflection curves show a significant reduction in stiffness beginning at this point. The moment-deflection curves for each of the prestressed overhangs became non-linear once cracking occurred, but the change in stiffness was not nearly as pronounced as in the CO-RU overhang, because these overhangs experienced significantly fewer cracks. Furthermore, the nonlinearity in the moment-deflection curves for the prestressed overhangs did not begin until higher load levels than for the CO-RU overhang. This is because the cracking loads for these overhangs were higher than for the CO-RU overhang, increasing with increasing levels of post-tensioning. The maximum moment reached by each overhang was also significantly different. This is discussed in greater detail in Sections 3.7 and 4.6.

At loads approaching ultimate, Figures 3.16 and 3.18 show an abrupt reduction of load with an increase in deflection. A loud bang was heard during the tests at the same load levels. The loud bangs and drop in load are believed to be the result of slippage between the 5" x 7" x 1" and 8" x 2" x 12" plates in the loading assembly (see Figure 2.32), occurring with the release of a frictional restraining force between the plates. With the release of the frictional restraint, the

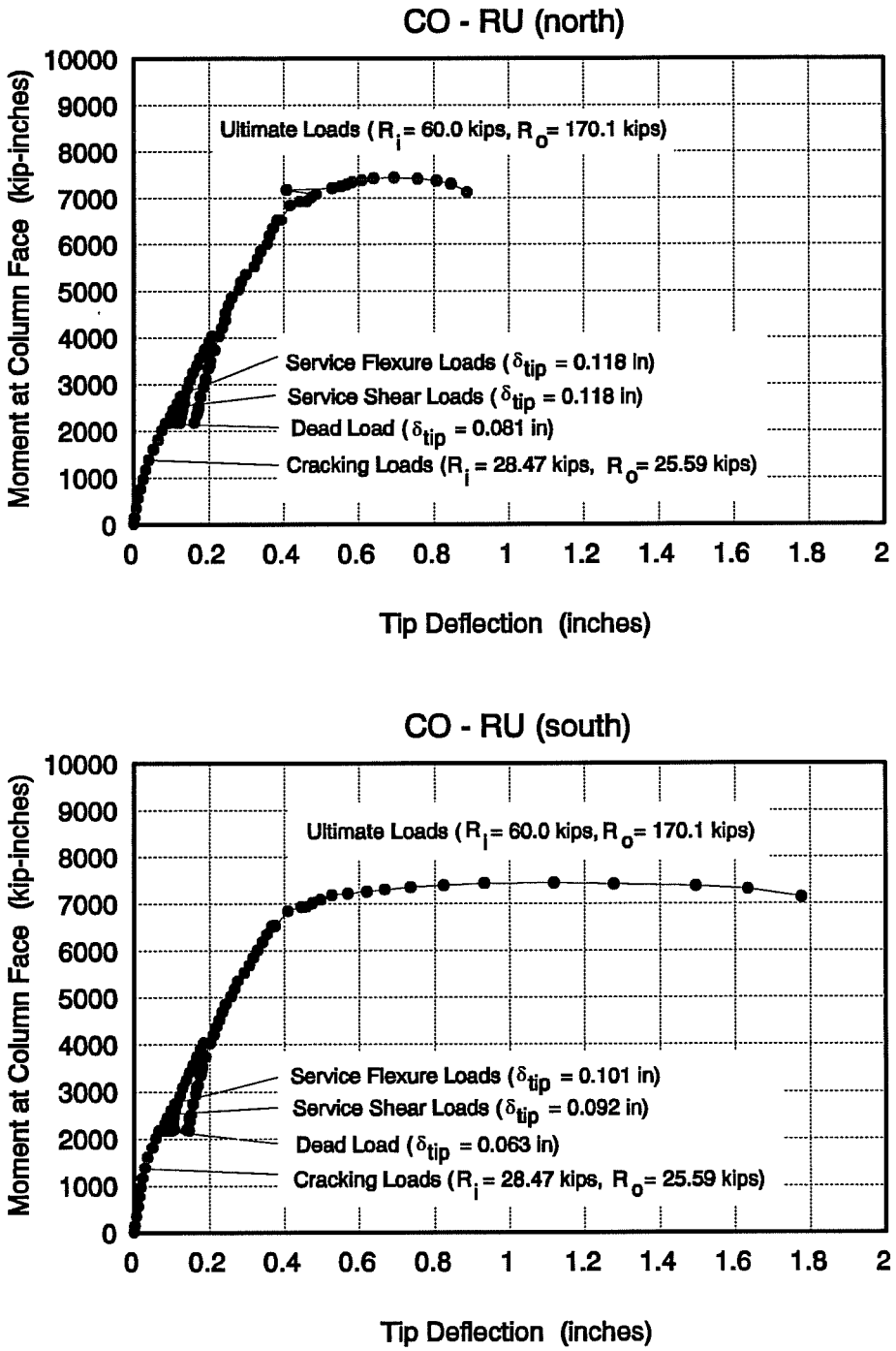

Figure 3.15 Moment-Deflection Curves for the CO-RU Overhangs (north and south)

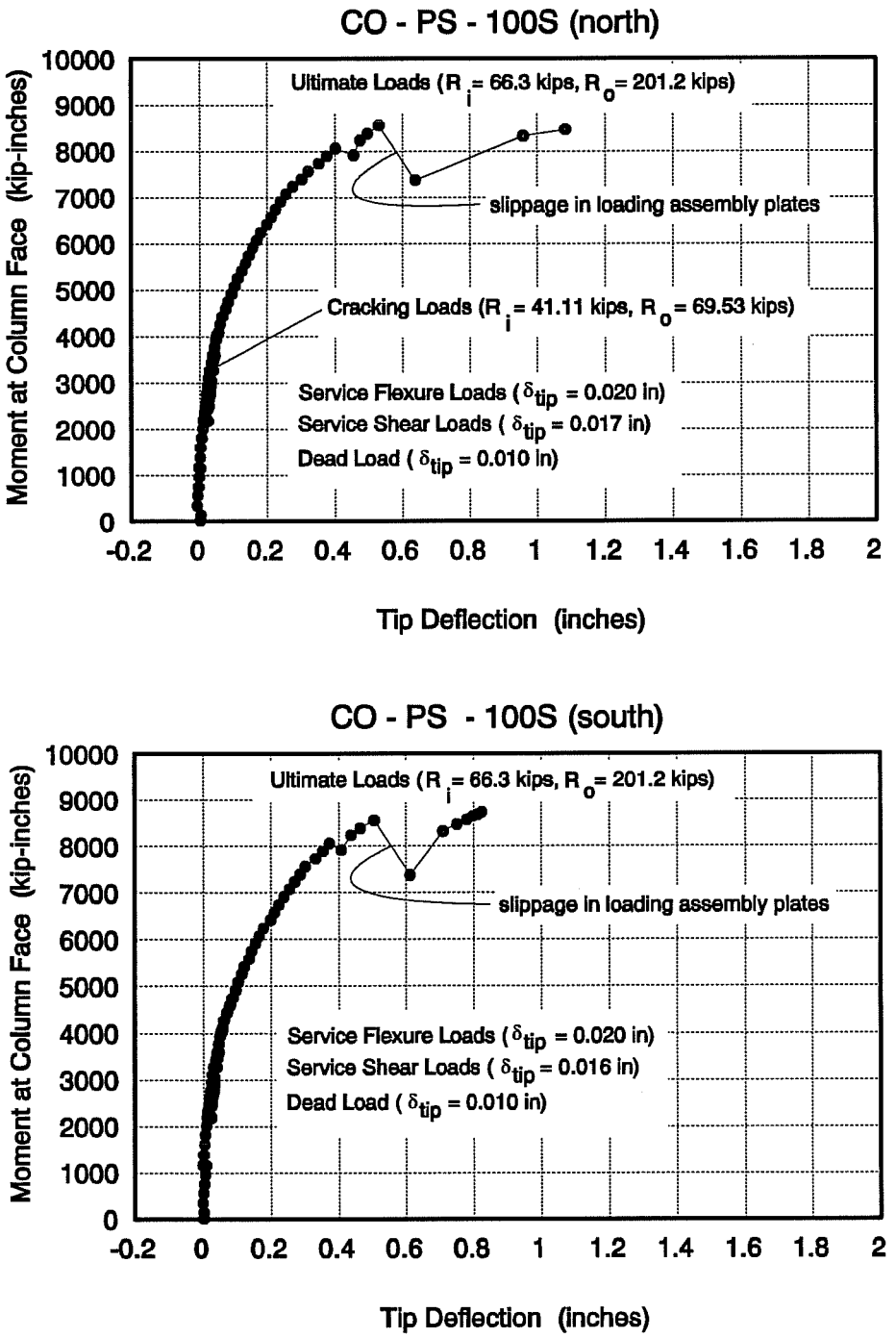

Figure 3.16 Moment-Deflection Curves for the CO-PS-100S Overhangs (north and south)

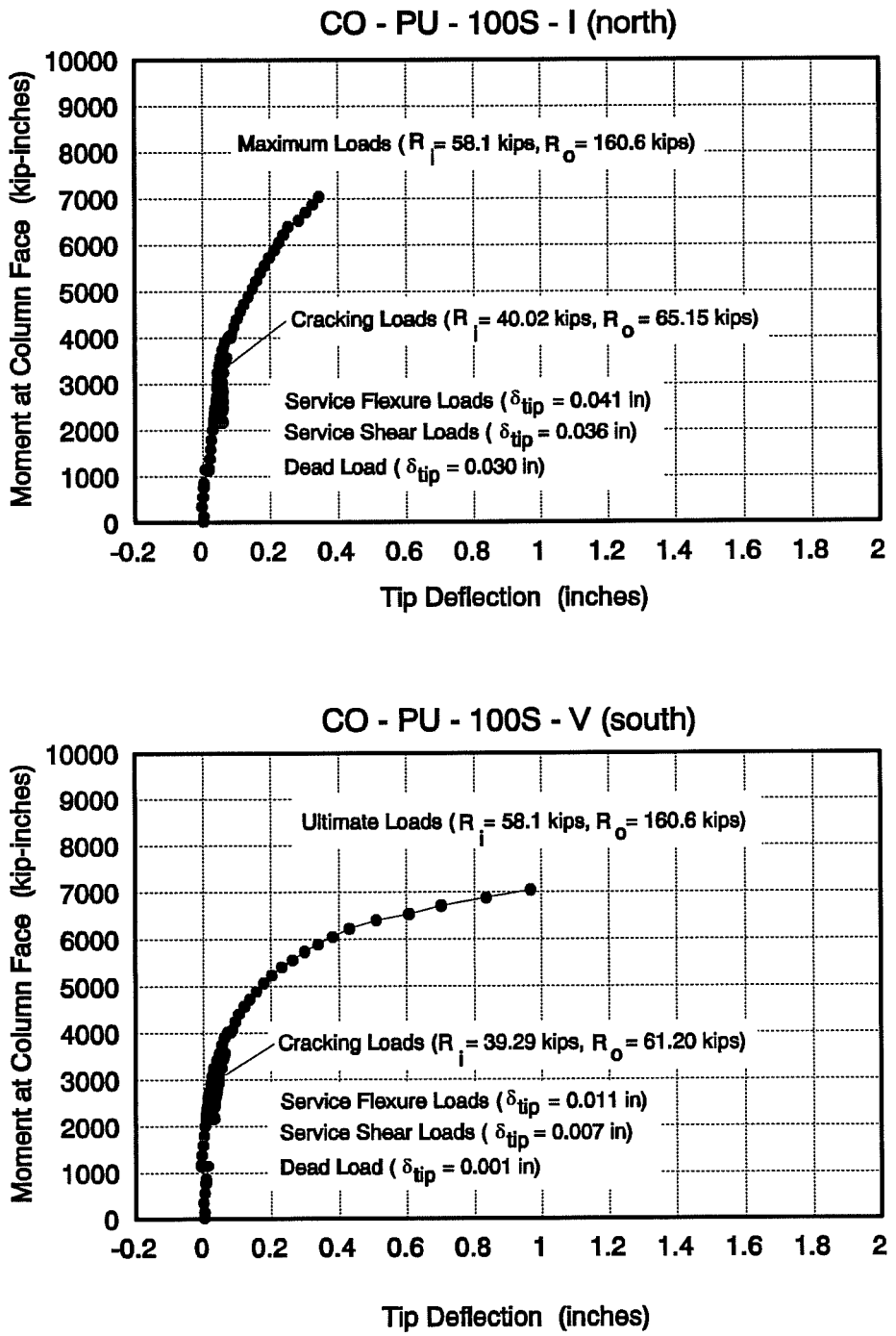

Figure 3.17 Moment-Deflection Curves for the CO-PU-100S-I and CO-PU-100S-V Overhangs

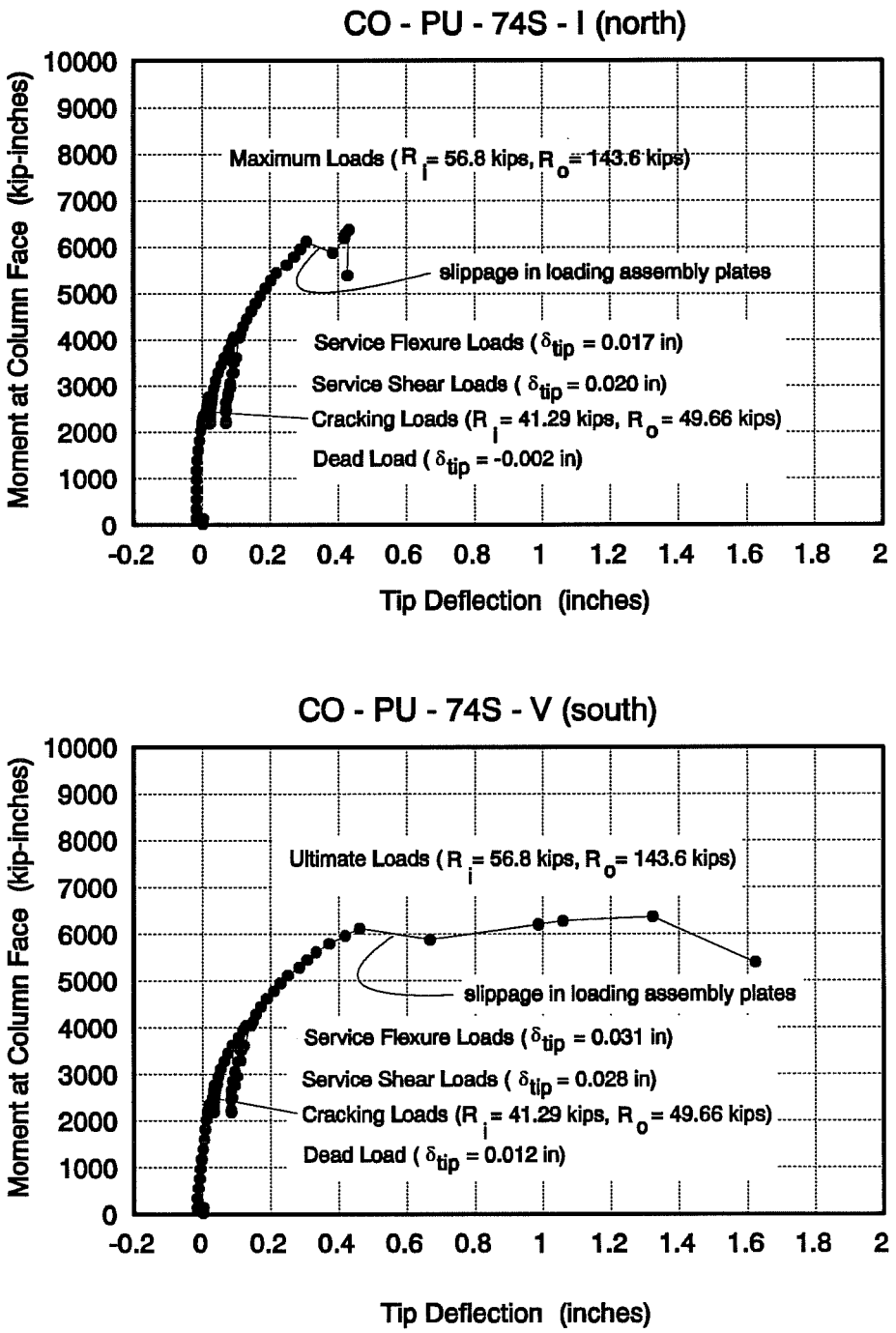

Figure 3.18 Moment-Deflection Curves for the CO-PU-74S-I and CO-PU-74S-V Overhangs

overhang experienced a sudden increase in the elongation of the top fiber and downward tip deflection.

This is a likely explanation since the position of the loading rams was fixed so that they were not able to move outward as the top fiber was elongating under increasing loads. The 4" x 4" x 8" blocks of the loading assembly were in contact with the concrete specimen where it was possible to develop a higher frictional force than between the adjacent steel plates. The outward movement of the 4" x 4" x 8" blocks progressed smoothly until the maximum frictional force that could develop between the adjacent steel plates was exceeded. At this point it is believed that the plates slipped, causing the loud bang and allowing the top fiber to elongate and the tip deflection to increase suddenly. With the sudden increase in deflection and extension of the ram piston, the hydraulic pressure on the rams would have decreased causing a sudden reduction in the load.

In the testing of the CO-PS-100S and CO-PU-74S overhangs, loading was resumed after the loud bang until the maximum loads were reached. The final loads were slightly higher than the loads when the bang was heard.

In the testing of the CO-PU-100S overhangs, a similar loud bang was heard. But for this specimen, no additional loading was applied to the overhangs. Thus, it is possible that slightly higher loads may have been reached if loading had been resumed. However, crushing of the concrete in the compression zone of the CO-PU-100S-V overhang was occurring, so it is believed that any increase in load over the maximum loads reached would have been minor.

3.6 Summary of Dead Load and Service Load Deflections

Table 3.10 summarizes the tip deflection for each overhang under superstructure dead load, service flexure loads, and service shear loads. The tip deflections were measured at 46" from the column face.

As expected, the CO-RU overhangs exhibited the largest deflections at service loads with a maximum tip deflection of 0.118 inches under service flexure loads. The service load deflection is largely influenced by the number of cracks on the overhang, so it is expected that the CO-RU overhang would have the greatest deflection.

The tip deflections of the CO-PS-100S, CO-PU-100S, and CO-PU-74S overhangs were all significantly lower and were very small. This is because the post-tensioning prevented or dramatically limited the cracking of these overhangs at service loads.

Specimen #	Overhang	Overhang Tip Deflection (inches)		
		Dead Load	Service Flexure Loads	Service Shear Loads
1	CO-RU (north)	0.081	0.118	0.118
	CO-RU (south)	0.063	0.101	0.092
2	CO-PS-100S (north)	0.010	0.020	0.017
	CO-PS-100S (south)	0.010	0.020	0.016
3	CO-PU-100S-I	0.030	0.041	0.036
	CO-PU-100S-V	0.001	0.011	0.007
4	CO-PU 74S-I	-0.002	0.017	0.020
	CO-PU-74S-V	0.012	0.031	0.028

Table 3.10 Dead Load and Service Load Deflections

A more detailed analysis of the service load deflections of each overhang is presented in Section 4.4.

3.7 Summary of Maximum Test Loads and Comparison to Required Design Moment

The maximum test loads for each overhang are summarized in Table 3.11 along with the corresponding moment at the face of the column, $M_{n\ test}$. Each of these values is substantially above the factored moment, M_u = 4036 k-in, determined from the design loading using the AASHTO load factors. In the design of all flexural reinforcement, the basic AASHTO approach given by Equation [3-1] was used

$$M_u \leq \phi M_n \qquad [3\text{-}1]$$

In these laboratory experiments with carefully controlled and measured dimensions and material properties, the use of Φ values complicates interpretation when comparing test results ($M_{n\ test}$)

to design values (M_u). For more consistent comparison, Equation [3-1] will be rearranged as

$$\frac{M_u}{\Phi} \leq M_n \qquad [3\text{-}1a]$$

and the comparison of test results ($M_{n\ test}$) will be made to the required design moment, M_u/Φ, equal to 4036 / 0.9 = 4484 k-in. These ratios are also included in Table 3.11.

Specimen #	Overhang	Maximum Inside Reaction, Ri test (kips)	Maximum Outside Reaction, Ro test (kips)	Maximum Test Moment Mn test (kip-in)	Required Design Moment, Mu/phi (kip-in)	Mn test / Mu/phi
1	CO-RU	60.0	170.1	7440	4484	1.66
2	CO-PS-100S	66.3	201.2	8734	4484	1.95
3	CO-PU-100S-I	58.1*	160.6*	7044*	4484	1.57
	CO-PU-100S-V	58.1	160.6	7044	4484	1.57
4	CO-PU-74S-I	56.8*	143.6*	6364*	4484	1.42
	CO-PU-74S-V	56.8	143.6	6364	4484	1.42

* proof loads

Table 3.11 Maximum Test Loads and Comparisons to Required Design Moment

The values in Table 3.11 were used to generate Figure 3.19 which shows the relationship of the maximum test loads to the required design moment, as well as the relative capacities of each overhang. Since the CO-PU-100S-I and CO-PU-74S-V overhangs were not loaded to failure, the maximum test loads can only be regarded as proof loads and the actual capacities of these overhangs would be higher than what is shown.

It is clear from Figure 3.19 that each overhang had ample capacity to resist factored loads. As suspected, the current AASHTO based reinforced concrete and prestressed concrete overhangs had the greatest strength and were extremely overdesigned. The CO-PS-100S overhang had the greatest capacity, which was expected since a service load design approach was used to proportion the post-tensioning. The CO-PU-100S-I and V overhangs were not as overdesigned as the AASHTO designs, but still had substantial excess capacity. The CO-PU-74S-I and V overhangs were closer to the required strength but still quite conservative.

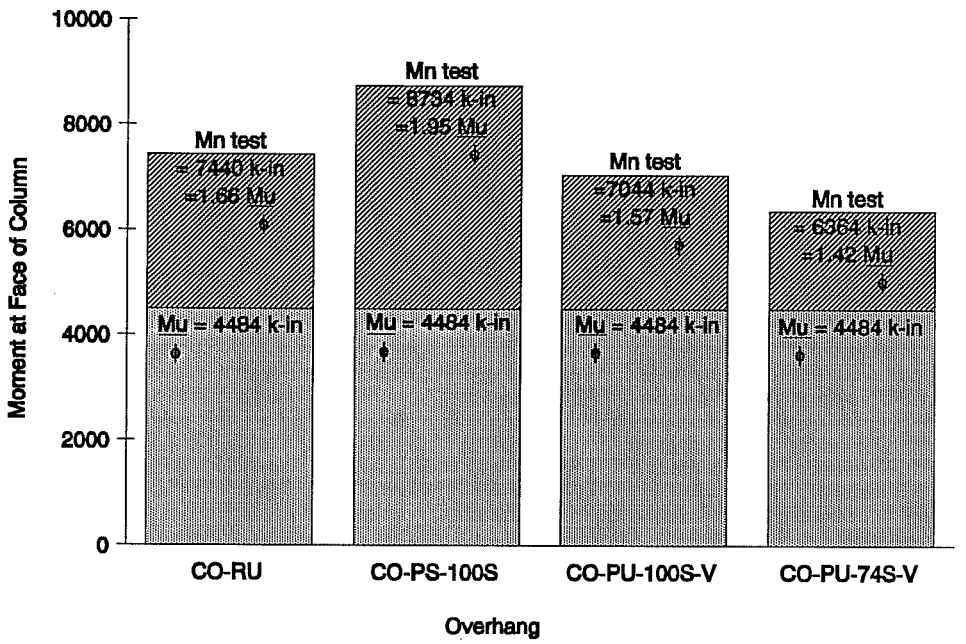

Figure 3.19 Comparisons of Test Moments to Required Design Moment

The difference in the capacities of the CO-PU-100S-V and CO-PU-74S-V overhangs was expected since in the CO-PU-74S-V overhang, several of the No. 2 reinforcing bars for the primary moment reinforcement were located in place of the skin reinforcement on the sides and top faces, whereas, for the CO-PU-100S-V overhang, all of the primary moment reinforcement was in addition to the side face and top face reinforcement.

A more detailed discussion of the overhang capacities is presented in Section 4.6.

3.8 Failure Modes

Although the number of cracks and the ultimate capacities of each of the four failed overhangs were very different, the mode of failure of each was essentially the same. Each overhang experienced a typical flexural failure, as depicted by the cracking patterns shown in

Figures 3.3 through 3.6. The failures were accompanied by yielding of the horizontal tension reinforcement (see Section 3.9) at the maximum moment section and crushing of the concrete compression zone at the juncture of the bottom of the overhang and the column.

3.9 Reinforcing Strains

3.9.1 General

The results of selected strain gages are presented in this section. In general, the results of strain gages on the horizontal reinforcement are presented as plots of the steel strain versus the moment in the overhang from applied loads at the location of the gage. Results from the strain gages on the vertical shear stirrups are plots of the steel strain versus the shear in the overhang from applied loads at the location of the gage. All plots are for the full range of test loading. No plots are included for strains on the post-tensioning strand as none of these strain gages were operating after post-tensioning was completed.

It is important to keep in mind that maximum strains in the reinforcement will occur where cracks cross the reinforcement. The gage only measures the strain in the reinforcement at the location of the gage which may or may not coincide with the location of cracks, so the recorded strains may not be the maximum strain experienced by the reinforcement.

3.9.2 CO-RU Overhang

Strain gages were used on the reinforcement in both the north and south CO-RU overhangs, but most gages were located in the north overhang. Only a few gages were used in the south overhang and these gages were placed in identical locations to gages in the north overhang. The gages in the south overhang were only used to verify that the straining of the reinforcement in each overhang was the same, as it should have been since the reinforcing designs were identical and the loading was symmetrical. Examination of the data from gages on both overhangs revealed that the straining of the steel on each overhang was in fact essentially the same. Therefore, only results from the strain gages on the north overhang will be presented.

Figures 3.20 through 3.22 show results of strain gages on the primary moment, shear-friction, and side face reinforcement. The plots show that at final failure all gages recorded strains in excess of the yield strain for the respective reinforcement at the face of the column.

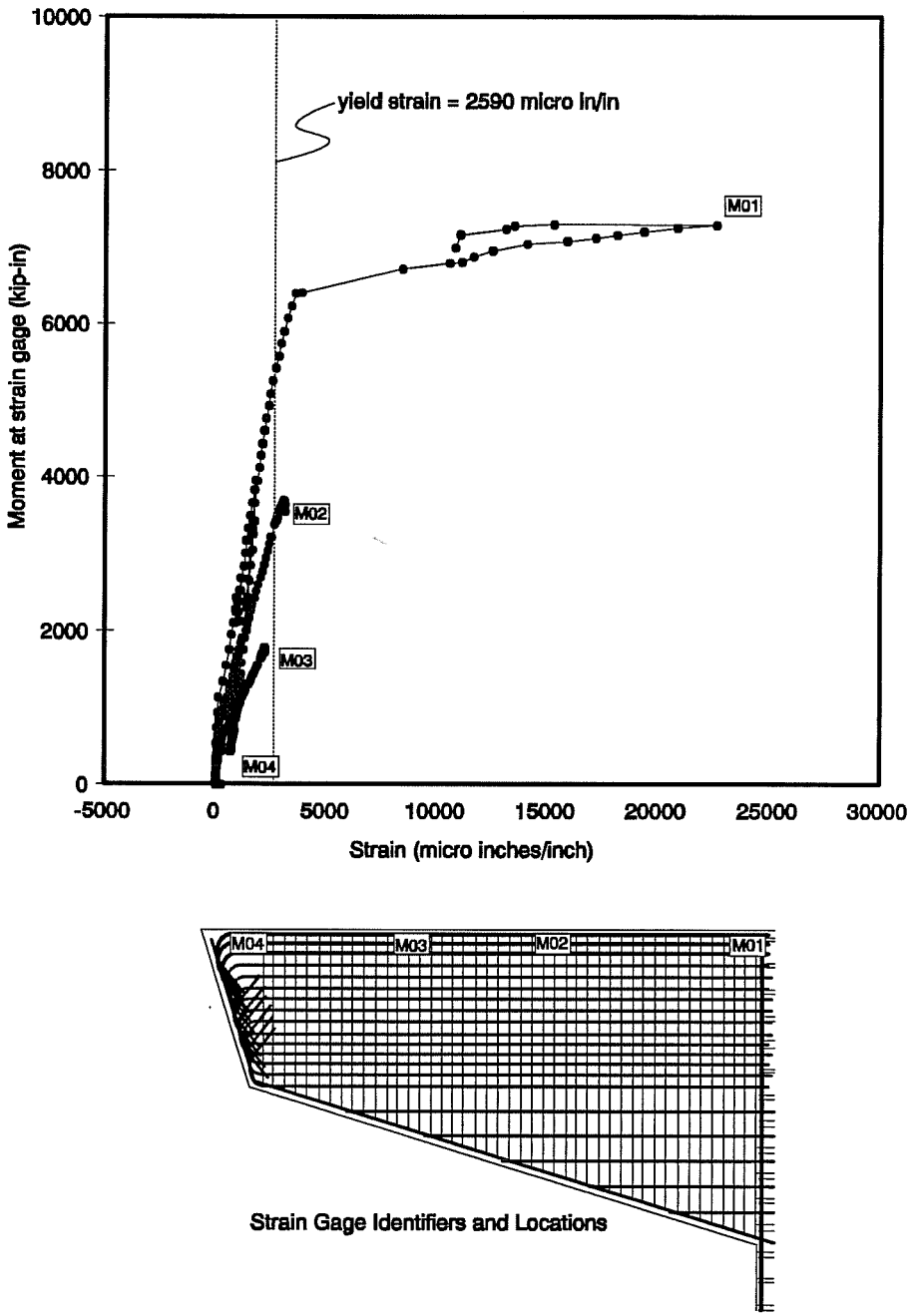

Figure 3.20 Strain Gages on the Moment Reinforcement in CO-RU (north) Overhang

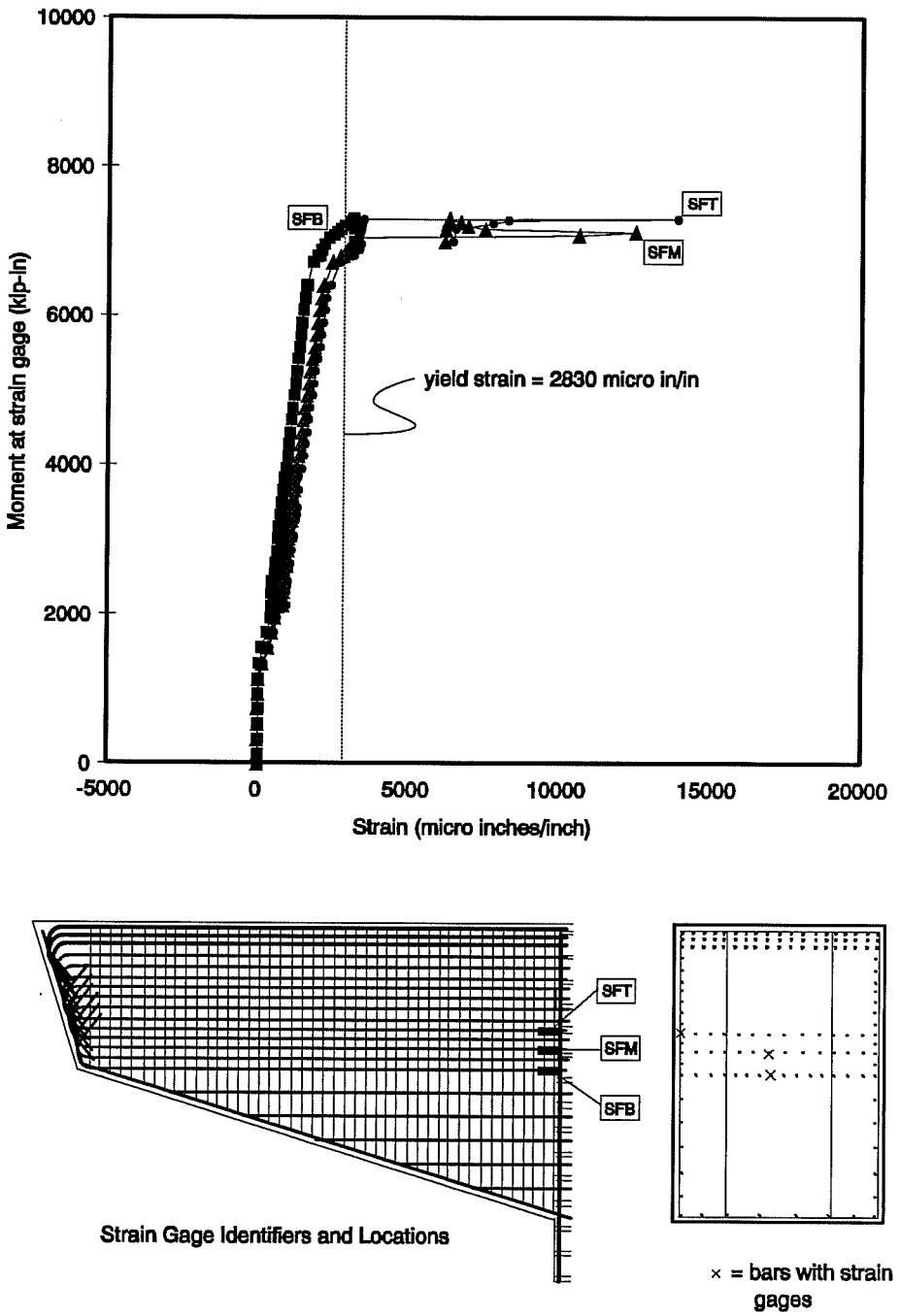

Figure 3.21 Strain Gages on the Shear-Friction Reinforcement in CO-RU (north) Overhang

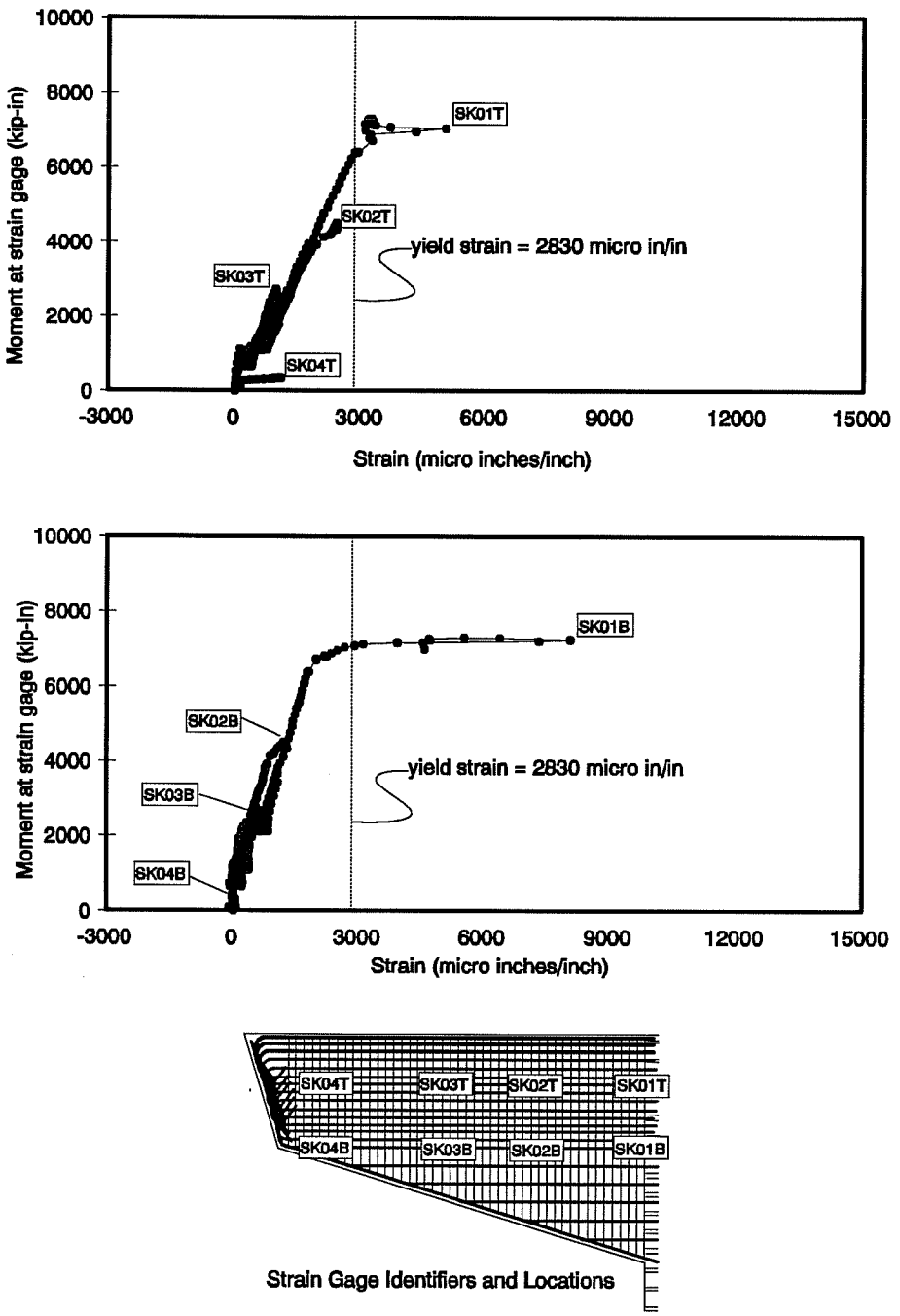

Figure 3.22 Strain Gages on Side Face Reinforcement in CO-RU (north) Overhang

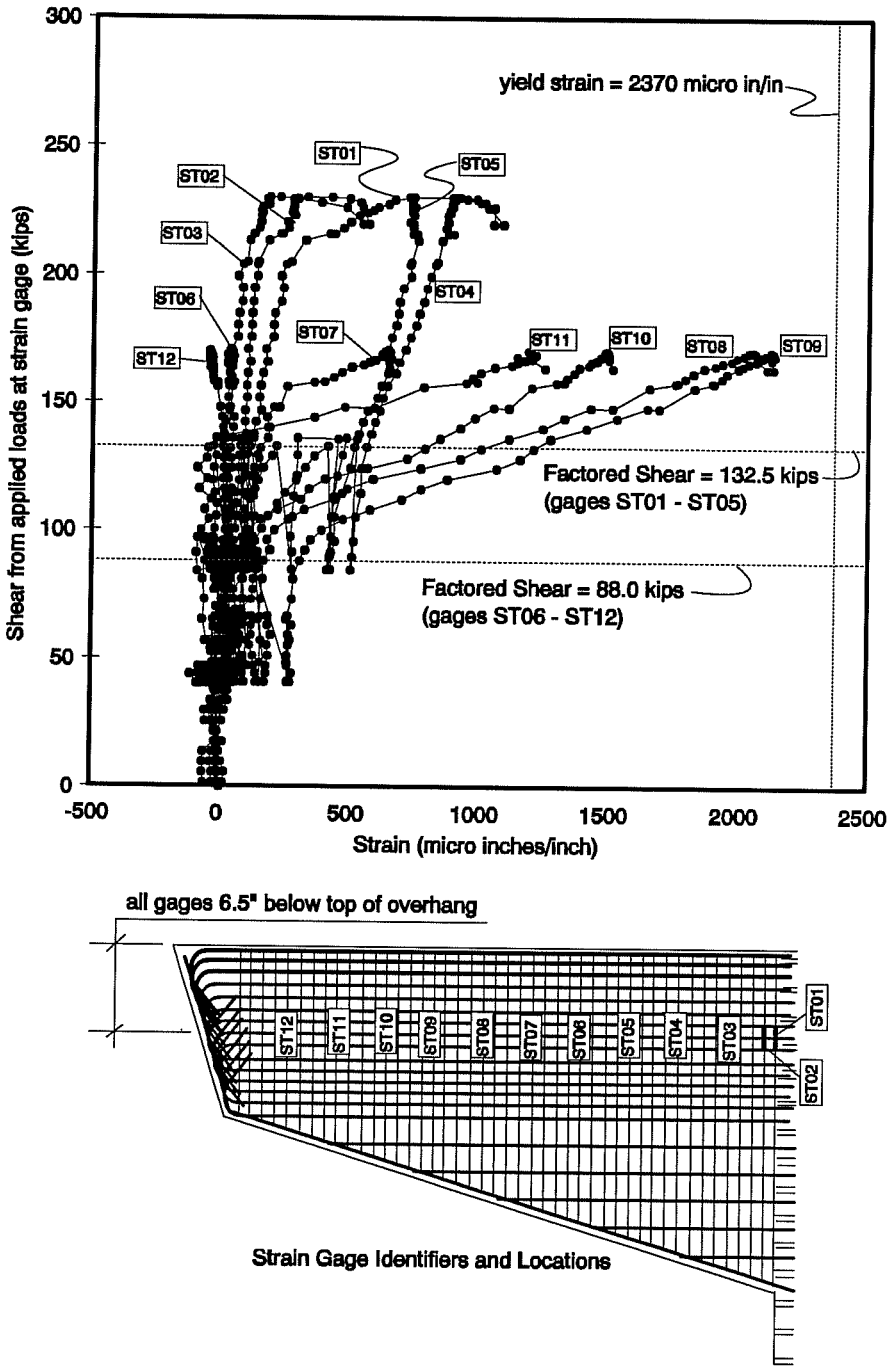

Figure 3.23 Strain Gages on Shear Stirrups in CO-RU (north) Overhang

However, at factored load levels, none of the side face nor shear-friction reinforcement had yielded.

Figure 3.23 shows results of the strain gages on the vertical shear stirrups. These reveal that no yielding of the vertical shear reinforcement was recorded. The most significant straining on the vertical stirrups was recorded on gages ST08, ST09, ST10, and ST11. These gages were located in the vicinity of cracks which formed parallel to the compression strut from the outside reaction. It can also be observed that at factored loads, straining of all stirrups was quite small with the maximum strains limited to approximately 500 micro inches/inch.

3.9.3 CO-PS-100S Overhang

Gaging of the reinforcement in this overhang was similar to the CO-RU overhang in that most of the gages were placed in only one overhang. In this overhang most of the gages were in the south overhang. Examination of gages in both overhangs revealed that steel strains were similar in both overhangs, so only results from the south overhang are presented.

Figures 3.24 and 3.25 show results of the strain gages on the shear-friction and side face reinforcement. The figures show that this horizontal reinforcement was well below yield at factored loads but at final failure had yielded at the face of the column.

In this overhang, almost no strains were recorded on the vertical stirrups so no plots are shown for these gages. The vertical shear stirrups were the same for this overhang as the CO-RU overhang and the same number and location of gages were used. The maximum strain in all gages was recorded on the second stirrup from the face of the column (see ST02 in Figure 3.23). The strain recorded by this gage was only 503 micro inches/inch at ultimate loads. The strain in this gage at factored flexure loads was only 104 micro inches/inch. This is not surprising since there was very little inclined cracking in this overhang, and no cracking in the outer region of the overhang in the vicinity of the compression strut from the outside reaction. It can be concluded from these observations that the shear capacity of the overhang would have been quite high even with a significant reduction in stirrups.

3.9.4 CO-PU-100S-I Overhang

Figures 3.26 and 3.27 show the results from the strain gages on the horizontal shear and side face reinforcement. These figures show that at maximum loads the horizontal shear

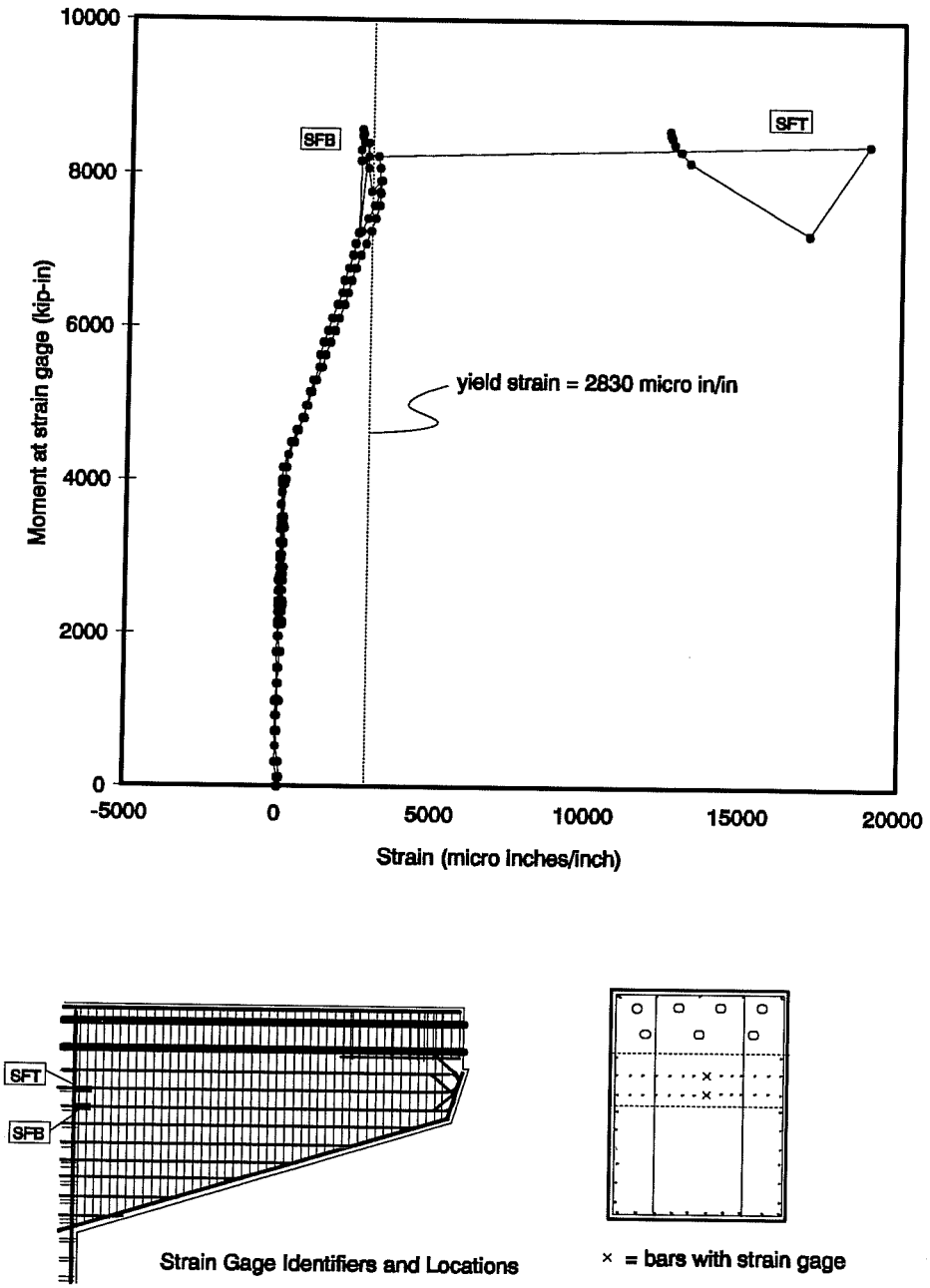

Figure 3.24 Strain Gages on Shear-Friction Reinforcement in CO-PS-100S (south) Overhang

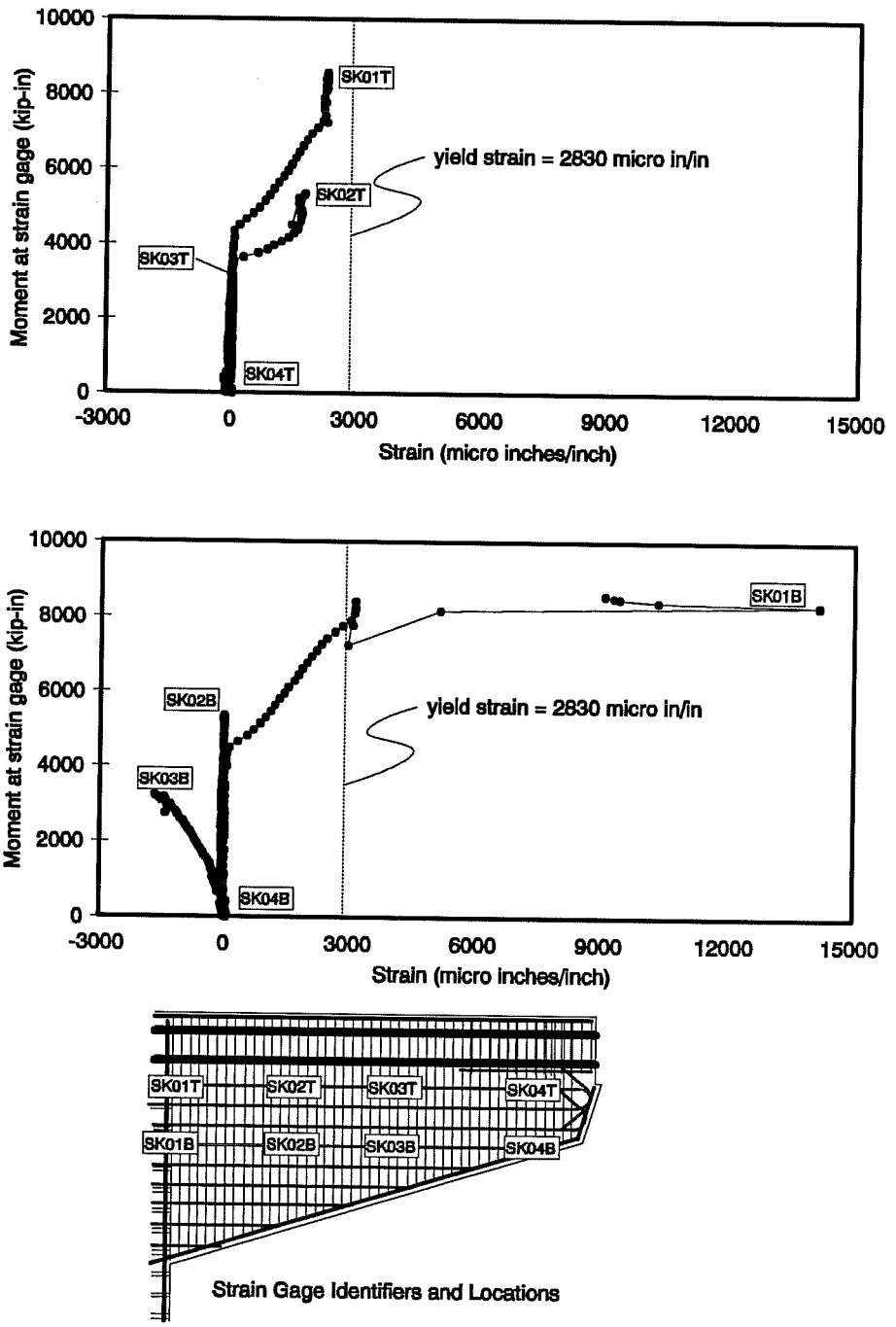

Figure 3.25 Strain Gages on Side Face Reinforcement in CO-PS-100S (south) Overhang

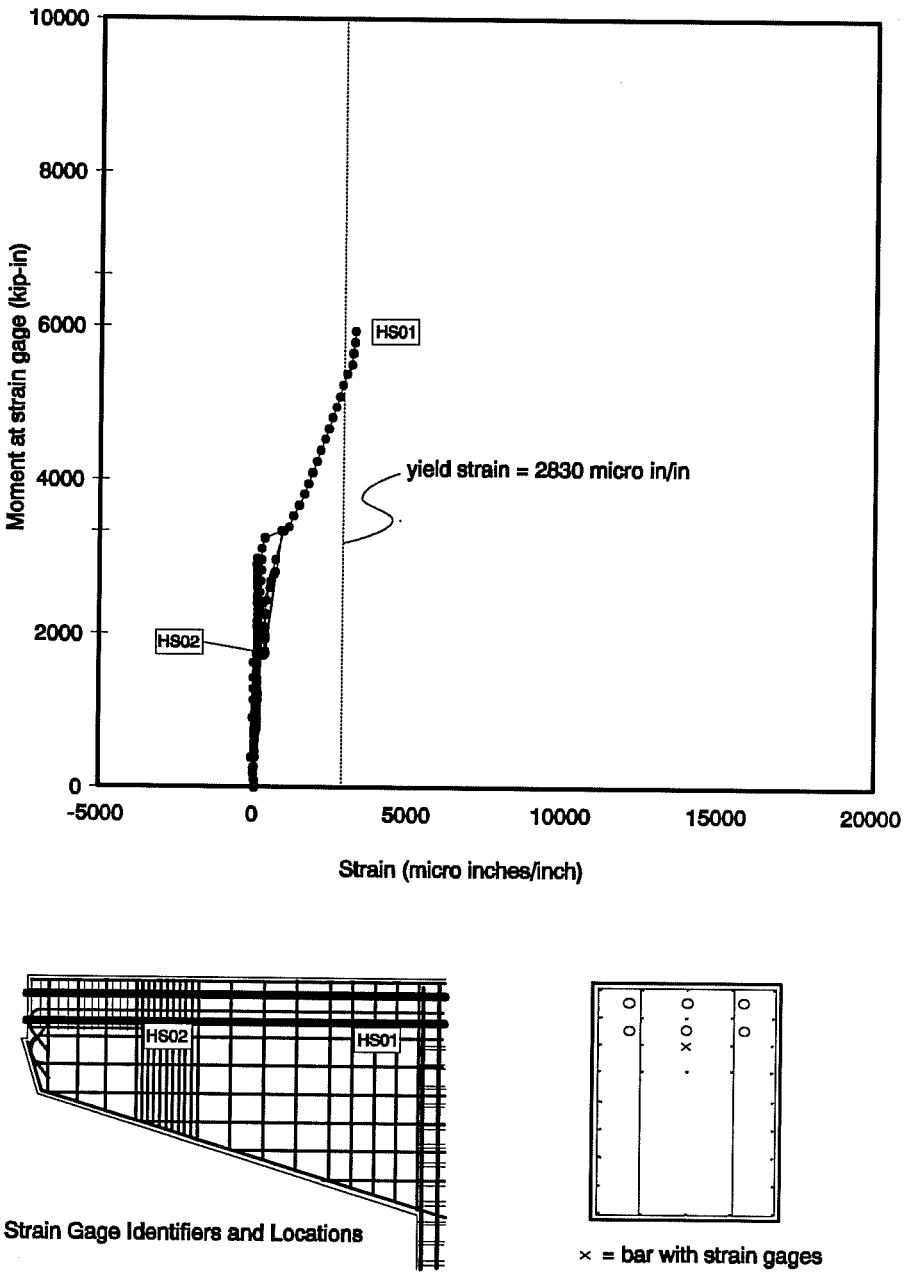

Figure 3.26 Strain Gages on Horizontal Shear Reinforcement in CO-PU-100S-I Overhang

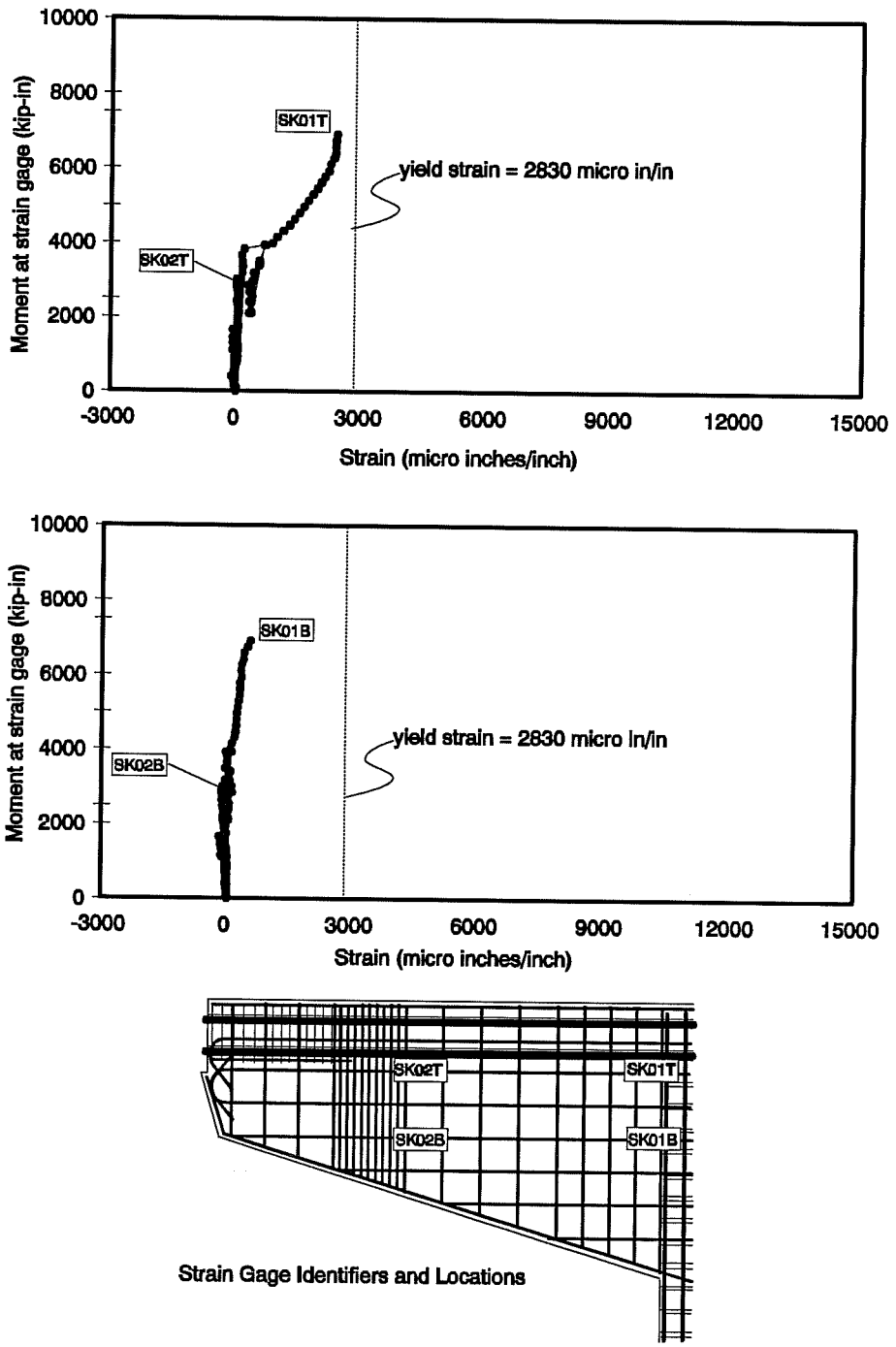

Figure 3.27 Strain Gages on Side Face Reinforcement in CO-PU-100S-I Overhang

reinforcement yielded at the face of the column even though this overhang was not loaded to failure.

The locations of strain gages used on the vertical shear stirrups are shown in Figure 3.28. No plots are given for any of these gages because only minimal strains were recorded. The maximum strain was recorded on gage ST01 which was 1370 micro inches/inch at maximum test loads and 225 micro inches/inch at factored flexure loads. Gage ST02 recorded the next highest strains which were 800 micro inches/inch at maximum test loads and 135 micro inches/inch at factored flexure load. These strains are very low at factored loads. Furthermore, gages on stirrups located in the vicinity of the anticipated shear crack shown in Figure 2.9 were even lower suggesting that the shear capacity of the overhang in this region would have been quite high even with significantly fewer stirrups.

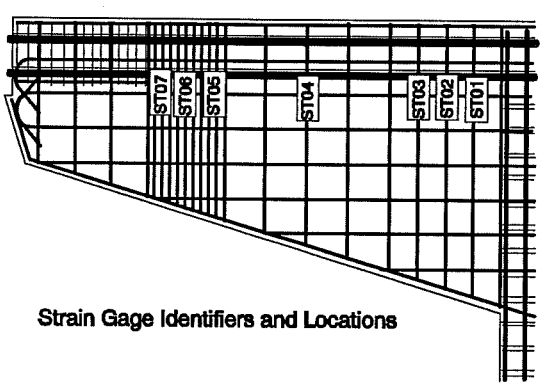

Figure 3.28 Strain Gages on Shear Stirrups in CO-PU-100S-I Overhang

3.9.5 CO-PU-100S-V Overhang

Figure 3.29 shows the results from the strain gages on the side face reinforcement. This figure shows that the side face reinforcement was well below yield at factored loads but by ultimate load had yielded at the face of the column.

The locations of strain gages used on the vertical shear stirrups are shown in Figure 3.30. The recorded strains on these gages were even lower than for the CO-PU-100S-I overhang. The maximum strain was recorded on gage ST20 which was 126 micro inches/inch at ultimate loads

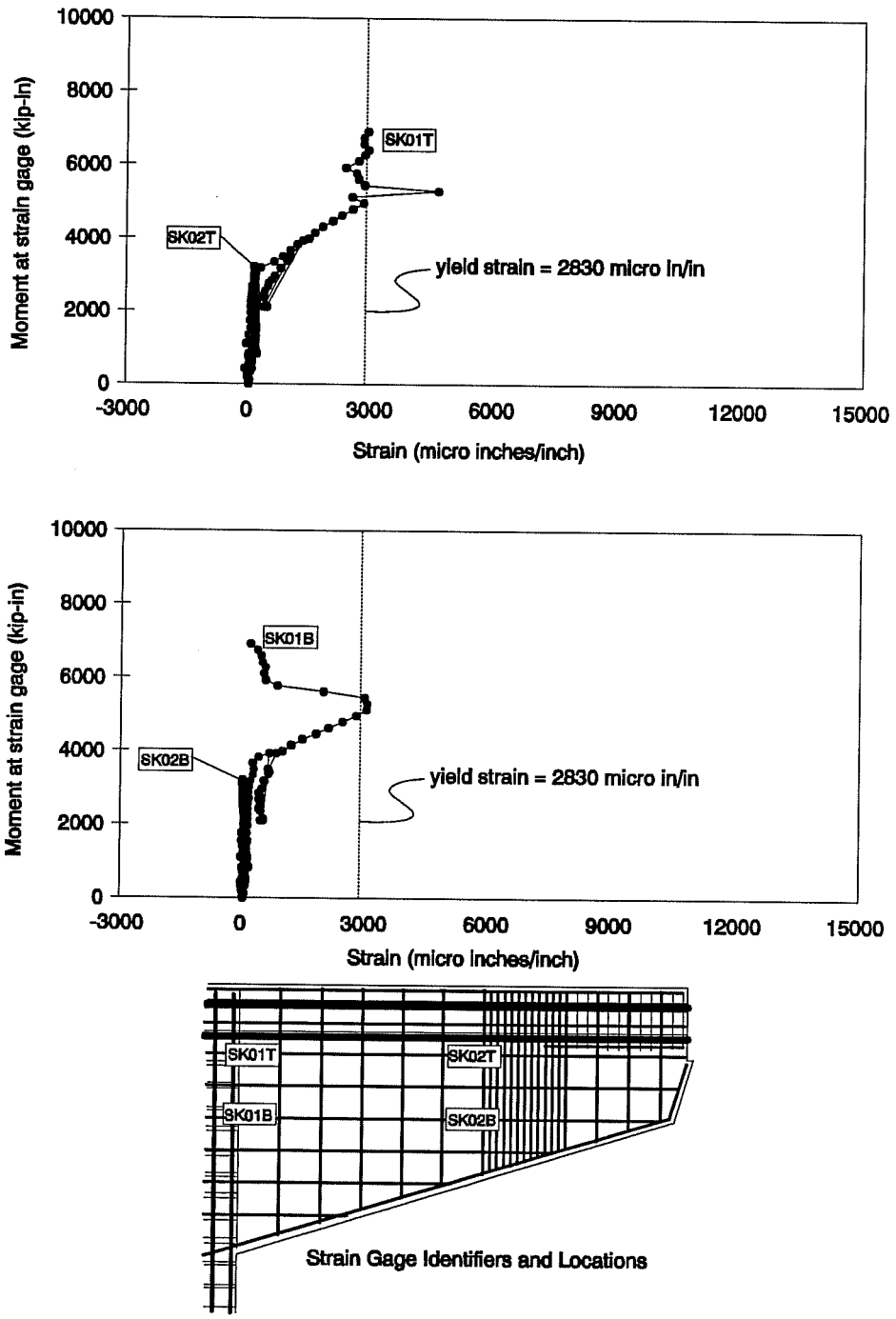

Figure 3.29 Strain Gages on Side Face Reinforcement in CO-PU-100S-V Overhang

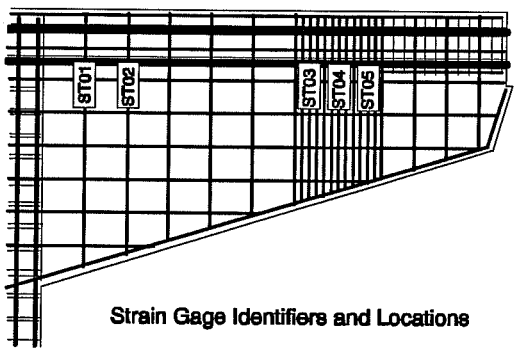

Figure 3.30 Strain Gages on Shear Stirrups in CO-PU-100S-V Overhang

and 32 micro inches/inch at factored loads. Again it can be said that the shear capacity of this overhang would have been quite high even with substantially fewer stirrups.

3.9.6 CO-PU-74S-I Overhang

Figures 3.31 through 3.33 show the results from the strain gages on the non-prestressed moment, horizontal shear, and side face reinforcement. These figures show that near factored loads the horizontal reinforcement yielded at the face of the column. The strain gage on the primary moment reinforcement at the face of the column (M01) was not working after the fabrication of the specimen so no results are shown for this gage.

Figure 3.34 shows the results of the strain gages on the vertical shear stirrups. Only a slight increase in stirrup strains can be observed over that of the vertical stirrups in the CO-PU-100S-I overhang. These strains are also quite low at both factored and maximum test loads. It can be concluded that the shear capacity of this overhang would have been substantial even with significantly fewer stirrups.

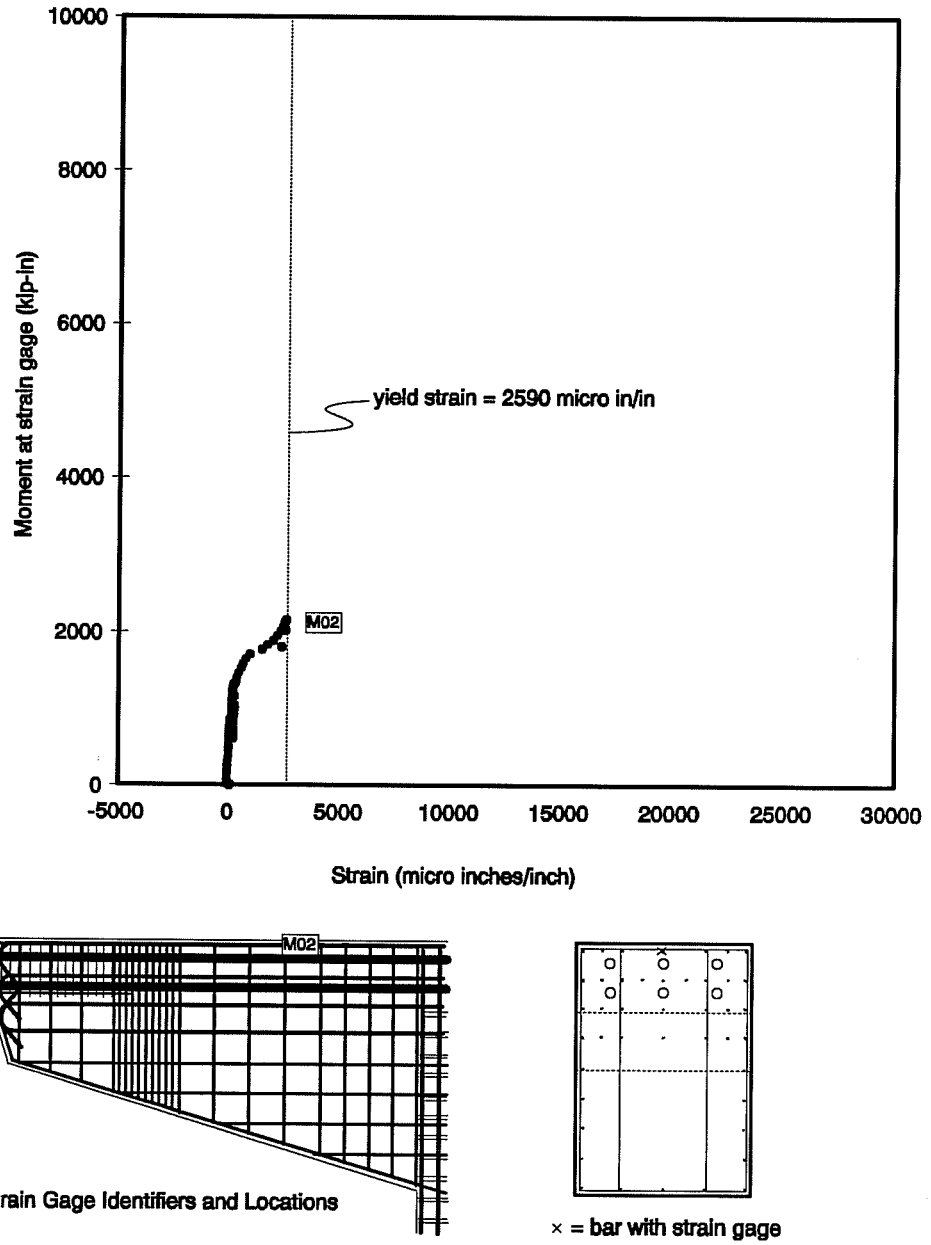

Figure 3.31 Strain Gages on Non-Prestressed Moment Reinforcement in CO-PU-74S-I Overhang

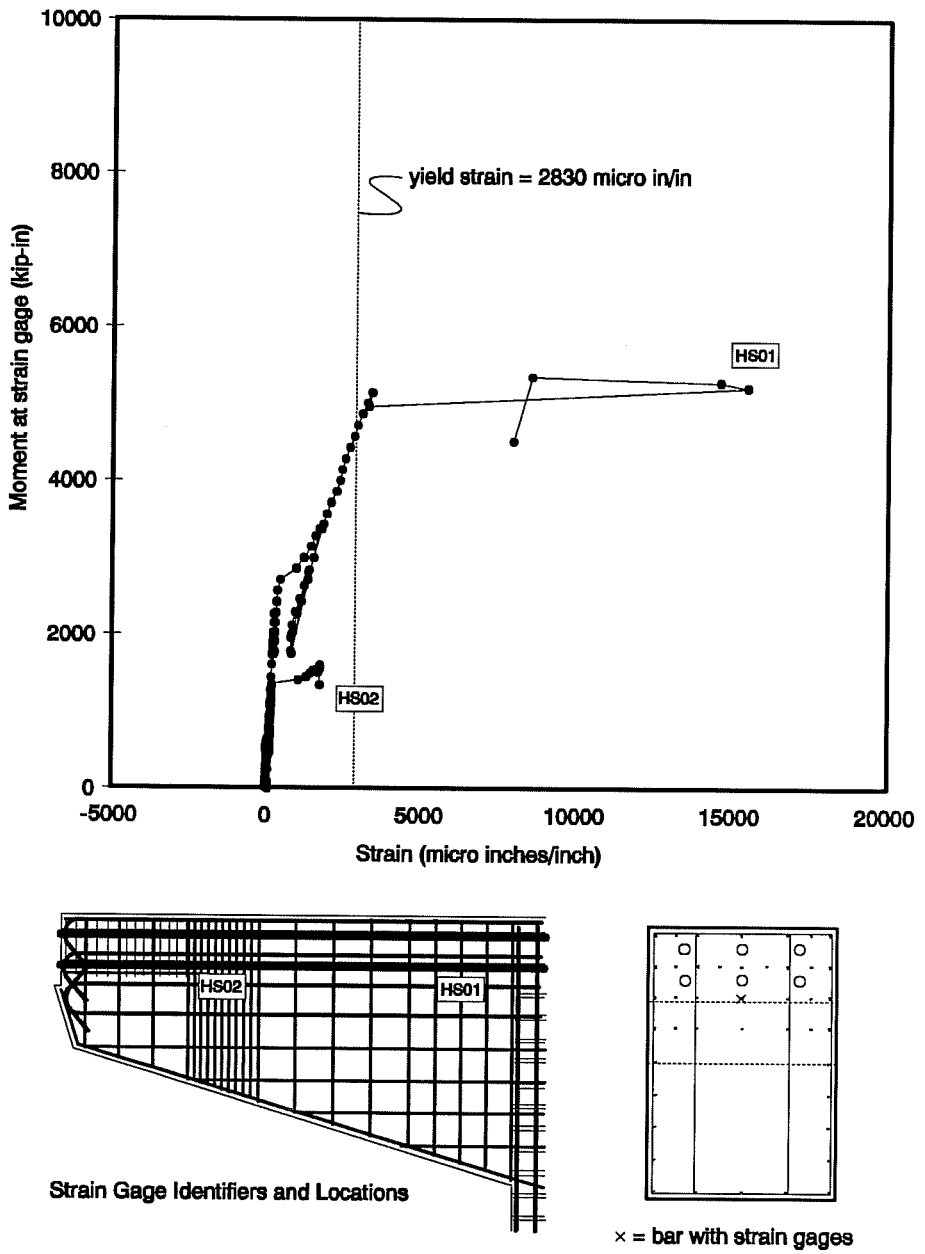

Figure 3.32 Strain Gages on Horizontal Shear Reinforcement in CO-PU-74S-I Overhang

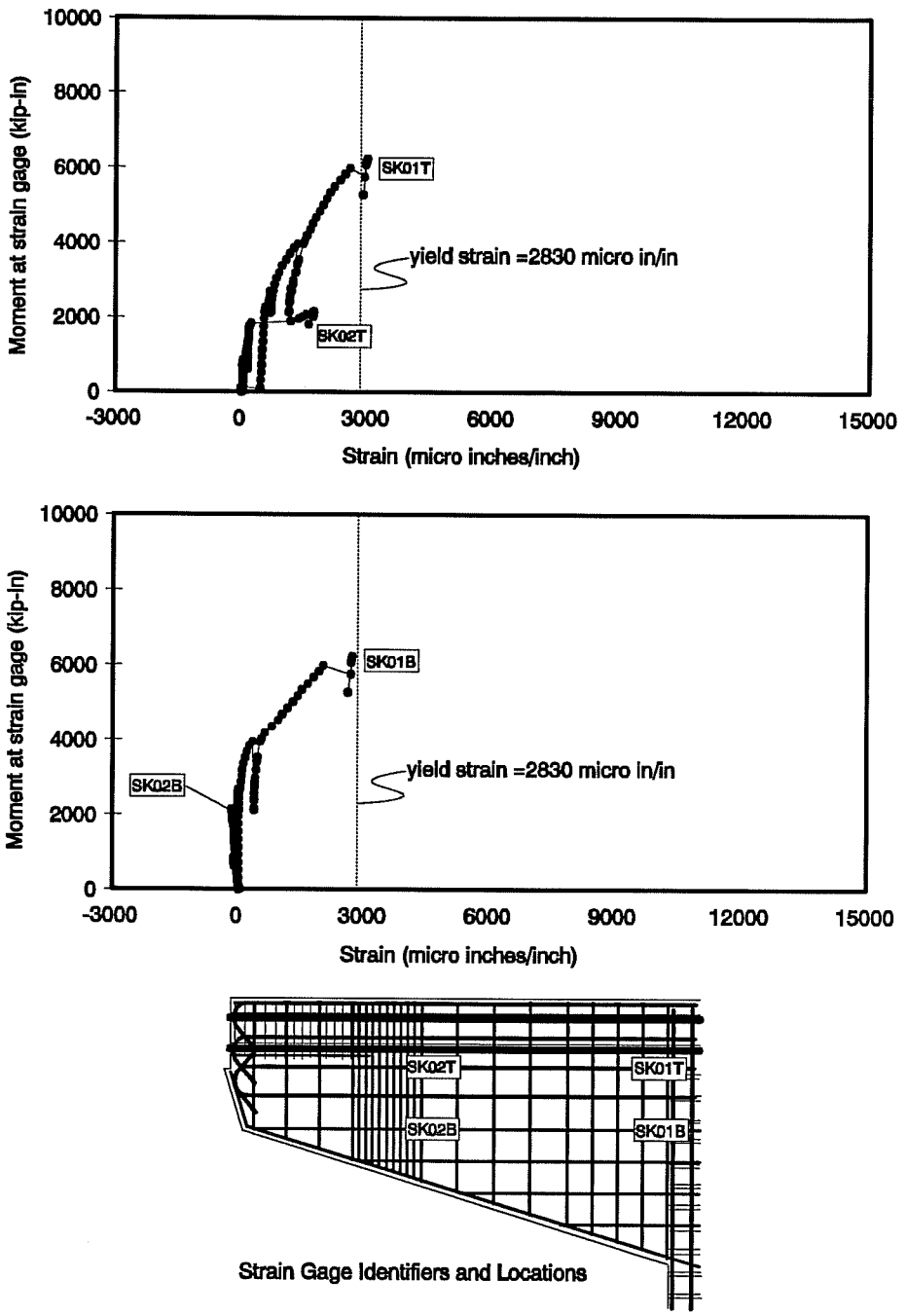

Figure 3.33 Strain Gages on Side Face Reinforcement in CO-PU-74S-I Overhang

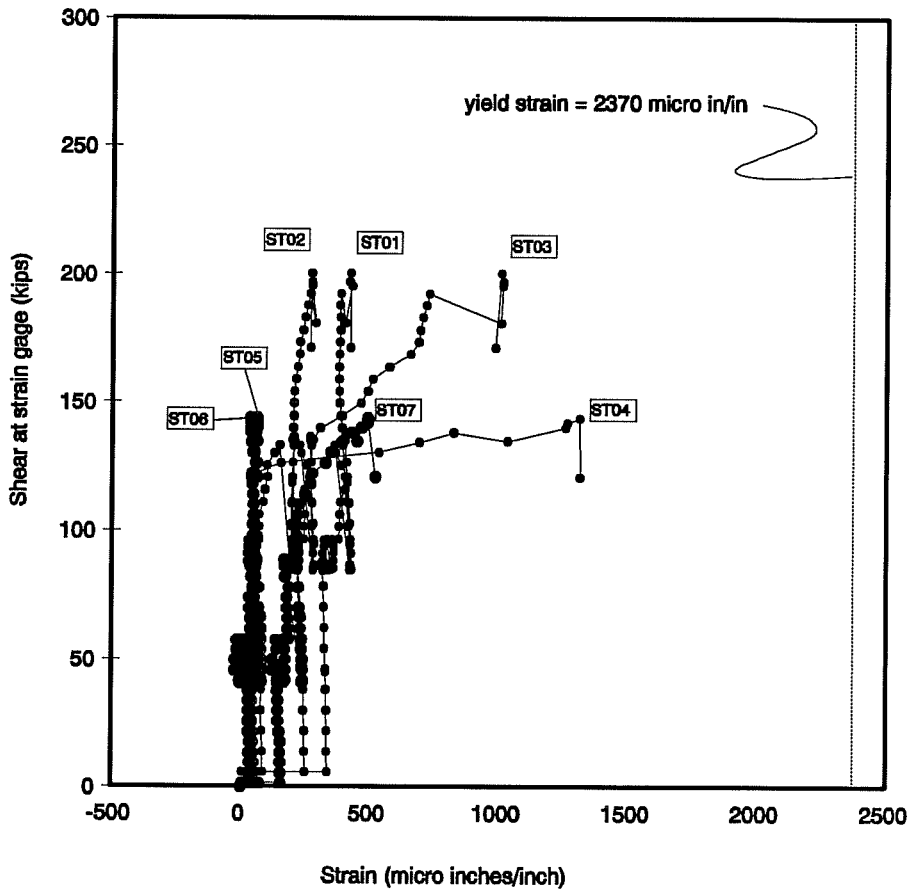

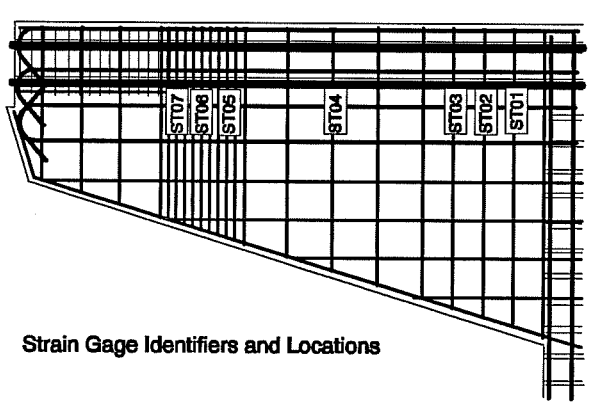

Figure 3.34 Strain Gages on Shear Stirrups in CO-PU-74S-I Overhang

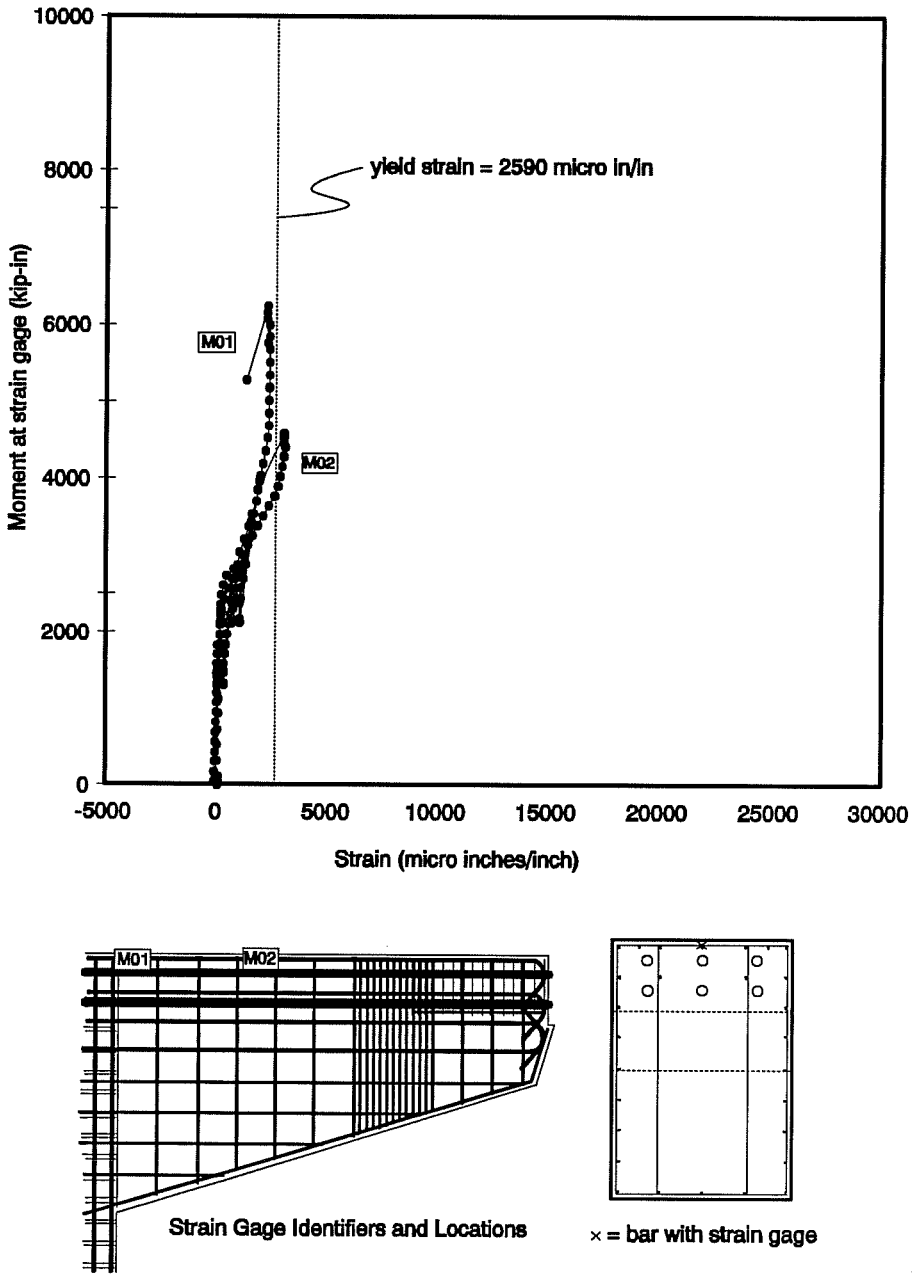

Figure 3.35 Strain Gages on Non-Prestressed Moment Reinforcement in CO-PU-74S-V Overhang

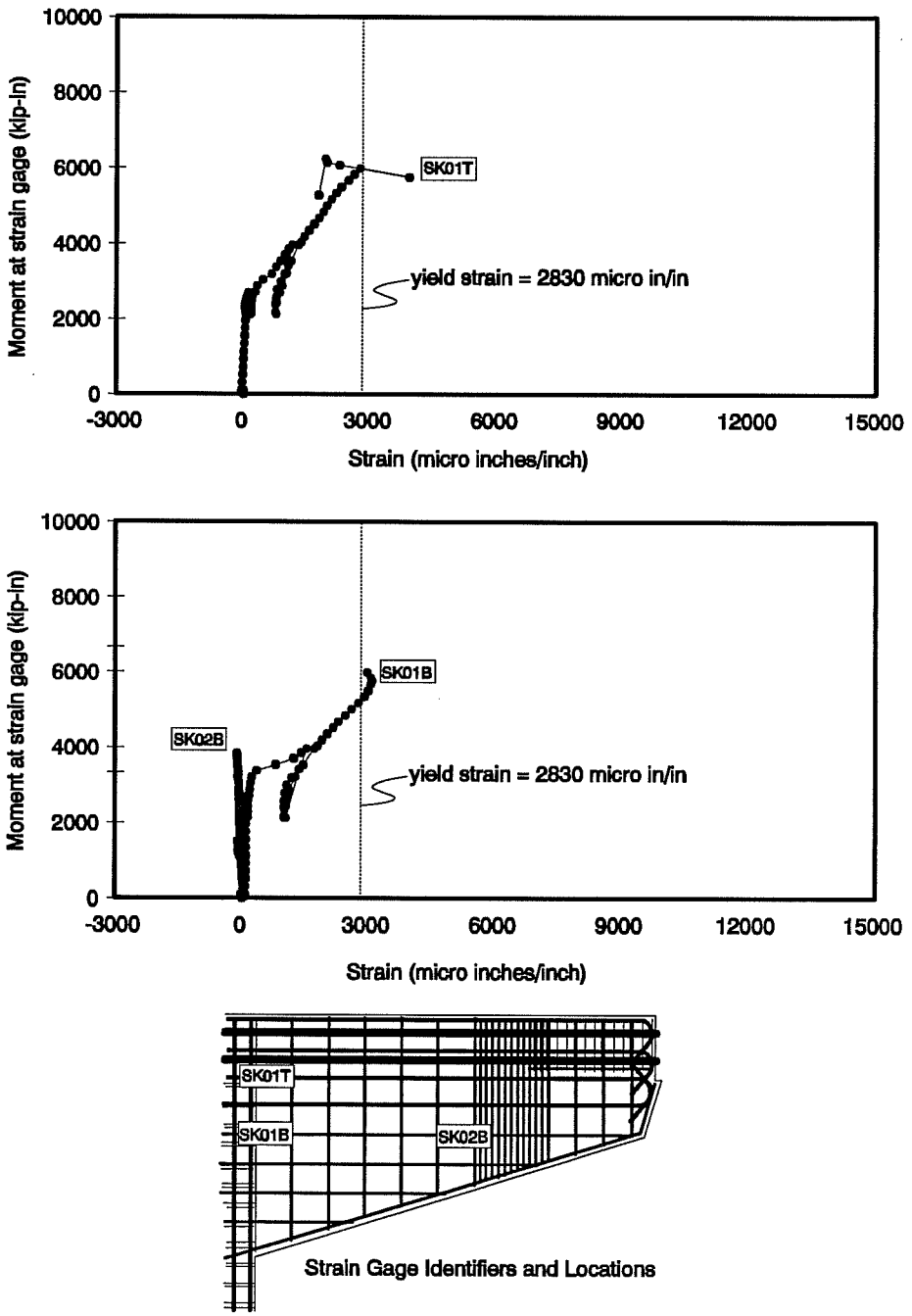

Figure 3.36 Strain Gages on Side Face Reinforcement in CO-PU-74S-V Overhang

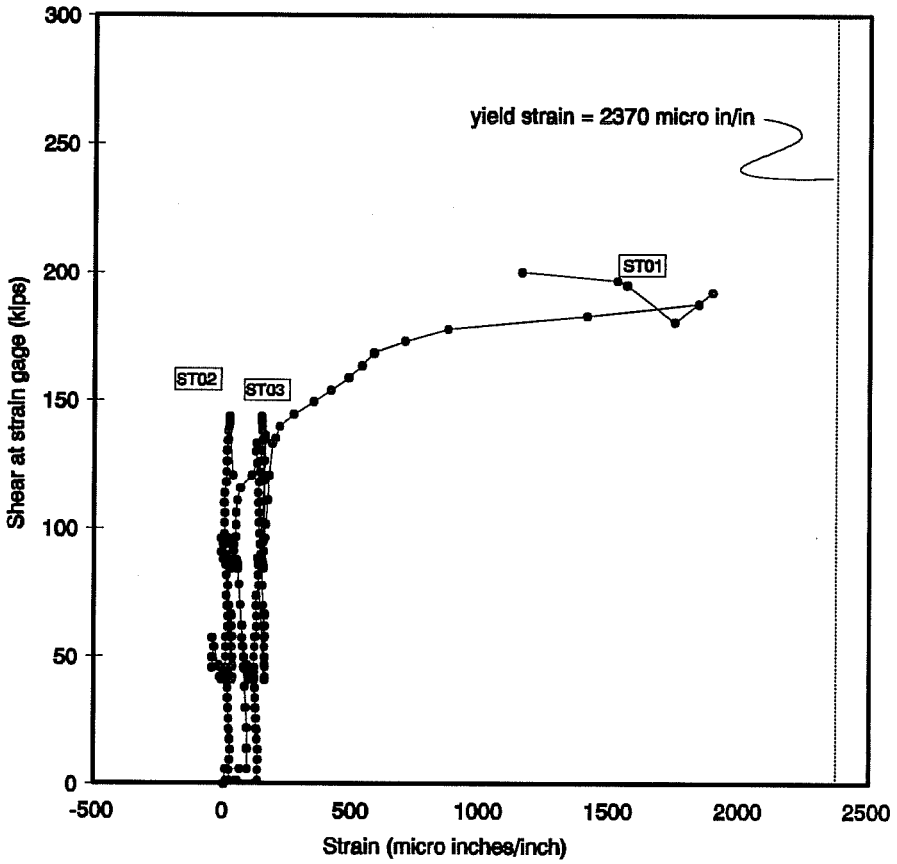

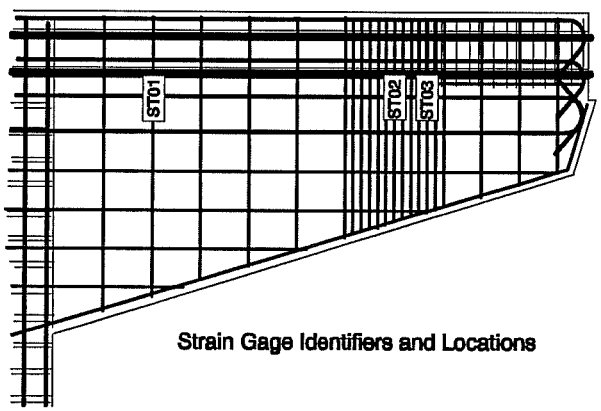

Figure 3.37 Strain Gages on Shear Stirrups in CO-PU-74S-V Overhang

3.9.7 CO-PU-74S-V Overhang

Figures 3.35 and 3.36 show the results from the strain gages on the non-prestressed moment and side face reinforcement. These figures show that the main flexural horizontal reinforcement was yielded at the face of the column even below factored load level and stayed at yield strain as substantially higher load was applied. The skin steel began working around service load level and yielded by ultimate loads.

Figure 3.37 shows the results of the strain gages on the vertical shear stirrups. Again it can be concluded that the shear capacity of this overhang would have been substantial even without any stirrups.

3.9.8 Summary of Strain Gage Results

The strain gage results confirm that yielding of the horizontal tensile reinforcement was occurring in all overhangs when the maximum test loads were reached. This is consistent with the typical flexural failure observed for each of the failed overhangs.

None of the gages on the vertical reinforcement recorded yield strains. The most significant strains were recorded on the stirrups in the CO-RU overhang, which is consistent with the higher number of inclined cracks observed in this overhang. Strains recorded on the stirrups in all of the prestressed overhangs except for CO-PU-74S-V were very low, suggesting that these overhangs would have had considerable shear capacity even with substantially fewer stirrups. The stirrups in the CO-PU-74S-V overhang near the support were very lowly stressed at factored load levels but did increase to about 85% yield at ultimate load.

3.10 Post Mortem Investigation

Each specimen was examined after the completion of testing to determine the condition of the reinforcement.

The concrete was removed from the maximum moment region of both overhangs of each specimen using a jack hammer. In both CO-RU overhangs and in the CO-PU-100S-I and CO-PU-100S-V overhangs, no fractured bars or evidence of necking down of any of the reinforcement was detected. In the north CO-PS-100S overhang, the two No. 2 reinforcing bars and the outer two 7 gauge wires in the top level of reinforcement were found to have fractured (see Figure

3.38). In the CO-PU-74S-V overhang, eleven No. 2 reinforcing bars on the south overhang were found to be fractured (see Figure 3.39).

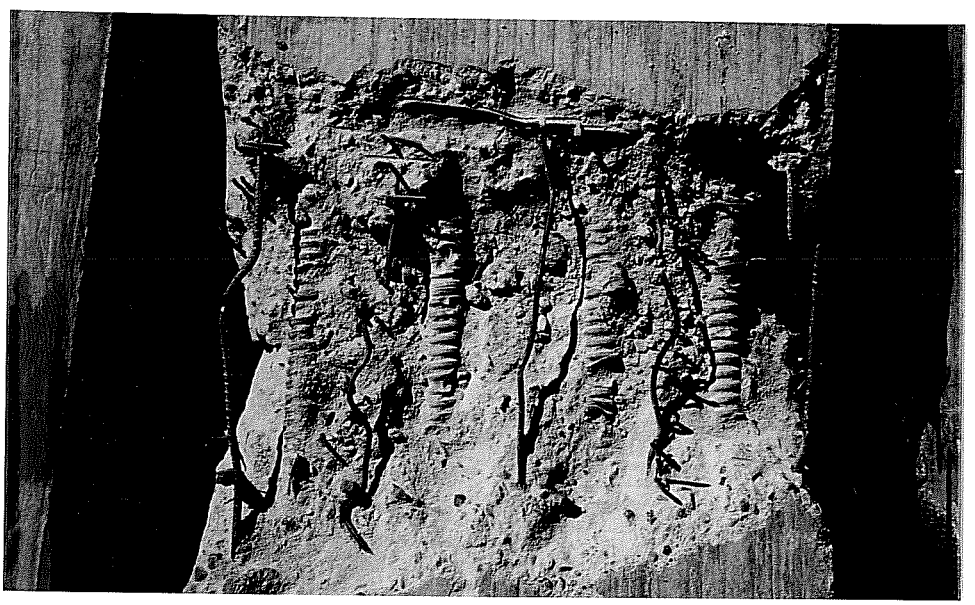

Figure 3.38 Fractured Tension Reinforcement in north CO-PS-100S Overhang

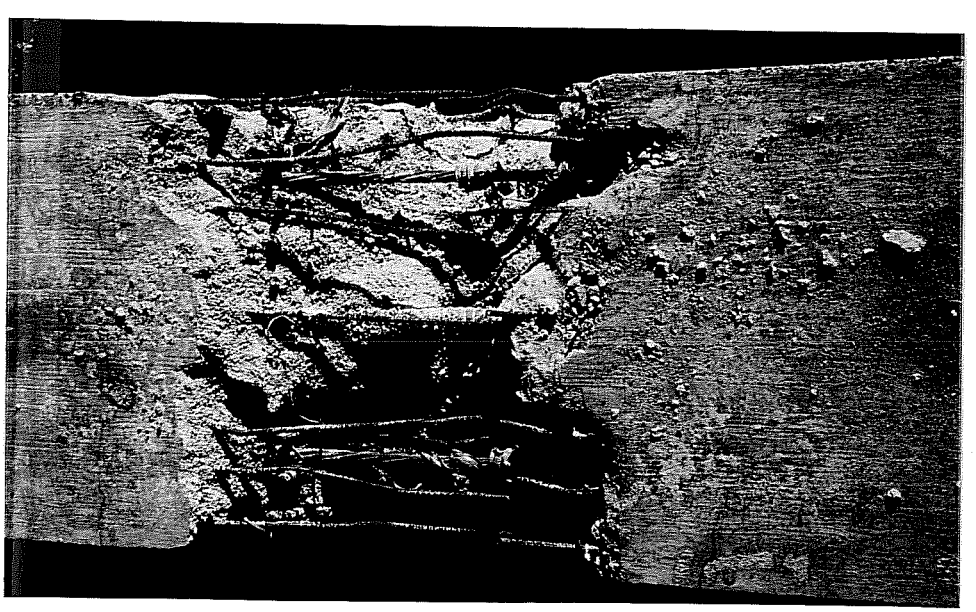

Figure 3.39 Fractured Tension Reinforcement in CO-PU-74S-V Overhang

All strands in the top level of each of the post-tensioned overhangs were removed from the specimens and the ducts and grout were removed from the strands. No broken strands or wires were detected.

CHAPTER 4
ANALYSIS OF TEST RESULTS

4.1 Comparison of Test Cracking Moments to Service Load Moment and Predicted Cracking Moments

Table 4.1 provides the ratio of the test cracking moment to the service flexure moment (2749 k-in) for each overhang. These ratios are plotted in Figure 4.1 which clearly shows the variation between overhangs.

Specimen #	Overhang	Observed Cracking Moment, Mcr Test (kip-in)	Mcr Test / M service	Predicted Cracking Moment, Mcr Pred (kip-in)	Mcr Test / Mcr Pred
1	CO-RU (north and south)	1394	0.51	1286	1.08
2	CO-PS-100S (north)	3272	1.19	2857	1.15
3	CO-PU-100S -I	3087	1.12	2611	1.18
	CO-PU-100S-V	2923	1.06	2607	1.12
4	CO-PU-74S--I	2499	0.91	2102	1.19
	CO-PU-74S-V	2222	0.81	2101	1.06

Table 4.1 Comparisons of Observed Cracking Moments to Service Moment and Predicted Cracking Moments

As mentioned in Section 3.2, the CO-RU overhang was cracked before the full dead load moment (2169 k-in) was applied. The CO-PU-74S-I and CO-PU-74S-V overhangs were cracked at loads above dead load but, as shown in Figure 4.1, were cracked below the service flexure moment. The CO-PS-100S, CO-PU-100S-I, and CO-PU-100S-V overhangs did not crack until loads above service flexure loads.

For those overhangs which cracked above service flexure loads, calculations were made to determine the multiple of the live load plus impact moment (580 k-in) that was acting in

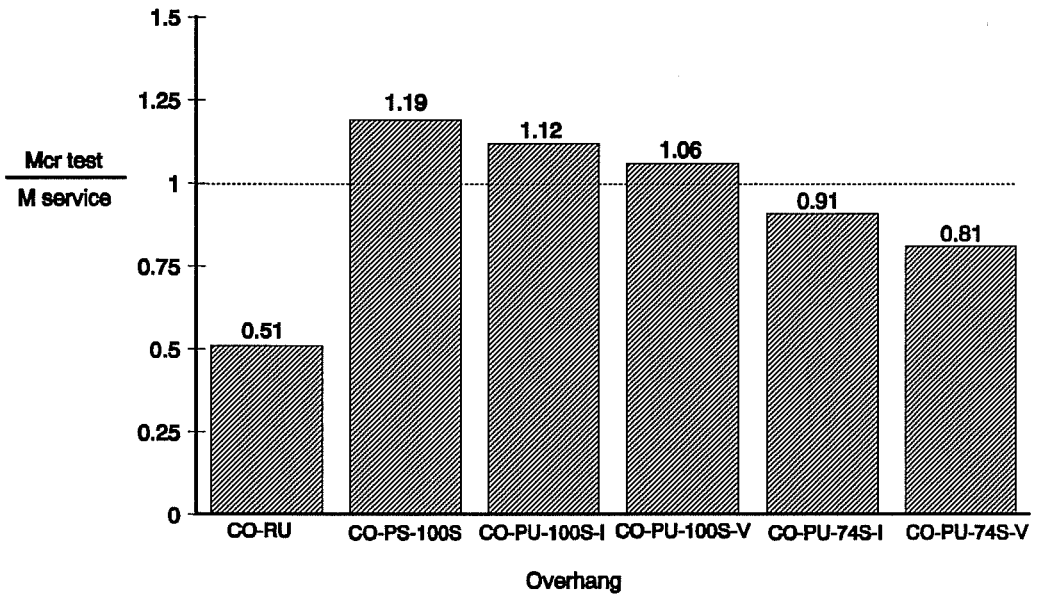

Figure 4.1 Ratio of Test Cracking Moments to Service Flexure Moment

combination with dead load moment to crack the overhang. For the CO-PS-100S overhang, the cracking moment corresponded to dead load plus 1.86 times the service flexure live loads plus impact. For the CO-PU-100S-I and CO-PU-100S-V overhangs, the cracking loads corresponded to dead load plus 1.54 and 1.26 times the service flexure live loads plus impact.

A prediction was made of the cracking moment for each overhang. The predicted cracking moment was determined from the load levels required to produce an extreme top fiber tensile stress in the concrete of $7.5\sqrt{f_c'}$, with the moment of inertia based on an uncracked transformed section.

The predicted cracking moments are also shown in Table 4.1, along with comparisons of the observed to predicted moments. For each overhang, it was found that the observed cracking loads were slightly higher than the predicted.

The fact that the observed cracking moments are consistently higher than the predicted is probably somewhat due to the difficulty of detecting a crack when it originates and may also

be a result of the concrete tensile strength being slightly above $7.5\sqrt{f_c'}$. Another possible reason for the difference could be lateral resistance provided by the test setup, as described in Section 3.5. It is important to note that some restraint of this type would be provided by the transverse stiffness of the superstructure in an actual bridge, since the bearings are restrained from movement in the transverse direction. On the other hand, the fact that the observed cracking loads in all of the prestressed specimens were higher than the predicted suggests that the stress in the post-tensioning was at least as high as the intended value of 160 ksi.

If the overhangs had cracked at the predicted moments, the CO-RU overhang would still have been cracked well below the dead load moment. The CO-PS-100S overhang would have been cracked at the dead load plus 1.19 times the service flexure live loads plus impact. The CO-PU-100S-I and CO-PU-100S-V overhangs would have cracked above dead load but before the full live load was reached. The CO-PU-74-I and CO-PU-74S-V overhangs would have been cracked slightly below the dead load moment.

It is noted that the concrete compressive strength for the CO-PU-100S overhangs was significantly higher than the assumed design strength of 5000 psi. If the concrete strength was equal to 5000 psi, both overhangs would have been expected to crack at slightly lower loads. Predicted cracking moments based on f'_c = 5000 psi would be revised to 2374 k-in for the CO-PU-100S-I overhang and 2371 k-in for the CO-PU-100S-V overhang. These values are even further below the service flexure moment but still above the dead load moment. Even if these revised predicted values are adjusted upward to reflect the same ratios of observed to predicted cracking moments as occurred in the test, the CO-PU-100S-I overhang would be expected to crack at 2801 k-in, which is only slightly above the service flexure moment, and the CO-PU-100S-V overhang would be expected to crack at 2655 k-in, which is slightly below the service flexure moment.

It is further observed that even the cracking moment of the CO-PS-100S overhang was not so high that the possibility of the overhang cracking can be ruled out altogether. If losses were high and prestress application was low due to friction, seating, etc., it is feasible that even this overhang could crack from an overload.

4.2 Fatigue Considerations

One consequence of an overhang being cracked at service loads is that the stress range experienced by the reinforcement (non-prestressed or prestressed) resulting from loads cycling between dead load and service loads will be increased over what would be experienced in a member that remains uncracked under service loads (ie. a fully prestressed overhang). This is important because the fatigue life of the reinforcement is reduced when subjected to higher stress ranges. An additional concern for prestressed reinforcement is the maximum level of stress in the reinforcement at service loads. As shown if Figure 4.1, the CO-RU, CO-PU-74S-I, and CO-PU-74S-V overhangs were cracked at service loads and the CO-PU-100S-I and CO-PU-100S-V overhangs could reasonably be expected to be cracked at or slightly above service loads.

Calculations were made for each overhang to determine the expected stress range in the top level of reinforcement. A cracked transformed section and an effective post-tensioning stress of 160 ksi were assumed in the calculations. The results of the calculations are shown in Table 4.2

Specimen #	Overhang	Stress in top bar or tendon at dead load, F-dl (ksi)	Stress in top bar or tendon at service flexure loads, F-serv (ksi)	Stress Range in top bar or tendon (F-serv) - (F-dl) (ksi)	F-serv / Fpu
1	CO-RU	31	39	8	********
2	CO-PS-100S	160	162	2	0.60
3	CO-PU-100S-I	161	170	9	0.63
	CO-PU-100S-V	161	171	10	0.63
4	CO-PU-74S-I	170	185	15	0.69
	CO-PU-74S-V	171	188	18	0.70

Table 4.2 Calculated Reinforcement Stresses at Dead Load and Service Load

The acceptability of the stress range for the CO-RU overhang was evaluated on the basis of the current AASHTO criteria. AASHTO Equation (8-60) gives the maximum allowable stress range as

$$f_f = 21 - 0.33f_{min} + 8(r/h) \qquad [4\text{-}1]$$

where f_f = stress range in ksi,

f_{min} = algebraic minimum stress level = 31 ksi, and

r/h = ratio of base radius to height of rolled on transverse deformations = 0.3.

From Equation [4-1] it was determined that the maximum allowable stress range, f_f, was equal to 13.2 ksi, which is greater than the calculated expected value of 8 ksi.

As shown in Table 4.2, the calculated stress ranges in the post-tensioning strand varied from a minimum of 2 ksi in the CO-PS-100S overhang to a maximum of 17 ksi in the CO-PU-74S-V overhang. For post-tensioned strand in metal ducts, Wollmann et al. (6), have recommended a maximum stress range of 14.5 ksi to ensure two million load cycles. The calculated stress ranges for both CO-PU-100S overhangs were below this value. However, the calculated stress ranges for both CO-PU-74S overhangs were slightly above the recommended maximum level. The implication of this for design is that measures must be taken to lower the expected stress range. This can be accomplished by adding additional mild reinforcement or by lowering the strand somewhat within the overhang. The latter would necessitate the use of a larger area of prestressed reinforcement.

The maximum calculated service load stress level in the post-tensioning strand was 188 ksi which occurred in the CO-PU-74S-V overhang. The current AASHTO specifications limit the maximum post-tensioning stress to $0.80f^*_y$. If f^*_y is taken as $0.90F_{pu}$, the maximum stress would be limited to $0.72F_{pu}$. On this basis, the maximum calculated stress level in the post-tensioning strand of all overhangs was acceptable.

4.3 Evaluation of Crack Widths

4.3.1 Crack Width Envelopes

To evaluate the crack width performance of each overhang, curves were generated which give the relationship between the moment at the face of the column and the maximum measured

crack width anywhere along the overhang. These curves are referred to as the "crack width envelopes" for each overhang.

The "crack width envelopes" were generated by first plotting the crack width readings of the "major" cracks on an overhang against the moment at the face of the column (see Figure 4.2). A "major" crack was defined in Section 3.4 to be any crack which had the greatest width of all cracks on the overhang at any single load stage. For those overhangs which were cracked before reaching service loads, multiple crack width readings were taken at the same load level because of the loading sequence (ie. loading, unloading, and reloading between dead load, service flexure loads, and service shear loads). Curves were determined for each "major" crack by connecting the maximum measured crack width points at successively increasing load levels as shown in Figure 4.2. Each of these individual "major" crack curves were then overlaid onto an additional graph (see Figure 4.3) and the "crack width envelopes" shown by the heavy lines were determined by connecting the points of maximum crack width for each load level from the "major" crack curves. For the CO-RU specimen, this was done for both overhangs (see Figures 4.4 and 4.5). The north and south overhang envelopes were superimposed onto yet another graph and the combined envelope was determined (see Figure 4.6). This envelope represents the maximum crack width at every load stage anywhere on both overhangs. The CO-PS-100S and CO-PU-100S-I overhangs had only one "major" crack each, so the plot of this crack gave the "crack width envelope" directly. The "major" crack plots and "crack width envelopes" for all remaining overhangs are given in Figures A.1 through A.8 in Appendix A.

The "crack width envelopes" incorporate the readings from the "major" cracks only. Furthermore, crack width readings taken after reaching factored flexure loads (Load Stage # 8) are not included.

4.3.2 Comparison of Overhang Crack Widths

The "crack width envelopes" for each overhang were overlaid onto a single combined display in Figure 4.7. This figure provides a useful reference for the comparison of the cracking performance of each overhang. It shows that at service flexure loads, the CO-PS-100S and CO-PU-100S overhangs were uncracked, and therefore, had the best service load crack width performance. The CO-RU, CO-PU-74S-I, and CO-PU-74S-V overhangs all had the same maximum width of 0.003".

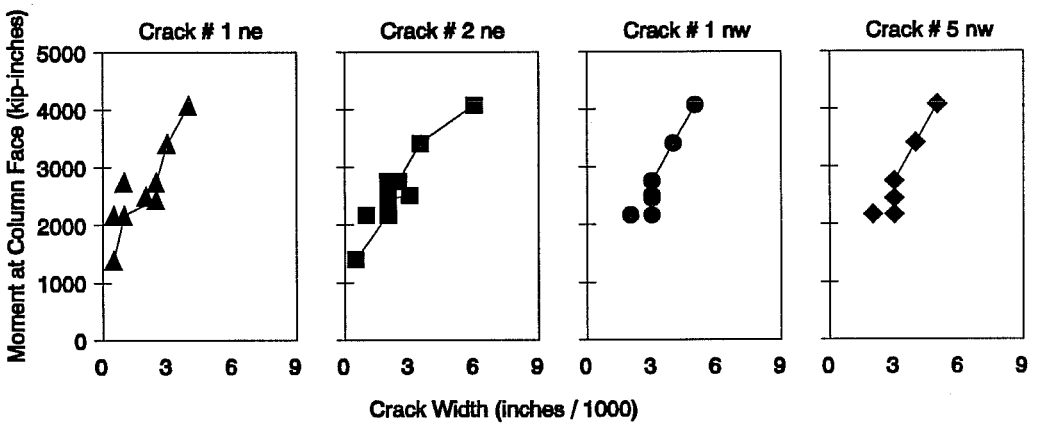

Figure 4.2 "Major" Crack plots for the north CO-RU Overhang

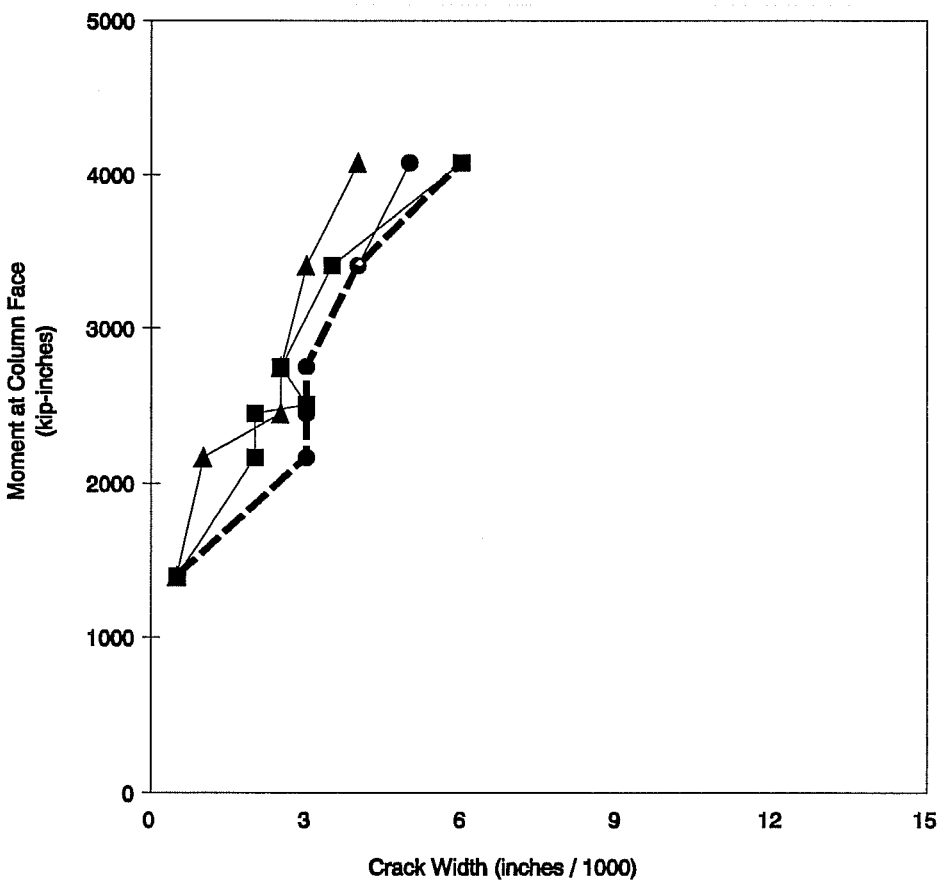

Figure 4.3 "Crack Width Envelope" for the north CO-RU Overhang

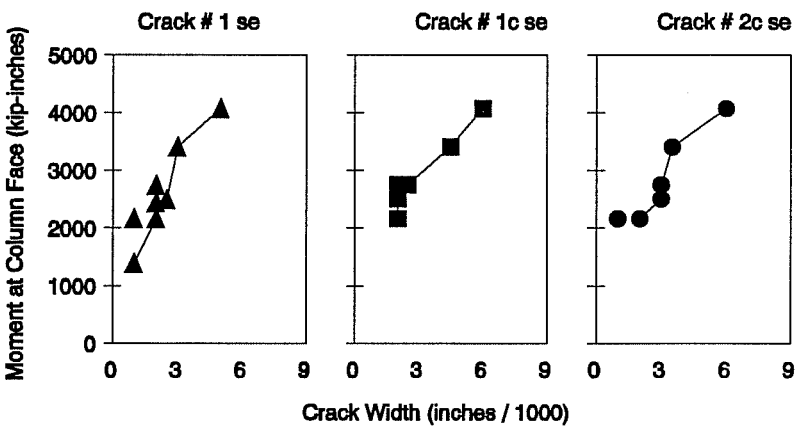

Figure 4.4 "Major" Crack plots for the south CO-RU Overhang

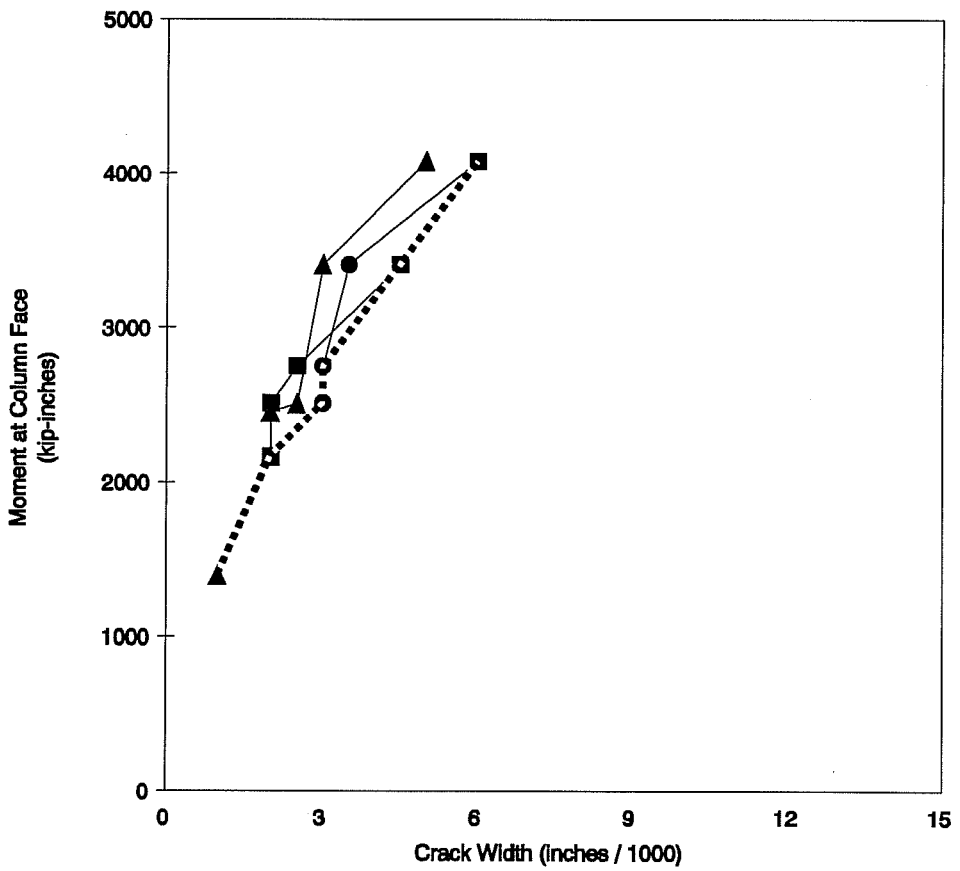

Figure 4.5 "Crack Width Envelope for the south CO-RU Overhang

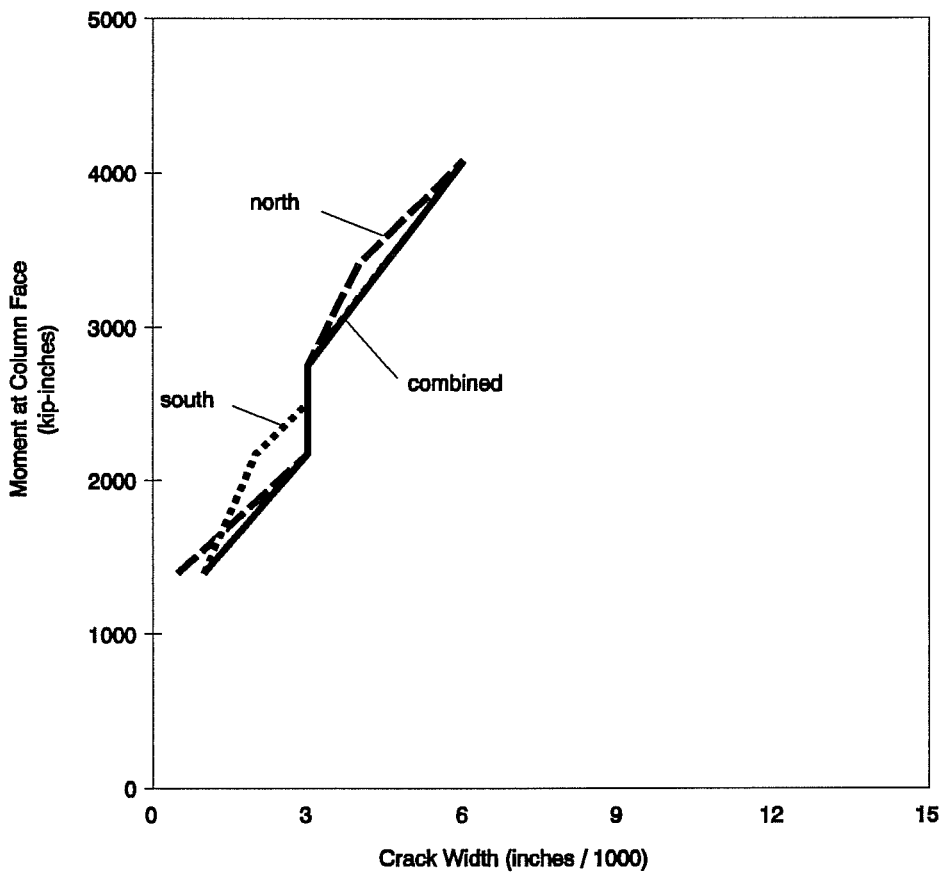

Figure 4.6 Combined "Crack Width Envelope" for the north and south CO-RU Overhangs

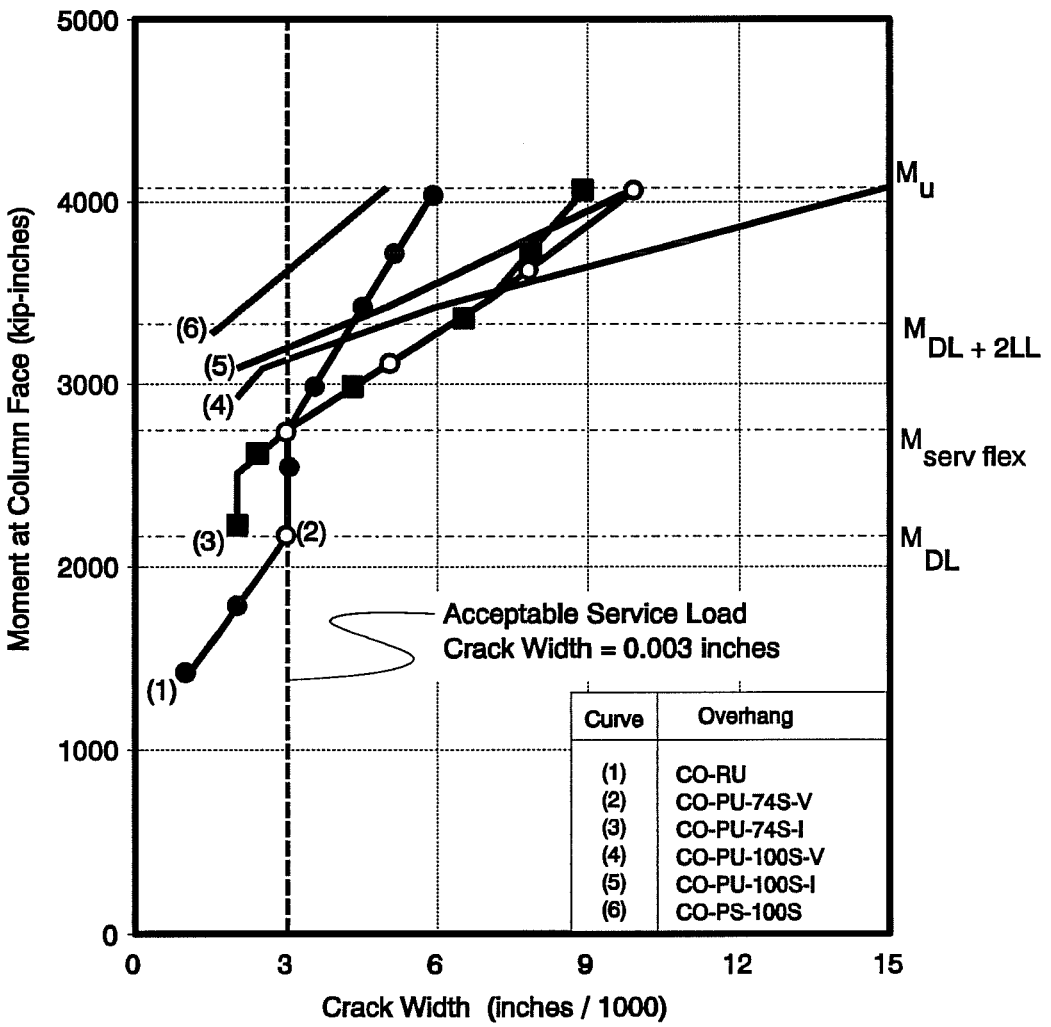

Figure 4.7 "Crack Width Envelopes" for all Overhangs

On Figure 4.7, an acceptable service load crack width of 0.003" is indicated. This is the 5.5 scale equivalent of the implicit limiting crack width value given by AASHTO for reinforced concrete members in moderate exposure conditions.

AASHTO gives the acceptable crack width implicitly in terms of a z factor using AASHTO Equation (8-61) (see Equation [2-4] in Section 2.3.1). Rearranging this expression gives:

$$z = f_s (d_c A)^{1/3} \qquad [4\text{-}2]$$

where z = quantity limiting distribution of flexural reinforcement,

f_s = stress in the reinforcing steel at service loads,

d_c = distance from the outside layer of reinforcement to the extreme fiber,

A = effective tension area of concrete surrounding the flexural tension reinforcement and having the same centroid as that reinforcement, divided by the number of bars or wires.

This equation is based on the following formula proposed by Gergely and Lutz (7) for the maximum probable crack width, w_c:

$$w_c = \frac{0.076}{1000} R f_s (d_c A)^{1/3} . \qquad [4\text{-}3]$$

The R term in this expression is the ratio of h_1 to h_2, where h_1 is the distance from the service load neutral axis to the extreme top fiber and h_2 is the distance to the top layer of reinforcement. AASHTO approximates the R term as 1.2. From these equations it follows that:

$$w_c = \frac{z}{10965} \qquad [4\text{-}4]$$

AASHTO recommends a maximum value for z of 170, for reinforced concrete members in moderate exposure conditions. This corresponds with a prototype crack width of 0.0155". Borges and Lima (8) have shown that crack widths in models tend to scale linearly with the scale factor. Reducing this width by the scale factor of the models gives an acceptable model crack width at service loads of 0.0028". Given that the accuracy of the crack readings

is ± 0.0005", a crack width of 0.0028" is essentially equal to 0.003".

The maximum crack widths (0.003") at service flexure loads for the CO-RU, CO-PU-74S-V, and CO-PU-74S-I overhangs, the only overhangs cracked at service loads, are essentially equal to the acceptable width.

Figure 4.7 also reveals the variation in ability of each overhang to control crack widths at loads above service loads. At factored loads, M_u, the maximum width occurred in the CO-PU-100S-V overhang which had the least number of bars of all overhangs. The CO-PU-100S-I and CO-PU-74S-V overhangs had the next largest widths followed closely by the CO-PU-74S-I overhang. The improved ability of these overhangs to control crack widths at factored loads is due to the increased quantities of mild reinforcement. The CO-RU and CO-PS-100S overhangs had the smallest crack widths at factored loads, again because of the large amount of reinforcement in these overhangs. Crack width at factored loads is a fairly meaningless value in view of the very high dead load moments which are factored.

At less severe, and more feasible, overload conditions of dead load plus two times the service flexure live load, the CO-RU and CO-PU-100S overhangs performed about the same with crack widths about 150% the AASHTO service level limit. The CO-PU-74S overhangs had crack widths about twice the AASHTO service level limits. Considering the elevated load levels these are quite well controlled. The CO-PS-100S overhang had the smallest widths being less than the AASHTO service level values under this overload.

All the "major" cracks on each specimen are shown in Figures 4.8 and 4.9 for the service flexure load and factored flexure load conditions, respectively. These figures indicate the location of the maximum crack width. The maximum crack width for all of the prestressed overhangs was at the extreme top fiber. However, this was not the case for the CO-RU overhang. This is consistent with the observations of Frantz et al. (3), that the widest cracks in a deep reinforced concrete flexural member may occur at depths below the primary moment reinforcement. A significant difference between the reinforcing patterns for the CO-RU overhang and the prestressed overhangs was the centroidal location of the primary moment reinforcement. This steel was concentrated at 1.39" from the top of the CO-RU overhang, while it varied from 3.25" to 3.6" in the prestressed overhangs. These distances in the prestressed overhangs correspond to approximately 13% of the maximum height of the overhang. The lower depth of the reinforcement in the prestressed overhangs appears to have influenced the location of the maximum crack width, providing greater crack width control throughout the full overhang depth.

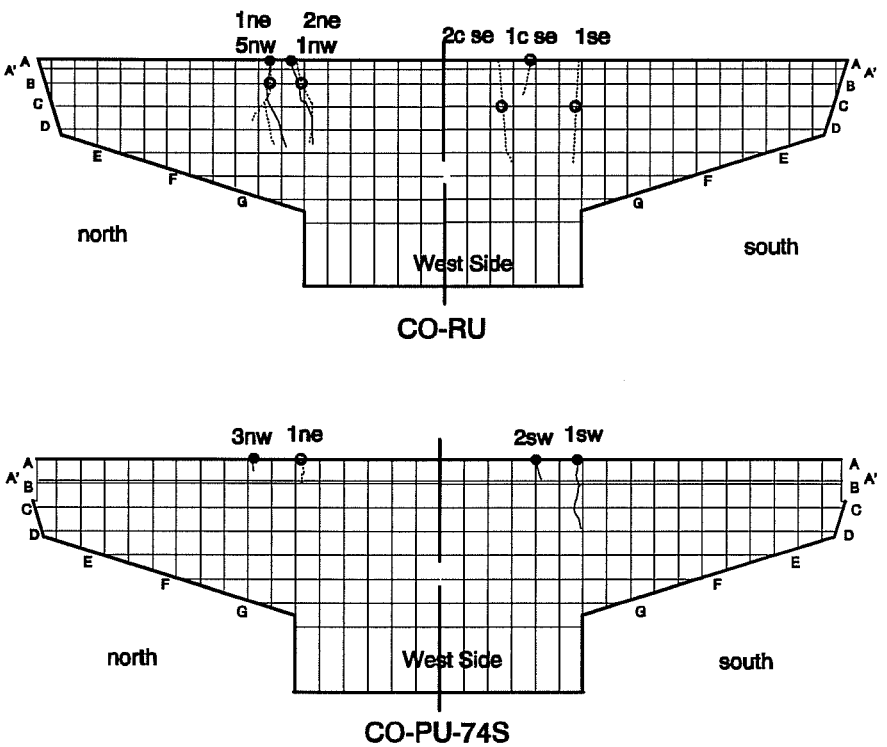

Figure 4.8 "Major" Cracks at Service Flexure Loads

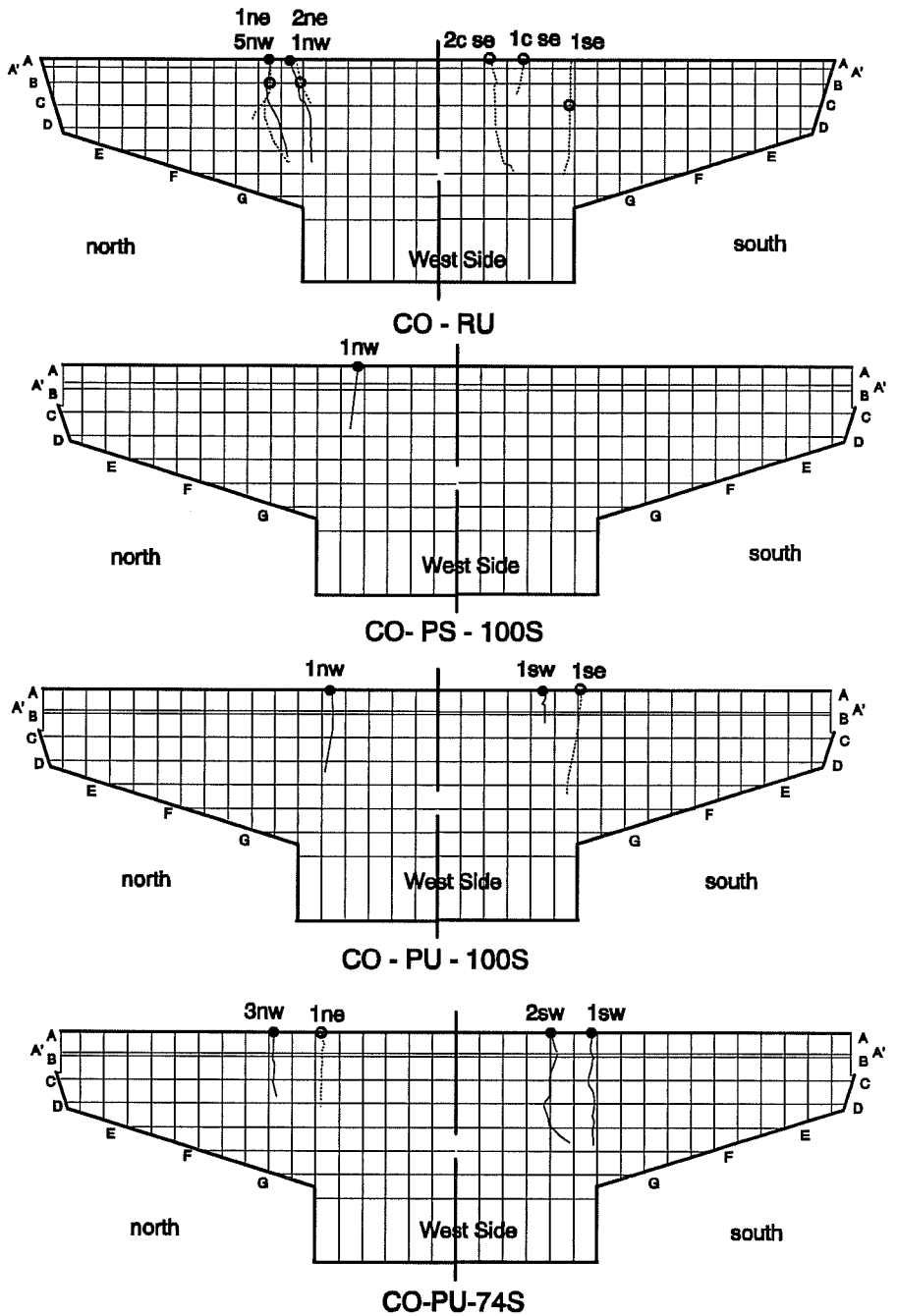

Figure 4.9 "Major" Cracks at Factored Flexure Loads

4.3.3 Prediction of Crack Widths

The Gergely and Lutz expression for the prediction of crack widths is only for reinforced concrete members. An expression is needed which is applicable to members designed with mixtures of non-prestressed and prestressed reinforcement, since no comparable expression has been widely accepted for use in such members.

A procedure which extrapolates the Gergely and Lutz equation to include post-tensioning tendons as well as reinforcing bars was developed in collaboration with fellow researcher, Bradley A. Wood. The procedure was used to predict the maximum crack widths for each overhang. In this procedure, a hypothetical value was used for the stress in the steel, f_s, which was taken as the change in stress from zero applied load to service loads, as determined from a linear service load strain profile based on the cracked section, at a distance d' from the extreme fiber. The location of d' was taken to correspond with the centroid of the primary moment reinforcement. The effective tension area was taken as the product of the overhang width and two times d'. Each post-tensioning strand was counted as one bar in determining the number of bars or wires within the effective tension area. These values are shown for each overhang in Table 4.3 along with the predicted maximum and measured service load crack widths.

Overhang	Distance to Centroid of Primary Moment Reinforcement, d' (inches)	# of Bars in Effective Tension Area	# of Tendons in Effective Tension Area	dc (inches)	Change in Stress in Reinforcement at d', fs (ksi)	Predicted Crack Width at Service Flexure Loads (inches)	Maximum Measured Service Load Crack Width (inches)
CO-RU	1.39	57	0	0.67	37.76	0.0029	0.003
CO-PS-100S	3.25	5	6	0.63	1.32	0.0002	0
CO-PU-100S-I	3.6	15	6	0.63	8.29	0.0012	0
CO-PU-100S-V	3.6	9	6	0.63	8.77	0.0014	0
CO-PU-74S-I	3.6	25	5	0.67	23.72	0.0031	0.003
CO-PU-74S-V	3.6	15	5	0.67	27.05	0.0040	0.003

Table 4.3 Predicted Crack Widths

The predicted widths for all of the prestressed overhangs are slightly larger, but very close to the actual measured widths. The greatest difference between the predicted and measured widths was for the CO-PU-74S-V overhang. The reason the predicted width for this overhang was higher than for the CO-PU-74S-I overhang was the higher f_s term and the reduced number of bars.

Keeping in mind that the accuracy of the crack measurements is ± 0.0005", the procedure appears to give a reasonably accurate prediction of the crack width and could be useful in the design of mixed reinforcement in overhangs. The predicted width would be conservative but not overly so.

4.4 Evaluation of Service Load Deflections

The service load deflections were summarized in Table 3.10 and are plotted in Figure 4.10. The CO-RU overhang had the greatest service load deflection of all overhangs with a value of 0.118".

For a span length, L, of 46", a maximum acceptable deflection of L/360 would equal 0.128". The maximum service load deflections for the CO-RU overhang can be expressed as L/390, which is clearly an acceptably small value.

The prestressed overhangs were extremely stiff with even smaller deflections. The maximum service load deflection measured for all of the prestressed overhangs occurred on the CO-PU-100S-I overhang and was 0.041", which corresponds to L/1122. The deflections for the CO-PU-74S overhangs were very close to, but slightly lower than this value. The fully prestressed overhang, CO-PS-100S, had a maximum service load deflection of 0.020", which corresponds to L/2300.

It was expected that the deflections in the prestressed overhangs would increase with decreasing amounts of prestressing. However, this trend is not evident in the measured deflections. The reason for this is probably that for such small deflections, the measurements were either beyond the accuracy of the linear potentiometers, or the frame on which the potentiometers were mounted was not perfectly rigid. In any case, these inaccuracies would be minor and it can be concluded that the deflections of all of the prestressed overhangs were very small.

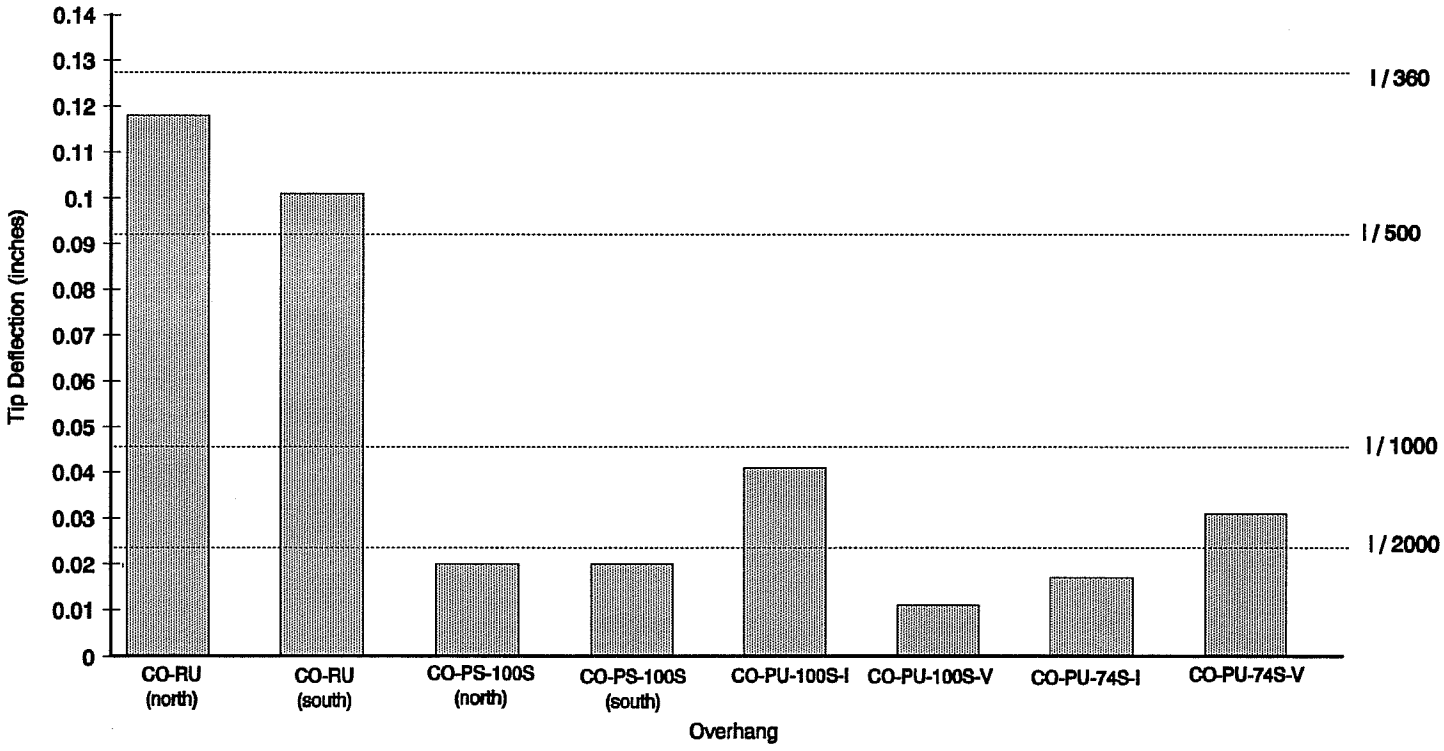

Figure 4.10 Service Load Tip Deflections

On the basis of this evaluation, it can be concluded that all of the specimens had sufficient stiffness to control service load deflections.

4.5 Comparison of Overhang Moment-Deflection Curves

The moment-deflection curves for the CO-RU(south), CO-PS-100S(north), CO-PU-100S-V, and CO-PU-74S-V overhangs were superimposed on Figure 4.11. The curves for the CO-PS-100S and CO-PU-74S-V overhangs were simplified to eliminate the abrupt changes occurring with the slippage of the plates in the loading assemblies (as explained in Section 3.5). Curves for the CO-PU-100S-I and CO-PU-74S-I overhangs are not included because these overhangs were not loaded to failure.

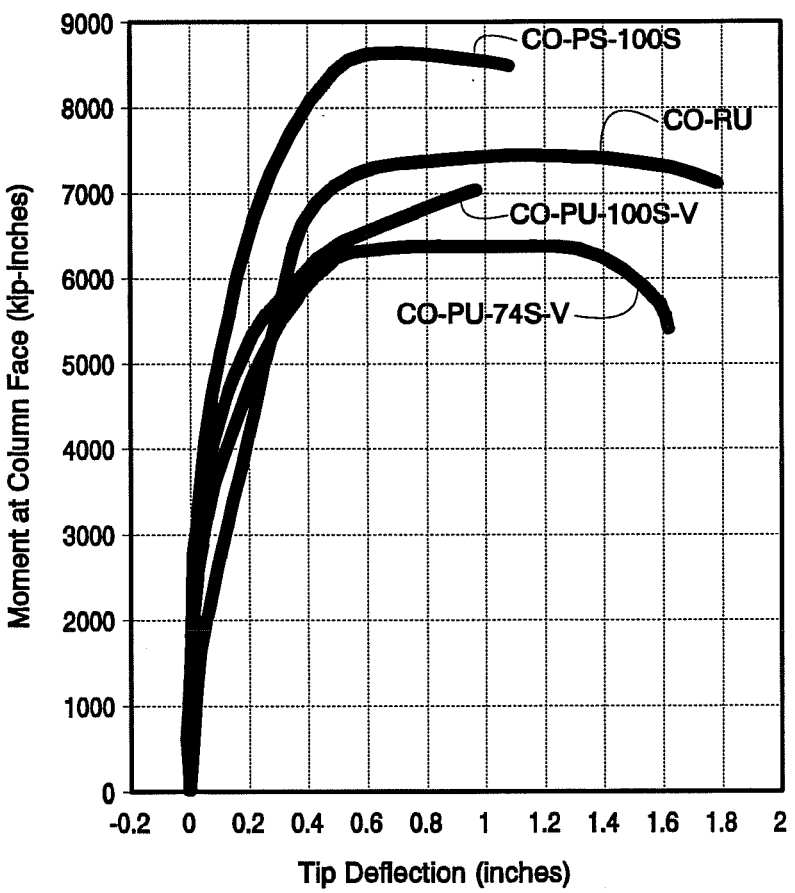

Figure 4.11 Comparison of Moment-Deflection Curves

Figure 4.11 provides a visual reference for comparison of the ductility of each overhang. As expected, the CO-RU overhang exhibited the greatest ductility. The ductility of the CO-PS-100S and CO-PU-100S-V overhangs was significantly less than the CO-RU overhang. The CO-PU-74S-V overhang, although not quite as ductile as the CO-RU overhang, demonstrated a considerable improvement in ductility over the current AASHTO design criteria used for the CO-PS-100S overhang. This is important from the standpoint of providing more warning of distress and possessing greater structural integrity in the case of accidental over-loading. The CO-PU-74S-V overhang developed almost 90% of the warning capability of the reinforced concrete overhang.

It can be concluded from this comparison that the ductility of an overhang designed with a mixture of non-prestressed and prestressed reinforcement can be significantly improved over a fully prestressed overhang and almost match that of a non-prestressed member.

4.6 Comparisons between Tested and Predicted Overhang Capacities

4.6.1 Moment at Face of Column

As previously mentioned in Section 3.7, each of the overhangs had ultimate moment capacities well in excess of the required factored moment, M_u. For each overhang, the excess moment capacity above M_u was primarily due to the use of various supplementary reinforcement such as shear-friction, horizontal shear, side face, and top bars, which was neglected in the calculations used to proportion the primary moment reinforcement. In addition, for the CO-PS-100S overhang, excess capacity was also provided due to the large quantity of post-tensioning required to satisfy the AASHTO service load design criteria.

As mentioned in Section 3.7, the excess capacity above the factored moment is also partly due to the fact that a strength reduction factor of 0.9 was used in the flexural design of each overhang, but the actual steel strengths were also used and the concrete strength for each overhang was higher than the strength assumed in the design. Therefore, capacities in the range of 10% over factored loads would have been expected even if all the supplementary steel was not used. From this it can be deduced that if strength reduction factors had not been used in the design, the ratios of $M_{n\ test}$ to M_u would have been approximately 10% lower. Even on this basis, the tested moment capacity of each overhang is still well above the factored moment.

All of the supplementary steel was accounted for in computations for the maximum predicted moment, $M_{n\ pred}$. These computations involved a detailed strain compatibility and

equilibrium solution for the critical moment section at the face of the column. A horizontal compression block and a linear strain profile was assumed with a maximum concrete compressive strain of 0.003 in/in. Assumed neutral axis depths were iterated until the tension and compressive forces in the section were equilibrated. In the case of each overhang, the computations predicted that virtually all of the reinforcement above the neutral axis would yield and the maximum steel strain in the top bars would be less than 0.02 in/in. The results of these calculations are shown in Table 4.4, along with the ratio of $M_{n\ pred}$ to M_u/Φ. These ratios reflect the increased capacity given to each overhang by the supplementary reinforcement.

Specimen #	Overhang	Maximum Predicted Moment, Mn pred (kip-in)	Required Design Moment, Mu/phi (kip-in)	Mn pred / Mu/phi	Maximum Test Moment, Mn test (kip-in)	Mn test / Mn pred
1	CO-RU	6519	4484	1.45	7440	1.14
2	CO-PS-100S	6935	4484	1.55	8734	1.26
3	CO-PU-100S-I	5876	4484	1.31	7044*	1.20
	CO-PU-100S-V	5575	4484	1.24	7044	1.26
4	CO-PU-74S-I	5341	4484	1.19	6364*	1.19
	CO-PU-74S-V	4872	4484	1.09	6364	1.31
* not loaded to failure so these are proof load values only (not included in average)					Average =	1.24

Table 4.4 Predicted Moment Capacities based on Linear Strain Profile and Comparisons to Required Design Moment and Test Moments

Table 4.4 also includes a comparison of $M_{n\ test}$ to $M_{n\ pred}$. For each overhang, the ratio of the test moment to the predicted moment was significantly greater than one. The average ratio is 1.24 (does not include the CO-PU-100S-I and CO-PU-74S-I overhangs since these were not loaded to failure). Therefore, it can be concluded that this method of calculation is quite conservative.

In an effort to explain the discrepancy between $M_{n\ pred}$ and $M_{n\ test}$, revised calculations of the moment capacities were made for the CO-RU, CO-PS-100S, CO- PU-100S-V, and CO-PU-74S-V overhangs. These calculations took into account strain hardening of the reinforcement. As mentioned in section 3.5, fractured No. 2 reinforcing bars were discovered in the CO-PS-100S

(north) and CO-PU-74S-V overhangs, so it was apparent that strains in the top bars for these specimens had reached the fracture strain of the No. 2 reinforcing bars of 0.08 in/in at the maximum test loads. Also, since the tip deflections for the CO-RU and CO-PU-100S-V overhangs at maximum test loads were at least as large as the tip deflections for the CO-PS-100S overhang at maximum loads, it was considered reasonable to assume that strains in the top bars of these specimens had to be approaching the 0.08 in/in range, even though no fractured bars were discovered.

To equilibrate the tensile and compressive forces in the calculations, while limiting the maximum concrete compressive strain to 0.003 in/in, it was necessary to assume a non-linear strain profile through the concrete compression zone. The revised maximum calculated moments, $M_{n\ calc}$, are shown in Table 4.5, along with the ratio of $M_{n\ test}$ to $M_{n\ calc}$. These ratios show that the maximum calculated moment still underestimates the tested moment capacity, but, the calculated capacity of each overhang is somewhat closer to the test results. The average of the four ratios is now 1.19.

Specimen #	Overhang	Maximum Calculated Moment, Mn calc (kip-in)	Maximum Test Moment, Mn test (kip-in)	Mn test / Mn calc
1	CO - RU	7017	7440	1.06
2	CO - PS - 100S	7286	8734	1.20
3	CO - PU - 100S - V	5656	7044	1.25
4	CO - PU - 74S - V	5023	6364	1.27
			Average =	1.19

Table 4.5 Maximum Calculated Moment Capacities based on Non-Linear Strain Profile and Strain Hardening of Reinforcement and Comparisons to Test Moments

The ultimate load of the post-tensioning strand used in the calculations was taken to be the ultimate load from the tensile tests that were performed on the strand. Each of the strands failed at the wedges in the tensile tests, so it may be assumed that the actual strength of the strand may be some 5 to 10 percent higher than assumed in the calculations based on the usual strand

efficiency factors. The difference between the maximum test moment and the maximum calculated moment may also be partially explained by the description given in Section 3.5 regarding the restraint of the top fiber by the loading rams. Note that the ratio of test to calculated moment for the CO-RU overhang in which fabric bearings were used is much closer to one.

4.6.2 Shear Capacity Predicted by AASHTO

Even though non of the overhangs had a shear failure, the shear capacity as predicted by the AASHTO shear provisions was determined for each overhang and compared to the maximum test loads. Since none of the overhangs failed in shear, the maximum test loads can only be regarded as proof loads.

The critical section of the overhang for shear was assumed to occur at Section a-a, shown in Figure 2.6. The predicted shear capacity was determined from Equation [2-5] with a strength reduction factor of 1.0.

For the CO-RU overhang, the V_c term was calculated using AASHTO Equation (8-48):

$$V_c = \left(1.9 \sqrt{f'_c} + 2500\ \rho_w \frac{V_u\, d}{M_u} \right) b_w\, d \qquad [4\text{-}5]$$

where ρ_w, V_u, M_u, and d were determined for Section a-a.

For the CO-PS-100S, both CO-PU-100S, and both CO-PU-74S overhangs, the V_c term was taken as the lesser of V_{ci} and V_{cw}. V_{ci} was determined from AASHTO Equation (9-27):

$$V_{ci} = 0.6 \sqrt{f'_c}\, bd + V_d + \frac{V_i\, M_{cr}}{M_{max}}, \qquad [4\text{-}6]$$

and AASHTO Equation (9-28):

$$M_{cr} = \frac{I}{Y_t}\left(6\sqrt{f'_c} + f_{pe} - f_d\right) . \qquad [4\text{-}7]$$

V_{cw} was determined from AASHTO Equation (9-29):

$$V_{cw} = \left(3.5\sqrt{f'_c} + 0.3 f_{pc}\right) bd + V_p . \qquad [4\text{-}8]$$

The V_s term was determined for all overhangs by summing all of the vertical stirrups located within a distance d/2 on either side of Section a-a. This is the region of the anticipated shear crack shown in Figure 2.6.

According to Equation [2-5], the predicted AASHTO shear capacity, $V_{n\ pred}$, is taken as the sum of V_c and V_s.

V_c, V_s, and $V_{n\ pred}$ are shown for each overhang in Table 4.6. Also listed are the shear applied to Section a-a at the maximum test loads, $V_{n\ test}$ (based on the maximum test loads and self weight of the outside 27.17" of the overhang), and the ratio of $V_{n\ test}$ to $V_{n\ pred}$. Since all of the ratios are substantially greater than one, it can be concluded that the AASHTO shear provisions are quite conservative.

Specimen #	Overhang	Maximum Applied Shear at Section a-a, Vn test (kips)	Predicted AASHTO Shear Capacity, Vn pred (kips)	Vn test / Vn pred
1	CO - RU	170.7*	132.4	1.29
2	CO - PS - 100S	201.8*	192.3	1.05
3	CO - PU - 100S - I	161.2*	143.0	1.13
	CO - PU - 100S - V	161.2*	146.7	1.10
4	CO - PU - 74S - I	144.2*	118.9	1.21
	CO - PU - 74S - V	144.2*	122.6	1.18
			Average =	1.16

* no shear failures so these are proof load values only

Table 4.6 Predicted AASHTO Shear Capacities and Comparisons to Maximum Test Loads

4.6.3 Shear-Friction Capacity Predicted by AASHTO

Even though none of the overhangs experienced a shear-friction failure, the predicted shear-friction capacity was determined for each overhang, according to the AASHTO corbel provisions which were outlined in Section 2.3.1, and the predicted capacities were compared to the maximum test loads. Since none of the overhangs failed in shear-friction, the maximum test loads can only be regarded as proof loads.

The predicted shear-friction capacity was determined by Equation [2-11], but was limited to the lesser of $0.2f'_cA_{cv}$ and $800A_{cv}$, according to the AASHTO provisions. The A_{vf} term in Equation [2-11] included all reinforcement which was determined to be yielded in the predicted moment capacity calculations. For the purpose of the calculation, the maximum stress in the reinforcement was taken as 60 ksi for the non-prestressed reinforcement and 220 ksi for the post-tensioning strand (60 ksi plus the effective prestressing of 160 ksi), according to the AASHTO provisions. The effective depth, d, was taken to the centroid of all yielded reinforcement.

Specimen #	Overhang	Tested Shear at Face of Column, Vsf Test (kips)	Predicted AASHTO Shear-Friction Capacity, Vsf Pred (kips)	Vsf Test / Vsf Pred
1	CO - RU	231.4*	354.4	0.65
2	CO - PS - 100S	268.8*	327.6	0.82
3	CO - PU - 100S - I	220.0*	311.4	0.71
	CO - PU - 100S - V	220.0*	296.9	0.74
4	CO - PU - 74S - I	201.7*	293.4	0.69
	CO - PU - 74S - V	201.7*	262.5	0.77
			Average =	0.73

* no shear failures so these are proof load values only

Table 4.7 Predicted AASHTO Shear-Friction Capacities and Comparisons to Maximum Test Loads

The $800A_{cv}$ limit controlled for the CO-RU and CO-PS-100S overhangs and Equation [2-11] controlled for both CO-PU-100S and both CO-PU-74S overhangs. The results of these

calculations are shown in Table 4.7, along with comparisons to the measured shear at the face of column at the maximum test loads. For each overhang, the ratio of tested shear to predicted shear-friction capacity was less than one. However, since the maximum test loads can only be considered proof loads, it cannot be concluded that the AASHTO shear-friction provisions overestimate the overhang capacities.

4.6.4 Predicted Capacities from Strut-and-Tie Model with only Vertical Ties in the Web

The strut-and-tie model shown in Figure 2.9 was used to predict the capacity of the CO-RU, CO-PS-100S, CO-PU-100S-V, and CO-PU-74S-V overhangs.

In the form shown in Figure 2.9, the model provides only a very simplified representation of the flow of forces in the overhang because it does not include a tie at each level of horizontal reinforcement. If the model were further refined for each overhang to take into account all the horizontal steel, and if it was assumed that a failure would not occur in tie T4, the predicted capacities would be the same as the maximum predicted moment capacities given in Section 4.6.1, since virtually all of the horizontal steel above the neutral axis was yielded at the maximum predicted moment.

Specimen #	Overhang	Maximum Test Outside Reaction, Ro test	Maximum Outside Reaction corresponding to yielding of horizontal reinf. (kips)	Maximum Outside Reaction corresponding to yielding of tie T4 (kips)	Capacity of tie T4 (reinf. only) (kips)	Maximum Predicted Outside Reaction, Ro pred (kips)	Ro test / Ro pred
1	CO-RU	170.1	147.8	111.3	44.5	111.3	1.53
2	CO-PS-100S	201.2	157.8	111.3	44.5	111.3	1.81
3	CO-PU-100S-V	160.6	125.1	120.6	48.2	120.6	1.28
4	CO-PU-74S-V	143.6	108.1	120.6	48.2	108.1	1.33

Table 4.8 Predicted Overhang Capacities by Strut-and-Tie Model (no V_c term included) and Comparisons to Tested Capacities

Values were determined for the inside and outside reaction corresponding to the maximum predicted moments, keeping the same relationship between R_i and R_o described in

Section 2.8.2 for loads approaching ultimate loads. The outside reactions at this level are shown in Table 4.8. These values for R_o represent the maximum outside reaction corresponding to yielding of the horizontal steel.

For the strut-and-tie model shown in Figure 2.9, equilibrium gives the relationship between the force in tie T4 and the outside reaction as:

$$T4 = 0.40R_o \qquad [4\text{-}9]$$

The capacity of tie T4 was determined for each overhang by summing all vertical steel crossing the anticipated shear crack shown in Figure 2.9. This capacity was used in Equation [4-9] to determine the maximum calculated load for R_o, corresponding to yielding of tie T4. For each overhang, the capacity of tie T4 and the maximum calculated load for R_o are listed in Table 4.8.

The lesser of the two values for R_o is the maximum predicted outside reaction, $R_{o\ pred}$, which represents the overhang capacity. Table 4.8 includes the ratio of the maximum value for the R_o reached in the test to $R_{o\ pred}$. In each case the ratios are substantially greater than one so it can be concluded that the predicted capacities from the strut and tie model with only vertical ties in the web are quite conservative.

Another observation is that for the CO-PU-74S-V overhang, the ratio of $R_{o\ test}$ to $R_{o\ pred}$ is essentially equal to the ratio of $M_{n\ test}$ to $M_{n\ pred}$, shown in Table 4.6. This is because yielding of the horizontal tension steel is predicted by both methods of computation of the capacity.

For the CO-RU, CO-PS-100S, and CO-PU-100S-V overhangs, yielding of tie T4 is predicted to occur before yielding of the horizontal steel. This was not the situation observed in the tests. The main reason the observed and predicted behaviors differed is believed to be that the strut-and-tie model provides no tensile concrete contribution to the capacity of tie T4. Therefore, the strength of the tie is underestimated and a failure of the tie is predicted. In reality, both the vertical reinforcement and the shear strength of the concrete at the location of tie T4 are available to carry the required force.

The shear capacity of the concrete was estimated for each overhang using equations [4-5] through [4-8], applied to each overhang section at the location of tie T4. This was added to the capacity of tie T4 for each overhang. The increased capacities of tie T4 are shown in Table 4.9. The maximum calculated outside reactions corresponding to the increased tie capacities are also shown in the Table 4.9.

Specimen #	Overhang	Vc term (kips)	Revised Capacity of tie T4 (reinf. + Vc term (kips)	Maximum Outside Reaction corresponding to failure of revised tie T4 (kips)	Maximum Predicted Outside Reaction, Ro pred (kips)	Ro test / Ro pred
1	CO-RU	50.8	95.3	238.3	111.3	1.15
2	CO-PS-100S	136.4	180.9	452.3	111.3	1.28
3	CO-PU-100S-V	106.3	154.5	386.3	120.6	1.28
4	CO-PU-74S-V	87.7	135.9	339.8	108.1	1.33

Table 4.9 Revised Predicted Overhang Capacities by Strut-and-Tie Model (V_c term included) and Comparisons to Tested Capacities

With the capacity of tie T4 being provided by both the V_c term and the reinforcement, failure of each overhang is predicted to occur with yielding of the horizontal reinforcement. This is what was observed in the tests. Thus, it seems reasonable to consider a concrete contribution to the strength of the tie.

An additional observation was made relating to the strength of tie T4. The required capacity of tie T4 from the strut-and-tie model with factored flexure loads applied is equal to 35.2 kips. It is noted that for each overhang the V_c term, determined by the AASHTO equations, is larger than the required capacity of the tie. Therefore, it is believed that each overhang would have had sufficient shear capacity to resist factored loads even if no shear stirrups had been provided. This is substantiated by the fact that only minimal strains were recorded by the gages on the shear stirrups at factored loads.

It is recognized that the fatigue tensile strength of the concrete would be much lower than the strength of the concrete in the tests. Because of this it is recommended that the stirrups still be used, although it seems reasonable to allow a reduction in the number of stirrups provided. It is proposed that allowing 1/2 of the AASHTO calculated V_c to contribute to the strength of the tie would be an acceptable design recommendation which would lead to a further reduction in the number of stirrups.

4.6.5 Effect of Concrete Efficiency Factors on Specimen Capacities Predicted by the Strut-and-Tie Method

It is important to note that the basic assumption in the assumed strut-and-tie model of a horizontal compression block at the bottom of the overhang with a height of 2.88", leads to compression stresses in that zone that are higher than the maximum levels recommended by Bergmeister et al. (9). Bergmeister recommends that the maximum concrete compression stress, f_{ce}, in unconfined nodes should be limited to $f_{ce} = \nu_e f'_c$, where $\nu_e = 0.9 - 0.25\, f'_c / 10000$ for $4000 < f'_c < 10000$ psi. For f'_c equal to 5000 psi, the recommended f_{ce} is equal to 3875 psi.

If the vertical height of the compression block is limited to 2.88", the resultant compression strut (see Figure 4.12) acting against struts C2, C_{sw}, C5, and C6, with factored flexure loads applied to the overhang, has a magnitude of 237.3 kips. The width of the node normal to the resultant compression strut is limited to 2.36" resulting in a principal compression stress in the node equal to 5586 psi. This value is well above the maximum allowable stress of 3875 psi.

To limit the compression stress in the node to 3875 psi, the vertical height of the node must be increased to approximately 4.3". This requires a flatter inclination for struts C2, C_{sw}, C5, and C6 which increases the load in the resultant strut to 243.0 kips.

Making this change to the model would increase the demand on the horizontal steel and lower the overhang capacities from what was predicted in Section 4.6.4. Therefore, the use of a strut-and-tie model, in which the compressive stresses are limited by concrete efficiency factors, is not recommended for predicting the overhang capacities.

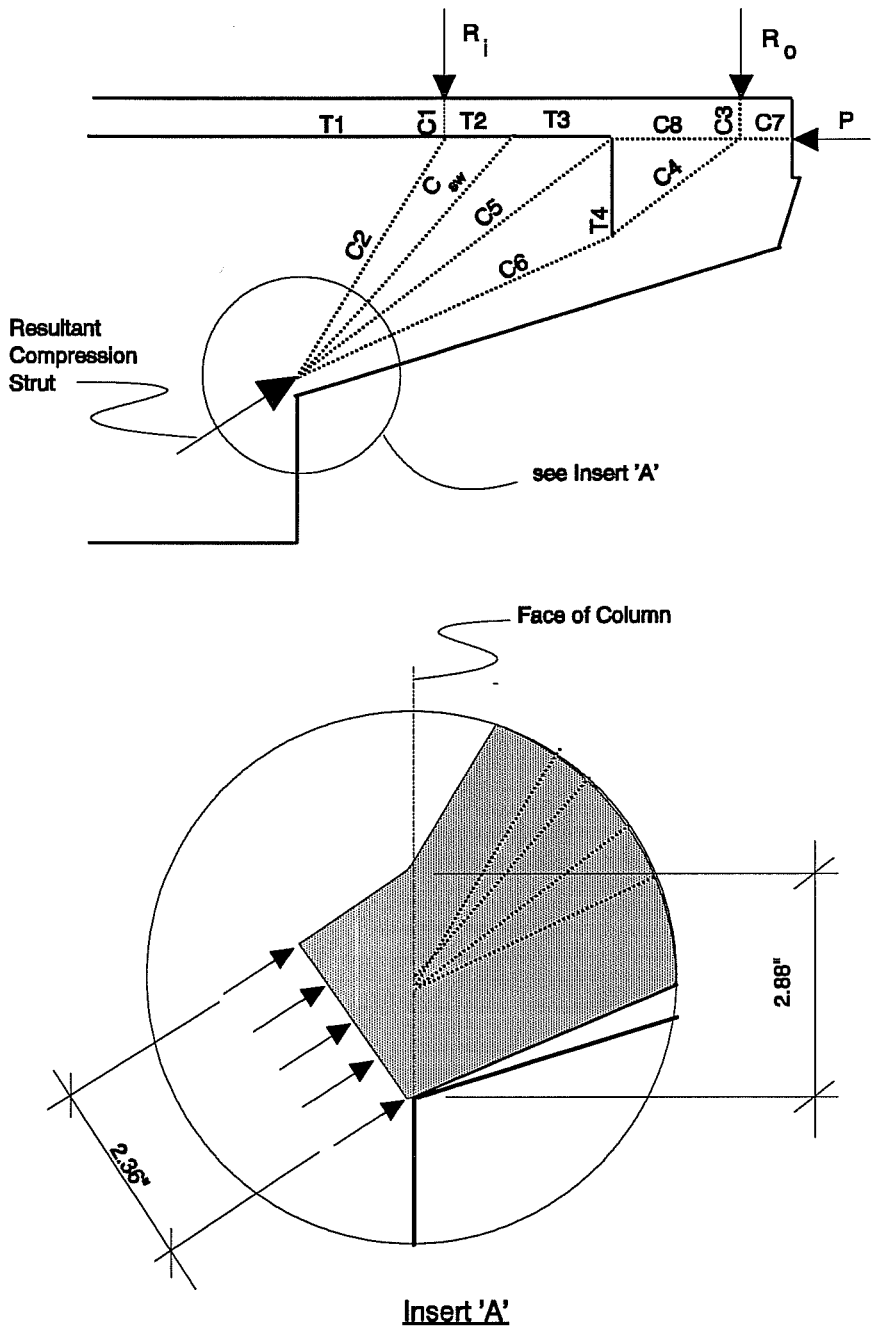

Figure 4.12 Detail of Compression Node at Bottom of Overhang

CHAPTER 5
OVERHANG CONSTRUCTABILITY AND ECONOMICS

5.1 Constructability

Close attention was paid to the ease or difficulty of constructing each overhang. The construction of each overhang involved forming, assembling the reinforcing cage, placing and consolidating the concrete, and the prestressing operation, if applicable. Forming was essentially the same for all overhangs, except that the prestressed overhangs required the use of the wooden insert forms to create a block-out for the post-tensioning14 anchorages. In a prototype overhang, this block-out would have to be patched after the post tensioning operation was completed. In general, it was observed that the difficulty of construction was in direct relationship to the total weight of reinforcement, including both prestressed and non-prestressed. This impacted both the difficulty of assembling the cage and the ease or difficulty of placing the concrete.

The reinforcing quantities for each 5.5 scale overhang were converted into equivalent prototype quantities and are shown in Tables 5.1 through 5.6. The mild reinforcement quantities were converted according to the relationships between model and prototype reinforcement shown in Table 2.1. The post-tensioning strands were converted into equivalent numbers of 19, 12, and 7 strand tendons.

Reinforcement Type	Reinforcement Size	Number of Bars	Length (ft)	Weight (lbs)
Primary Moment	No. 11	66	1273	7874
Shear -Friction	No. 8	38	1087	3773
Shear Stirrups	No. 6	42	2880	4002
Side Face	No. 8	22	345	1197
Bottom Bars	No. 8	10	235	814
			Total =	17660

Table 5.1 Equivalent Prototype Reinforcment Quantities for the CO-RU Overhang

Reinforcement Type	Reinforcement Size	Number of Bars or Tendons	Length (ft)	Weight (lbs)
Primary Moment	19 strand tendon	7	140	1985
"	12 strand tendon	1	20	179
			sub-total =	2164
Shear -Friction	No. 8	31	675	2340
Shear Stirrups	No. 6	42	2880	4002
Side Face	No. 8	18	98	342
Top Bars	No. 11	2	39	243
"	No. 8	4	59	205
Bottom Bars	No. 8	12	254	1573
Anchorage Hoops	No. 6	14	608	845
			sub-total =	9550
			Total =	11714

Table 5.2 Equivalent Prototype Reinforcement Quantities for the CO-PS-100S Overhang

Reinforcement Type	Reinforcement Size	Numberof Bars or Tendons	Length (ft)	Weight (lbs)
Primary Moment	19 strand tendon	6	120	1701
"	7 strand tendon	1	20	104
			sub-total =	1805
Horizontal Shear	No. 8	19	324	1124
Shear Stirrups	No. 6	20	1260	1751
Side Face	No. 8	10	94	328
Top Bars	No. 11	6	99	342
Bottom Bars	No. 8	6	127	441
Anchorage Hoops	No. 6	14	608	845
			sub-total =	4831
			Total =	6636

Table 5.3 Equivalent Prototype Reinforcment Quantities for the CO-PU-100S-I Overhang

Reinforcement Type	Reinforcement Size	Number of Bars or Tendons	Length (ft)	Weight (lbs)
Primary Moment	19 strand tendon	6	120	1701
"	7 strand tendon	1	20	104
			sub-total =	1805
Shear Stirrups	No. 6	20	1240	1723
Side Face	No. 8	18	213	737
Top Bars	No. 11	6	99	342
Bottom Bars	No. 8	6	127	441
Anchorage Hoops	No. 6	14	608	845
			sub-total =	4088
			Total =	5893

Table 5.4 Equivalent Prototype Reinforcement Quantities for the CO-PU-100S-V Overhang

Reinforcement Type	Reinforcement Size	Number of Bars or Tendons	Length (ft)	Weight (lbs)
Primary Moment	19 strand tendon	4	80	1134
"	12 strand tendon	1	20	179
			sub-total =	1313
Primary Moment	No. 11	17	324	2003
Horizontal Shear	No. 8	19	324	1124
Shear Stirrups	No. 6	20	1260	1751
Side Face	No. 8	10	94	328
Bottom Bars	No. 8	6	127	441
Anchorage Hoops	No. 6	14	608	845
			sub-total =	6492
			Total =	7805

Table 5.5 Equivalent Prototype Reinforcement Quantities for the CO-PU-74S-I Overhang

Reinforcement Type	Reinforcement Size	Number of Bars or Tendons	Length (ft)	Weight (lbs)
Primary Moment	19 strand tendon	4	80	1134
"	12 strand tendon	1	20	179
			sub-total =	1313
Primary Moment	No. 11	17	324	2003
Shear Stirrups	No. 6	20	1240	1723
Side Face	No. 8	10	94	328
Bottom Bars	No. 8	6	127	441
Anchorage Hoops	No. 6	14	608	845
			sub-total =	5340
			Total =	6653

Table 5.6 Equivalent Prototype Reinforcement Quantities for the CO-PU-74S-V Overhang

The CO-RU overhang based on the current AASHTO standards was by far the most difficult overhang to construct. The cage was very congested and contained multiple levels of horizontal reinforcement and numerous vertical stirrups making it very difficult to assemble. In terms of total poundage and linear feet of reinforcement, this overhang had substantially more than any other overhang, resulting in a very dense reinforcing cage with closely spaced bars throughout. The densely spaced reinforcement made placement and consolidation of concrete very difficult. This is an important consideration because poorly placed concrete will lead to long term durability problems.

The CO-PS-100S overhang based on the current AASHTO design specifications was also quite difficult to construct. Although the total linear feet and pounds of reinforcement were significantly lower than the CO-RU overhang, fabrication of the reinforcing cage was very difficult and the cage was quite congested. This is primarily because of the use of shear-friction steel and because of the large number of vertical stirrups that were used. Good placement and consolidation of the concrete was difficult to achieve because of the highly congested reinforcing cage.

The CO-PU-100-V overhang was by far the easiest to construct. This overhang had the lowest total poundage of reinforcement of all overhangs. The reduction of reinforcement resulted in greatly simplifying the process of assembling the cage and reducing congestion. With less congestion, it was much easier to place and consolidate the concrete. With better consolidated concrete, a more durable structure would be expected.

The CO-PU-100S-I overhang was also much easier to construct than either the CO-RU or CO-PS-100S overhangs. The presence of the horizontal shear steel made it slightly more difficult to construct than the CO-PU-100S-V overhang.

The CO-PU-74S-I and V overhangs were a little more difficult to construct than the CO-PU-100S-I and V overhangs, but both were significantly easier to build than either the CO-RU or CO-PS-100S overhangs.

Some work was unique to the post-tensioned specimens. The stressing operation had to be performed, wooden insert forms had to be used to form the block-out for the tendon anchorages, and in a prototype overhang, the block-outs would have to be patched. However, it is felt that the reduction in the congestion of the cage resulting from the use of post-tensioning more than offset the added difficulty of performing these operations.

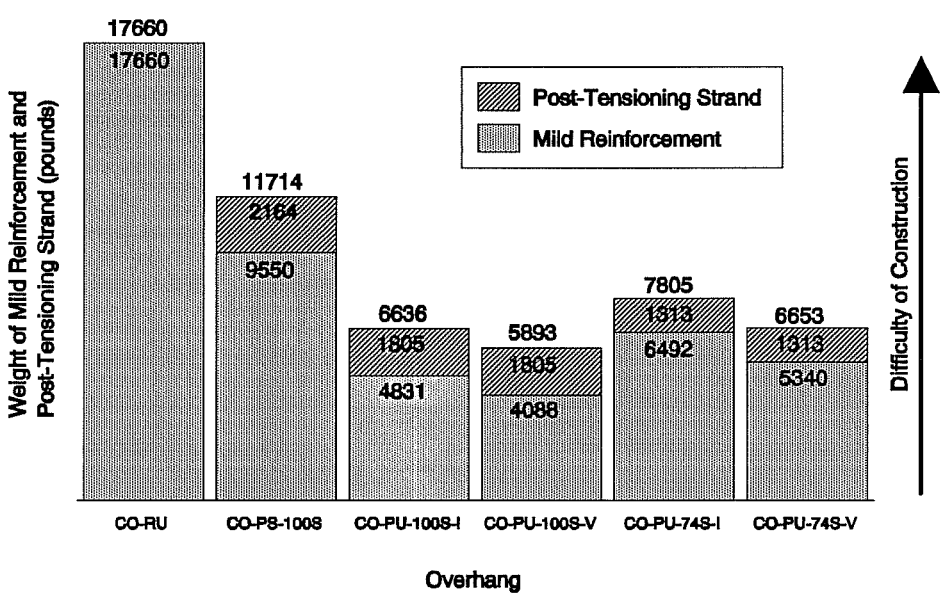

Figure 5.1 Comparison of Total Weight of Reinforcement for each Prototype Overhang

The relative difficulty of construction of each overhang is depicted graphically in Figure 5.1 which was generated on the basis of total pounds of reinforcement (non-prestressed and prestressed) in each overhang.

5.2 Construction Cost Estimates

Cost estimates were obtained from a representative of a local construction company (10) for each overhang. The estimates are for mild reinforcement and post-tensioning only. The estimator assumed that the cost of forming and supplying and placing concrete would be essentially the same for each overhang. (The assumption of no variation in placing costs regardless of type of cage and reinforcement congestion is at great variation with the author's laboratory observations). It was also assumed that each type of overhang was the only overhang on a project in which 25 overhangs were required. This influenced the cost for tieing and erecting the reinforcement which was variable depending on the quantity of reinforcement used. The unit costs for purchasing materials did not vary with the quantity of usage.

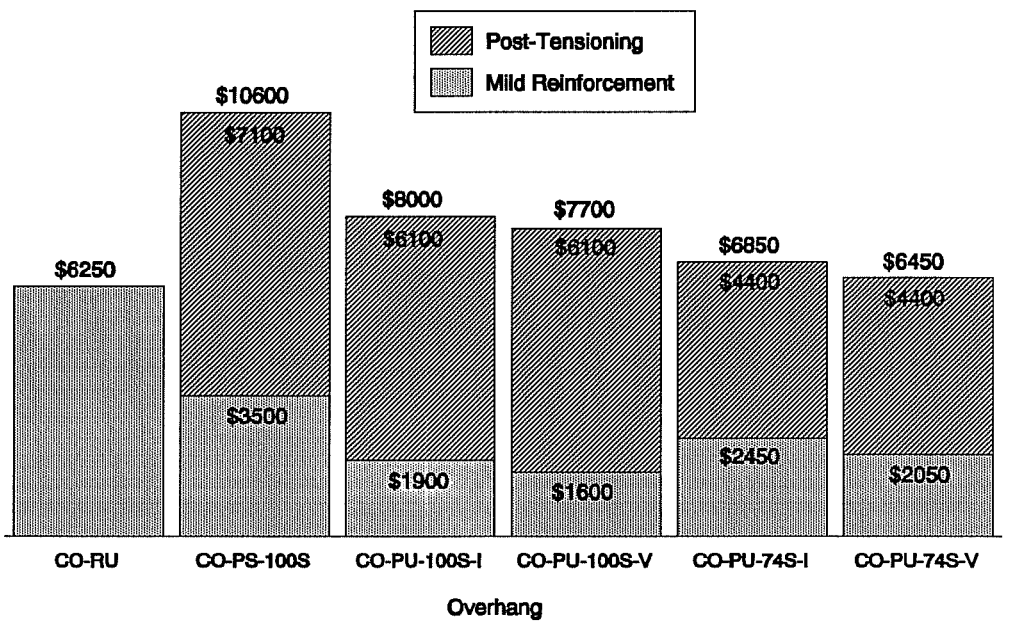

Figure 5.2 Comparison of Cost Estimates for the Reinforcement in each Prototype Overhang

Figure 5.2 presents the cost for each overhang. The lowest estimates were for the CO-RU and CO-PU-74S-V overhangs which had very nearly the same estimated costs. The estimate for the CO-PU-74S-I overhang was slightly higher. The CO-PU-100S-I and CO-PU-100S-V overhang costs were higher still followed by the CO-PS-100S overhang which was the most expensive. The trend revealed in the estimates is that the cost increases with increasing amounts of post-tensioning. Thus, any reduction in the amount of post-tensioning used will result in a cost savings. The reason the CO-RU and CO-PU-74S-V overhangs had essentially the same cost is that the CO-RU overhang had such a large amount of reinforcement.

5.3 Summary

In summary, it is observed that by implementing the alternative design procedures that were used in the CO-PU-100S and CO-PU-74S overhangs, the constructability can be greatly improved and significant cost savings over the AASHTO designed fully prestressed overhang can be realized. The improved simplification of concrete placement resulting from the significant reduction of congestion should lead to better consolidation of concrete and, consequently, more durable structures. A design similar to the CO-PU-74S-V overhang could be provided at essentially the same cost as the CO-RU overhang with significantly improved constructability and durability. If credit is given for improved constructability by reduction of congestion, the CO-PU-74S-V overhang would almost certainly be the most economical.

CHAPTER 6
DESIGN RECOMMENDATIONS

6.1 General Discussion of Design Recommendations

Based on the results of this research, it is possible to make several recommendations for the design of large cantilever overhangs. The recommendations are specifically directed at overhangs of intermediate lengths for which application of the current AASHTO specifications are ambiguous and lead to significantly overdesigned, difficult to construct, and possibly expensive overhangs. A design procedure similar to that which was used in the design of the CO-PU-100S-V and CO-PU-74S-V overhangs is proposed.

Overhangs designed by the proposed approach would be easier to construct than current AASHTO designs for either reinforced concrete or fully post-tensioned concrete, and would have significantly less overdesign. The resulting overhangs could be provided at a substantially lower cost than the AASHTO fully post-tensioned designs and at about the same cost as the AASHTO reinforced concrete designs. Furthermore, the simplification of the construction process, specifically the placement of concrete, should lead to better consolidation of concrete, more durable structures, and possibly further cost savings.

As demonstrated by this research, such an approach would result in overhangs which have good serviceability and adequate strength. While each of the new overhang designs had moment capacity substantially above what is required for factored loads, it is important to realize that any reduction in the amount of reinforcement would probably result in unacceptable service load crack width performance. This is especially true for the CO-PU-74S overhangs which had crack widths right at the maximum acceptable level. It appears that some minimum threshold amount of strength overdesign must be provided in order to achieve good serviceability and it is believed that the CO-PU-74S overhangs were very close to that amount.

The shear reinforcement design for the CO-PU-100S-V and CO-PU-74S-V overhangs was based on a simple strut-and-tie model incorporating only vertical ties in the webs. This is recommended over the approach taken for the companion CO-PU-100S-I and CO-PU-74S-I overhangs which utilized inclined ties in the web. This is because no significant differences were

observed in the service load performance of overhangs designed by the two differing approaches and designs based on the inclined ties were more difficult to construct.

One-hundred percent of the primary moment reinforcement in the CO-PU-100S-V overhang was provided by post-tensioning and the CO-PU-74S-V overhang utilized a mixture of prestressed and non-prestressed reinforcement. No definitive recommendation of one of these overhangs over the other is suggested because each has its own merits. For example, the CO-PU-100S-V overhang was by far the easiest to construct and had better crack control than the CO-PU-74S-V overhang. However, the CO-PU-74S-V overhang had acceptable crack control and was cheaper to construct than the CO-PU-100S-V overhang. Also the CO-PU-74S-V overhang had better ductility than the CO-PU-100S-V overhang. The design approach used for either overhang would be essentially the same. This decision would be up to the designer depending on the relative importance given to economics, constructability, and ductility.

6.2 Summary of Recommended Design Procedure

1. Design Primary Moment Reinforcement

   Use an ultimate strength design approach based on conventional AASHTO provisions for flexural capacity of rectangular sections. Use the appropriate formulas for non-prestressed and/or prestressed reinforcement (which assume a horizontal rectangular concrete compressive stress block) to determine the area and centroidal location of the reinforcement. The distance from the top of the overhang to the centroid of the reinforcement should be approximately 13% of the maximum depth of the overhang to provide control of crack widths through the full overhang depth.

2. Design Shear Reinforcement

   Develop a simple strut-and-tie model with the same basic configuration shown in Figure 2.9. The model should include only vertical ties in the web and it should incorporate the compressive stress block assumed in the primary moment reinforcement design.

   Determine the force which is required to be carried by the vertical web tie (tie T4 in Figure 2.9) from nodal equilibrium. Determine the shear capacity of the concrete at the location of the web from conventional AASHTO shear provisions. Allow one half of the AASHTO V_c concrete shear capacity to partially satisfy the force requirement of

the tie and provide vertical shear stirrups to carry the remaining force. Position these stirrups in a closely spaced pattern centered on the tie location. Provide minimum shear stirrups throughout the remainder of the overhang.

3. Design Side Face, Top, and Bottom Reinforcement

   Place minimum longitudinal skin reinforcement on the top, bottom, and sides as recommended by Frantz et al. (3). Determine the quantity as required to satisfy current AASHTO shrinkage and temperature steel requirements.

   Perform a cracked transformed section analysis to determine the net change in reinforcement stress with service load moment applied to the overhang. Check fatigue stress range and add reinforcement as required. Use the procedure outlined in Section 4.3.3 to determine the predicted crack widths. Iterate the crack width prediction procedure, adding steel to the top and sides as necessary to limit the predicted crack width to an acceptable level.

CHAPTER 7
SUMMARY AND CONCLUSIONS

7.1 Summary

An experimental investigation was conducted into the design and behavior of large cantilever bridge pier overhangs of intermediate lengths for which application of the current AASHTO code is ambiguous and leads to members which are overdesigned, difficult to construct, and uneconomical.

Four specimens, with two overhangs each, were constructed and tested. Six different reinforcing patterns and design procedures were represented in the eight overhangs.

The first specimen had two identical overhangs (CO-RU) each designed according to current AASHTO standards for reinforced concrete, using only mild reinforcement. The second specimen had two identical overhangs (CO-PS-100S) each designed according to current AASHTO standards for fully prestressed concrete in which service load stresses governed. The shear design for these overhangs was based on AASHTO shear provisions and included both vertical shear stirrups and horizontal shear-friction steel.

Both overhangs on the third specimen (CO-PU-100S-I and CO-PU-100S-V) were designed using only post-tensioning strand for the primary moment reinforcement. However, the quantity of post-tensioning was determined on the basis of an ultimate strength design philosophy, in contrast to the working stress design used in the second specimen. The shear reinforcement for both overhangs was determined from strut-and-tie modelling. The strut-and-tie model for one of the overhangs incorporated inclined ties in the web, leading to both vertical and horizontal shear reinforcement, while the strut-and-tie model for the other overhang included only a single vertical tie in the web, leading to only vertical shear reinforcement.

The primary moment reinforcement in both overhangs of the fourth specimen (CO-PU-74S-I and CO-PU-74S-V) was also designed according to an ultimate strength approach, but these overhangs used a combination of non-prestressed reinforcement and prestressed reinforcement. The shear reinforcement for these overhangs was the same as for the overhangs of the third specimen.

One overhang of each specimen was loaded to a complete flexural failure. The service load performance of all eight overhangs was evaluated on the basis of data collected in the tests. Construction cost estimates based only on reinforcement costs were obtained for each of the six overhang types. Comparisons were made between the service load performance, ultimate behavior, and reinforcement economics of each overhang.

The results of this study were used to formulate a design procedure which is recommended for use on large cantilever overhangs of intermediate length.

7.2 Conclusions

1. Overhangs designed according to current AASHTO standards, both reinforced concrete (CO-RU) and fully prestressed concrete (CO-PS-100S) with service load stresses governing have significantly more strength than required for factored loads.

2. Overhangs designed according to current AASHTO standards, both reinforced concrete and fully prestressed concrete have highly congested reinforcing cages making them difficult to construct.

3. An alternative design approach utilizing strut-and-tie modelling and either reductions in the amount of post-tensioning based on ultimate criteria (CO-PU-100S-I and CO-PU-100S-V) or combinations of non-prestressed and prestressed reinforcement based on ultimate criteria (CO-PU-74S-I and CO-PU-74S-V) can be successfully employed in the design of large cantilever overhangs. Such designs contain significantly reduced amounts of reinforcement and consequently are much easier to construct.

4. Overhangs designed according to current AASHTO standards and by the alternative approach have acceptable service load performance both with respect to deflections and crack widths.

5. Overhangs designed by the alternative approach have greater strength than required for factored loads, but designing them with less strength may jeopardize their service load performance.

6. For overhangs designed with amounts of post-tensioning such that the overhang will be cracked at service loads, the stress range on the strand can be sufficiently high that it needs to be checked in the design process to ensure adequate fatigue life. Some measures such as adding supplemental mild reinforcement or decreasing the eccentricity of the post-tensioning may be necessary.

7. The crack widths of post-tensioned specimens can be predicted by a procedure given in Section 4.3.3 which extrapolates the Gergely and Lutz equation. This procedure appears to be sufficiently accurate to be useful in design.

8. The ductility of an overhang designed with a combination of non-prestressed and prestressed reinforcement can approach that of a reinforced concrete overhang.

9. All of the overhangs tested experienced a flexural failure. The shear strength of all of the tested overhangs was very high and adequate shear capacity for factored loads could probably be achieved with an even further reduction in stirrups than that used in the overhangs designed according to the alternative approach.

10. Based on consideration of reinforcement cost only, the construction cost of the overhangs is significantly increased with increasing amounts of post-tensioning. This makes the AASHTO fully prestressed design (CO-PS-100S) the most expensive of the overhangs evaluated. The AASHTO reinforced concrete design (CO-RU) had the lowest cost of all overhangs evaluated, but the CO-PU-74S-V Overhang could be built at about the same cost. With reasonable credit given for reduction of congestion, the CO-PU-74S-V overhang would probably be the most economical.

APPENDIX

"Major" Crack Plots and "Crack Width Envelopes"

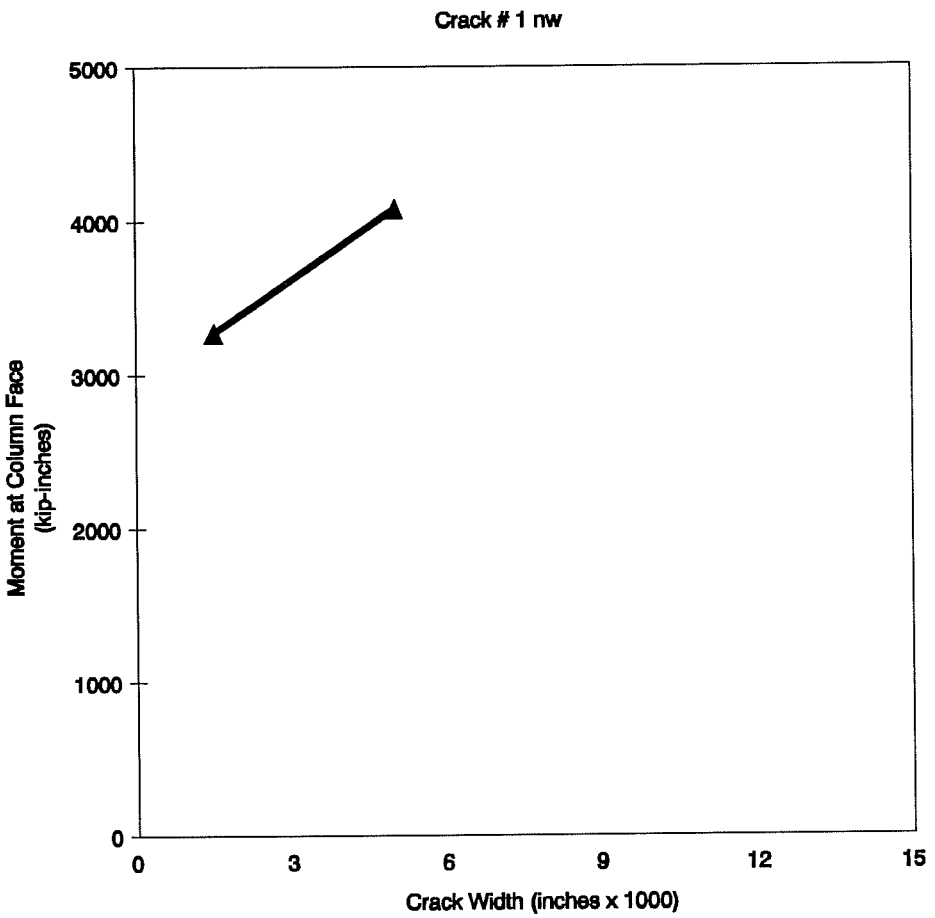

Figure A.1 "Crack Width Envelope" for the CO-PS-100S Overhang

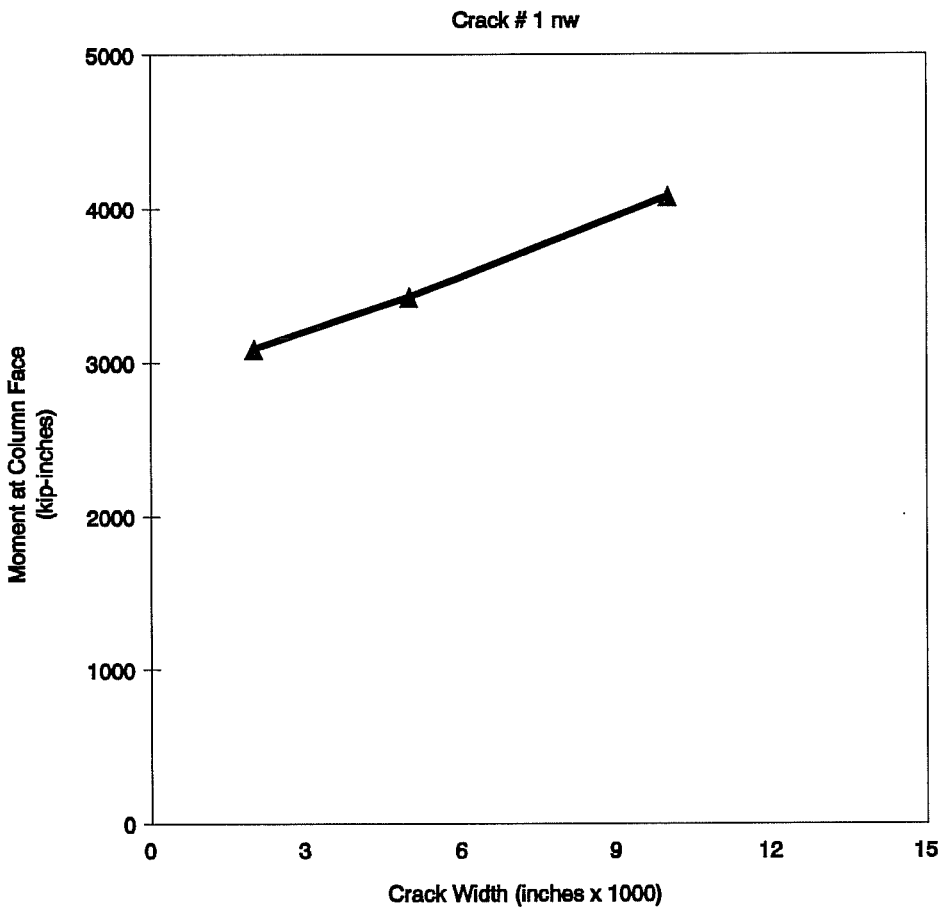

Figure A.2 "Crack Width Envelope" for the CO-PU-100S-I Overhang

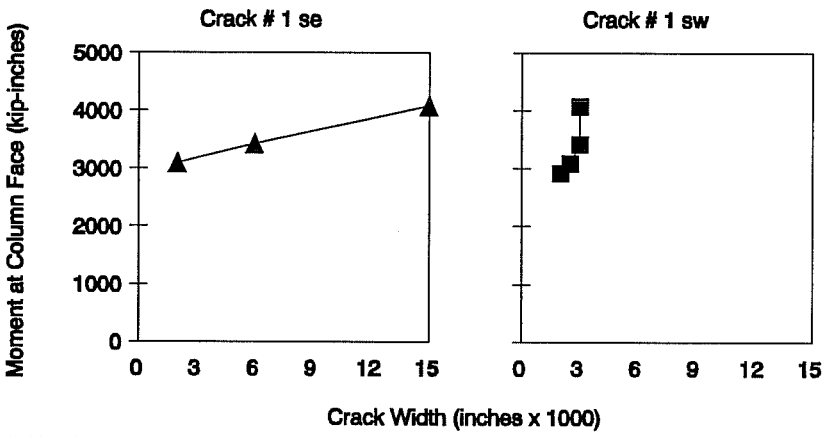

Figure A.3 "Major" Crack Plots for the CO-PU-100S-V Overhang

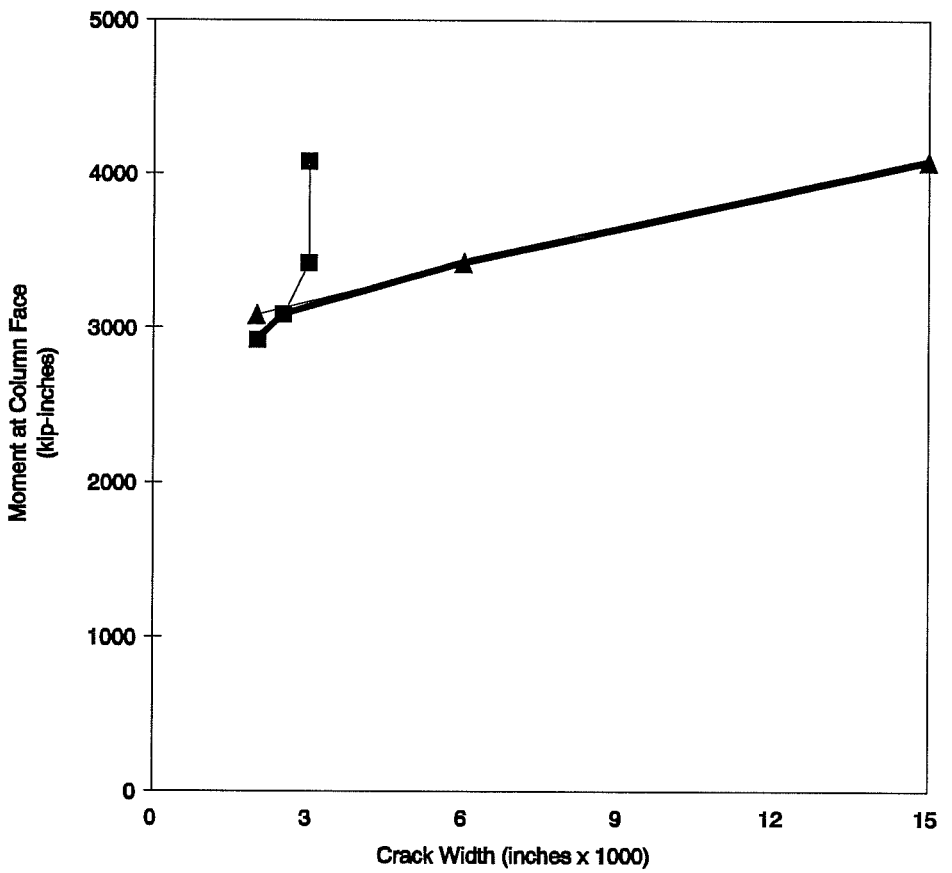

Figure A.4 "Crack Width Envelope" for the CO-PU-100S-V Overhang

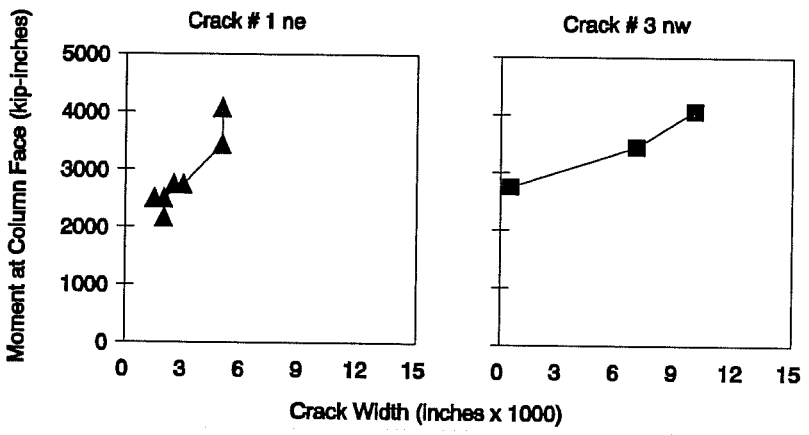

Figure A.5 "Major" Crack Plots for the CO-PU-74S-I Overhang

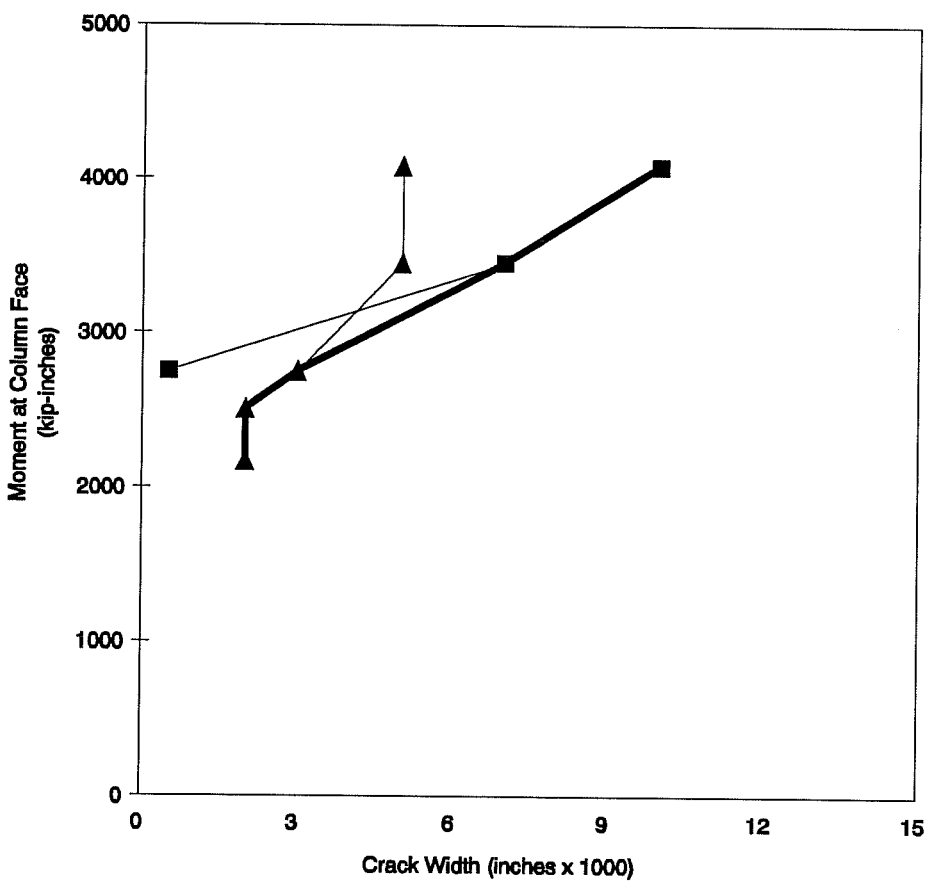

Figure A.6 "Crack Width Envelope" for the CO-PU-74S-I Overhang

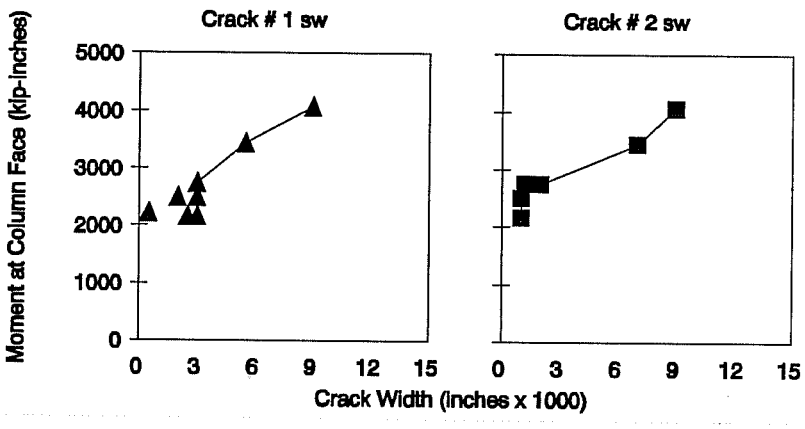

Figure A.7 "Major" Crack Plots for the CO-PU-74S-V Overhang

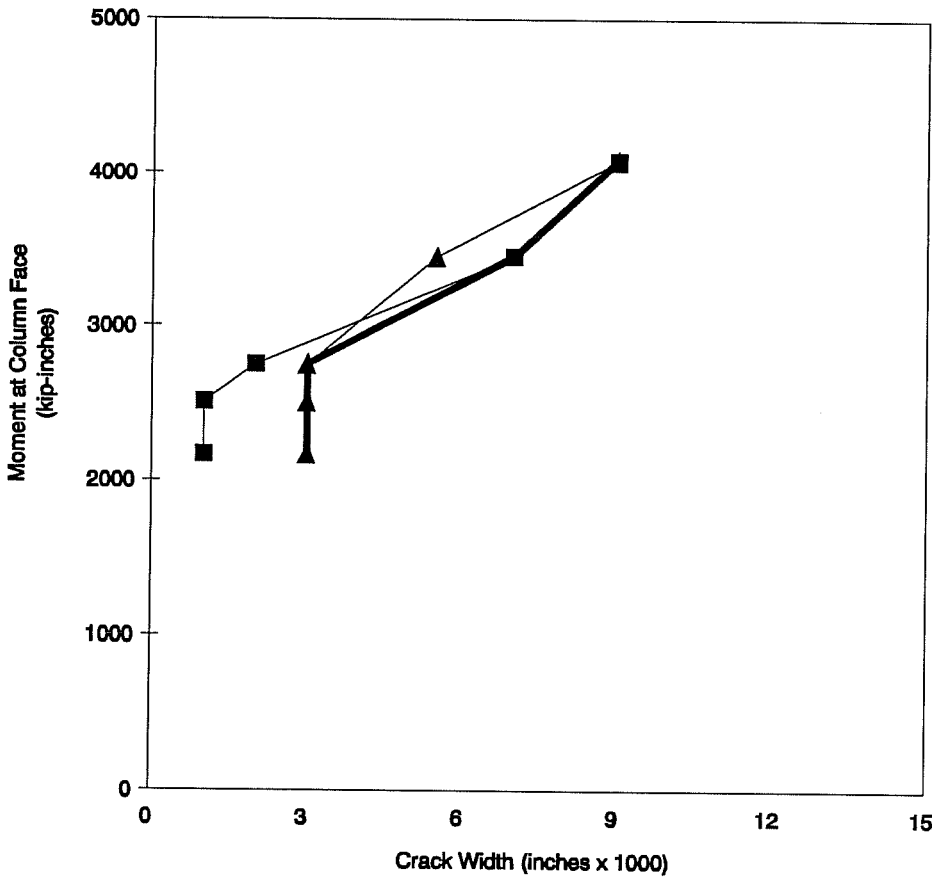

Figure A.8 "Crack Width Envelope" for the CO-PU-74S-V Overhang

REFERENCES

(1) American Association of State Highway Transportation Officials (AASHTO), Standard Specifications for Highway Bridges, Fourteenth Edition, 1989.

(2) Schlaich, J., Schafer, K., and Jennewein, M., "Toward a Consistent Design of Reinforced and Prestressed Concrete Structures," PCI Journal, Vol. 32, No. 3, May-June 1987, pp. 74-151.

(3) Frantz G.C., and Breen J.E., "Control of Cracking on the Side Faces of Large Reinforced Concrete Beams", The University of Texas at Austin, Center for Transportation Research, Research Report 198-1F, September 1978.

(4) Breen, J.E., Burdet, O., Roberts, C., Sanders, D., and Wollmann, G., "Anchorage Zone Reinforcement for Post-Tensioned Concrete Girders," National Cooperative Highway Research Program, Report No. 356, August 1991.

(5) Texas Department of Transportation, 1992 Standard Specifications for Construction of Highways, Streets, and Bridges.

(6) Wollmann, G.P., Yates, D.L., Breen, J.E., and Kreger, M.E., "Fretting Fatigue in Post-Tensioned Concrete," The University of Texas at Austin, Center for Transportation Research, Report No. 465-2F, November 1988.

(7) Gergely, P. and Lutz, L., "Maximum Crack Width in Reinforced Concrete Flexural Members," Causes, Mechanism, and Control of Cracking in Concrete (SP-20). Detroit: American Concrete Institute, 1968, pp. 87-117.

(8) Borges, F. and Lima, A., "Crack and Deformation Similitude in Reinforced Concrete," RILEM, No. 7, June 1960.

(9) Bergmeister, K., Breen, J.E., Jirsa, J.O., Kreger, M.E., "Detailing Reinforcement in Concrete Structures," The University of Texas at Austin, Center for Transportation Research, Report No. 1127-3F, May 1993.

(10) Written Correspondence with Michael W. Tanner, P.E., Senior Estimator, Austin Bridge & Road, Inc., Dallas, Texas.

VITA

Scott Douglas Armstrong was born in Minneapolis, Minnesota on January 28, 1962 to Raymond Gordon and Joan Altemus Armstrong. After graduation from highschool in San Antonio, Texas, he attended Texas A & M University where he received a Bachelor of Science in Civil Engineering in 1984. Following graduation, he accepted employment with a general civil engineering consulting firm in San Antonio where his work assignments were concentrated in the area of residential land development. He later accepted a position in a design office at the Texas Department of Transportation in San Antonio. For four years he worked on a variety of assignments related to construction plan preparation for several phases of the San Antonio Downtown "Y" Project. This was a multi-facetted urban freeway rehabilitation project involving the elevation of several lanes of interstate highway with the use of precast segmental box girder bridges. He then transferred to a residency office for three years where he served as Project Engineer on one of the San Antonio Downtown "Y" projects. He was registered as a professional engineer in Texas in 1991. In the fall of 1992, he was accepted into the Department's graduate program and entered the University of Texas at Austin. He then returned to the Department's Design Division, accepting a position in the bridge design section.

Permanent Address: TXDOT
11th & Brazos
Austin, Texas 78701

This thesis was typed by the author.